7-2016

ENCODING OF SALTATORY TACTILE VELOCITY IN THE ADULT OROFACIAL SOMATOSENSORY SYSTEM

Rebecca Custead
University of Nebraska-Lincoln, rcustead@huskers.unl.edu

ENCODING OF SALTATORY TACTILE VELOCITY IN THE ADULT OROFACIAL SOMATOSENSORY SYSTEM

by

Rebecca Custead

A DISSERTATION

Presented to the Faculty of

The Graduate College at the University of Nebraska

In Partial Fulfillment of Requirements

For the degree of Doctor of Philosophy

Major: Human Sciences

Under the Supervision of Professor Steven M. Barlow PhD

Lincoln, Nebraska

July, 2016

ENCODING OF SALTATORY TACTILE VELOCITY IN THE ADULT OROFACIAL SOMATOSENSORY SYSTEM

Rebecca Custead, Ph.D.

University of Nebraska, 2016

Advisor: Steven M. Barlow

Processing dynamic tactile inputs is a key function of somatosensory systems. Closely tied to skilled motor activity, neural velocity encoding mechanisms are crucial for both neurotypical movement production and recovery of function following neurological insult. To date, little is known about tactile velocity encoding in trigeminal networks that process complex cutaneous afferent information associated with facial sensation, proprioception, and oromotor feedback.

In this project, high resolution functional magnetic resonance imaging (fMRI) was used to investigate the neural substrates of velocity encoding in the human orofacial somatosensory system during saltatory (discontinuous, "jumping") pneumotactile inputs to the unilateral orofacial skin in 20 healthy adults. A custom multichannel, scalable pneumotactile array was used to present 5 stimulus conditions: 5 cm/s, 25 cm/s, 65 cm/s, ALL-ON synchronous activation, and ALL-OFF. The spatiotemporal organization of cortical and subcortical blood oxygen level-dependent (BOLD) response as a function of stimulus velocity was analyzed using general linear modeling (GLM) of single-subject and pooled group fMRI signal data.

Results showed that unilateral, sequential saltatory inputs to the right lower face produced localized, predominantly contralateral BOLD responses in primary somatosensory (SI), secondary somatosensory (SII), posterior parietal cortex (PPC), primary motor (MI), supplemental motor area (SMA), and insula, whose spatial organization was dependent on velocity. Additionally, ipsilateral cortical and insular BOLD response was noted during slower velocity presentations (5cm/s, 25 cm/s). In 70% of the subjects (N=14), ipsilateral cerebellar BOLD response was seen during the slower velocities (5cm/s, 25cm/s) and the ALL-ON condition, in regions consistent with the dentate and interpositus nuclei.

These results indicate rapid neural adaptation via a scalability of networks processing temporal cues associated with velocity. In addition to pure somatosensory response, activations of neural regions associated with motion production, perception, and planning may indicate close physiological ties with functional motor systems, and provide access to avenues for sensorimotor rehabilitation. Based on these preliminary results, the current project has the potential to create a neurotypical hemodynamic response (HRF) model of cortical velocity processing networks following a novel velocity stimulation paradigm, which in turn could lead to new neurodiagnostic and neurotherapeutic applications.

Acknowledgements

This work has been supported in part by the Barkley Doctoral Fellowship, Department of Special Education and Communication Disorders, with access to imaging facilities and equipment made possible by the Center for Brain, Biology & Behavior, both at the University of Nebraska-Lincoln.

Thank you to my mentor Steven Barlow, PhD, for his brilliance and enthusiasm, for teaching me how to focus my curiosity, and showing me the elegance of solid science. I now see the world as a wondrous puzzle waiting to be explored (onward we go!). Great appreciation is also extended to the members of my dissertation committee who have provided wisdom and encouragement, including; Yingying Wang, PhD, Angela Dietsch, PhD, and Greg Bashford, PhD.

Fond thanks to Austin Rosner, PhD (my roommate and sounding board) and Hyuntaek Oh, MS, ABD, for their limitless friendship and support. Thank you to my parents who lead by example, love me fiercely, and let me find my way. Thank you to my husband Len, my joy and my sanctuary. I eagerly look forward to the future ahead.

Table of Contents

List of Figures

List of Tables

Abbreviation Key

BOLD…… Blood-oxygenation level dependent
CBF……Cerebral blood flow
CNS…….....Central nervous system
CSF……Cerebrospinal fluid
deoxyHb…….Deoxyhemoglobin
EPI……..Echo-planar imaging
EPSP……...Excitatory postsynaptic potential
FA……...Fast-adapting
fMRI …… Functional magnetic resonance imaging
FWHM……...Full width half maximum
GLM……..….General linear model
HRF…….....Hemodynamic response function
IPSP……Inhibitory postsynaptic potential
MI……..…….Primary motor cortex
MNI……Montreal Neurological Institute
oxyHb…….....Oxyhemoglobin
PPC…….....Posterior parietal cortex
ROI ……Region of interest
SAI…….Slowly adapting, type I
SAII....……..……..Slowly adapting, type II
SI…….....Primary sensory cortex
SII……..……..Secondary sensory cortex
SMA……...Supplementary motor area
TE……...Echo time
TR……...Repetition time

CHAPTER ONE: INTRODUCTION

The processing of continuous tactile information is a key function of somatosensory systems. Closely tied to movement and skilled motor activity, accurate tactile percepts of direction and velocity are crucial mechanisms in both healthy movement production and recovery of function following neurological insult. To date, little is known about saltatory tactile velocity encoding in trigeminal somatosensory networks within the lower face of humans.

Specific Aims

To map the spatiotemporal organization of the cortical network which encodes the velocity of saltatory (discontinuous, 'jumping') pneumotactile stimuli (5 cm/s, 25 cm/s, 65 cm/s) delivered through a 5-channel array of TAC-Cells positioned unilaterally over perioral and buccal skin surfaces in 20 neurotypical young adults (age 19-30 years). High resolution 3T fMRI was used to map the brain's hemodynamic response to this new form of scalable pneumotactile stimulation, with saltatory velocity presentation order randomized along with two control conditions. MRI signal processing and analysis focused on: (1) characterization of the overall neural response as a function of saltatory pneumatic stimulus velocity using whole brain, single-subject analysis, and (2) quantification of active neural networks for velocity processing (group-analysis) using general linear modeling (GLM) techniques.

Background, Significance, and Rationale

Living organisms must move and interact continuously with the surrounding world. Accordingly, highly evolved plastic mechanisms within the nervous system allow for accurate interpretations of both incoming stimuli and internally-driven movement throughout the lifespan. At any given time, the outside environment and somatosensory systems present a wealth of input to the cerebral cortex and subcortical structures which can be coded by various specialized networks. This coded information is crucial for successful motor planning and corresponding behavior. Loss or impairment of sensory coding networks has a detrimental effect on motor function, while conversely, even partial recovery of sensory networks can have a profoundly beneficial effect on sensorimotor recovery in disease (Hamdy et al., 1998; Kaelin-Lang et al., 2002; Wu et al., 2006).

The goal of the current study is to identify the neural networks responsible for encoding the saltatory traverse velocity of tactile stimulation presented to the perioral and buccal region of the human face. In many research paradigms, stimulation of the facial region in neuroimaging environments has proven to be technically challenging. Standard electromechanical- and piezoceramic/piezoelectric-based stimulating devices require feed wires and large source currents to function, both of which can interfere with MR signal acquisition, or become heated by radiofrequency pulses if not properly shielded (Harrington et al., 2000; Blankenburg et al, 2003; Antal et al., 2014; Lipworth et al., 2015). Similarly, some pneumatic stimulators involve complex set-ups, and are not easily adapted to applications that include participants with neurological disease, or time-restricted imaging paradigms (Servos et al., 1999; Briggs et al., 2004; Huang et al.,

2007). The pneumotactile stimulator in the present study can be applied quickly to the skin of any population using double adhesive tape collars, and presents a form of saltatory tactile input that can be adjusted to fit unique study designs (Popescu et al., 2013; Venkatesan et al., 2014; Custead et al., 2015; Rosner & Barlow, 2015).

Characterization of the spatiotemporal organization of velocity networks in the facial somatosensory system of neurotypical participants is expected to lead to a long line of future projects, designed to unravel aspects of aberrant touch processing in brain disease and injury states. Ultimately, the long-term research goal is to delve into the powerful link between sensory and motor systems in rehabilitation and functional recovery. This project represents a first step in a comprehensive line of research that will contribute to our understanding of somatosensory processing, neural circuit plasticity, and sensorimotor connectivity. The following sections describe key elements of neural touch processing and current theories of velocity discrimination. Lastly, a method for comprehensive fMRI analysis of these processes is outlined, and applied to a cohort of neurotypical adults.

Tactile Processing

Mechanoreceptors and First Order Tactile Pathways

The reception of mechanical stimuli that is coded as tactile sensation (discriminative touch, pressure, vibration, temperature or injurious/noxious contact) occurs through a well-studied process of mechanotransduction. For all mammals

including humans, the major region specified for mechanotransduction with the outside environment is the largest sensing organ in the body: the skin.

The volley of neural activity that result from contacting skin are mediated by different types of primary afferents and their specialized receptor terminals, each of which are tuned to encode select characteristics of incoming stimuli and are referred to as *tactile units* (Vallbo & Johansson, 1984). The cell bodies of the primary tactile afferent are located in the dorsal root (neck to feet) or the trigeminal ganglia (head and face), from which they extend fibers that are classified according to axon myelination and conduction velocity. As such, Aα fibers are the largest myelinated afferent fibers with fast conduction times (120+ m/sec), and serve to innervate muscle spindle annulospiral endings. Aβ fibers are the next largest with conduction velocities in the ~30-75m/s range, which innervate most light touch receptors in the skin including various corpuscle types (Ruffini, Pacinian, Meissner), Merkel complexes, a majority of hair follicles, and keratinocytes. Aδ fibers are thinly myelinated (5-35 m/s), medium diameter fibers that serve sharp pain nociceptors, and lastly, C fibers are thin and unmyelinated (0.5-2 m/s), with distal processes that terminate as free nerve endings in peripheral tissue and are tuned to noxious thermal, chemical or mechanical stimuli through slow neuropeptide (substance P) or thermosensitive (TRP channels) mechanisms (Hursh, 1939; Johnson, 2001; Christensen & Corey, 2007; Tsunozaki & Bautista, 2009).

At the receptor end of the tactile unit, many terminals have specialized endings that are incorporated into a matrix of surrounding, non-nervous tissue. This interconnection with skin layers allows receptors to be highly sensitive to mechanical distortion such as stretch, pressure, vibration, flutter, and location variability, all of which

contribute to direction and velocity information (Chouchkov, 1973; Valbo & Johansson, 1984; Johnson, 2001).

Each mechanoreceptor's membrane is endowed with stress-gated ion channels that respond to mechanical forces, resulting in a depolarization of the terminal ending. In some instances, the frequency and extent of depolarizations are dictated by the duration and magnitude of the applied force (sustained force = sustained signaling), as in the case of slowly-adapting mechanoreceptors (SA) which tend to transmit low frequency, irregular or regular action potential signaling throughout sustained mechanical contact. In another population of mechanoreceptors, however, the generated potential is fast-adapting (FA), and the responding afferent signals are transient bursts of action potentials that tend to fall silent between the initial onset and final offset of mechanical contact, and remain quiescent during sustained static load to the surface of the skin. In addition to response pattern differences, both SA and FA receptors can be further subcategorized by the size and definition of their receptive fields.

For example, both SAI (Merkel complex) and FAI (Meissner's corpuscle) mechanoreceptors are located near the skin surface and have small, distinct receptive fields. In contrast, both SAII (Ruffini ending) and FAII (Pacinian and Golgi-Mazzoni corpuscle) receptors which lie deeper in the dermal layer have large, obscure receptive borders (Johansson et al., 1988; Johnson 2001; Mano et al., 2006; McGlone & Reilly, 2010). This arrangement and typing of receptors allows for a system of coding the all/none action potentials of tactile units into a much more complex and composite signal.

Touch processing therefore, begins with layers of coded information from finely tuned deformation- or stretch-sensitive units in the skin. The percept of mechanical

intensity, direction and velocity starts with the sensitivity and range of individual mechanoreceptors (Essick et al., 1988; Edin et al., 1995; Essick, 1998; Bensmaia, 2008). Later, touch processing necessitates the integration of patterns of activity from regional groups of mechanoreceptors, and ultimately requires the temporal and spatial summation of those patterns by higher level, central divisions of the nervous system (Kohn & Whitsel, 2002; Tommerdahl et al., 2010).

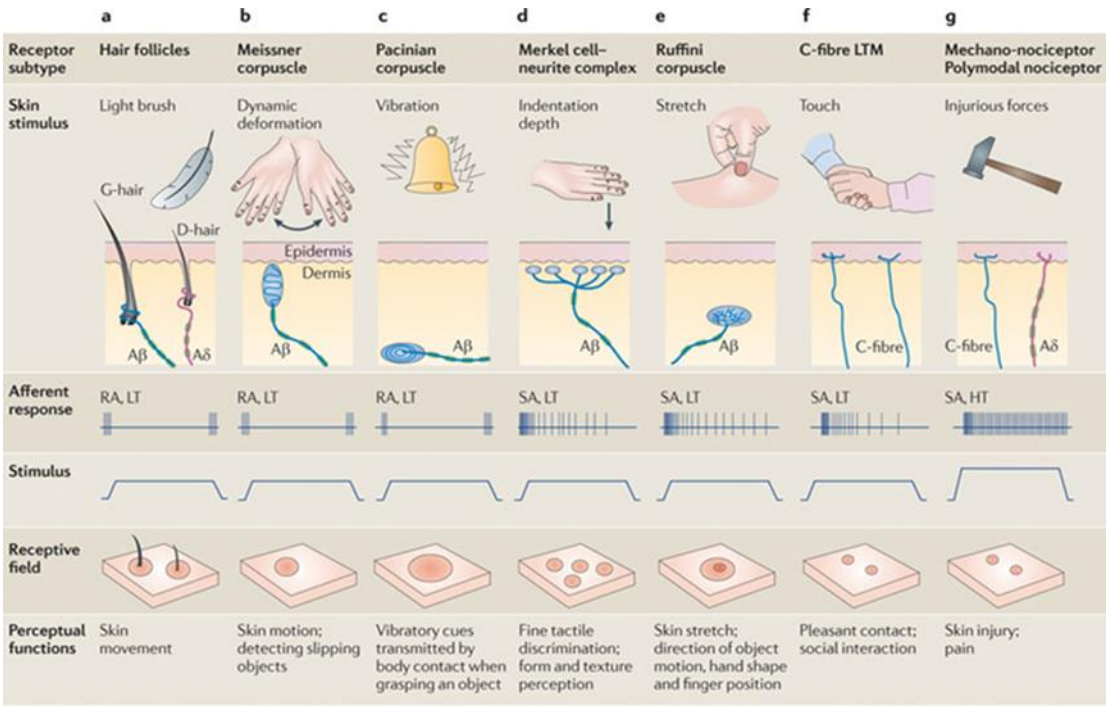

Figure 1.1 Human cutaneous mechanoreceptors. Illustration shows receptor subtypes (a-g), their corresponding response characteristics, receptive field boundaries and perceptual functions (modified from Delmas et al., 2011).

Second Order Tactile Pathways

The patterns of touch information obtained by peripheral receptors are conveyed to the central nervous system along somatotopically segregated pathways. For body regions below the neck, mechanoreceptive signals pass from the distal (receptor) process of the first order neuron to the proximal (axonal) process which extends directly into the dorsal region of the spinal cord. These first order neurons ascend ipsilaterally in designated tracts of the dorsal columns of the spinal cord, and make synaptic links to second order neurons in the gracile (lower trunk and legs) or cuneate (upper trunk and arms) medullary nuclei. From there, the second order neurons decussate and make synaptic connections with third order neurons in the thalamus (ventral posterolateral nucleus, VPL) before ascending to cortex (Brown, 1981; Hendelman, 2006).

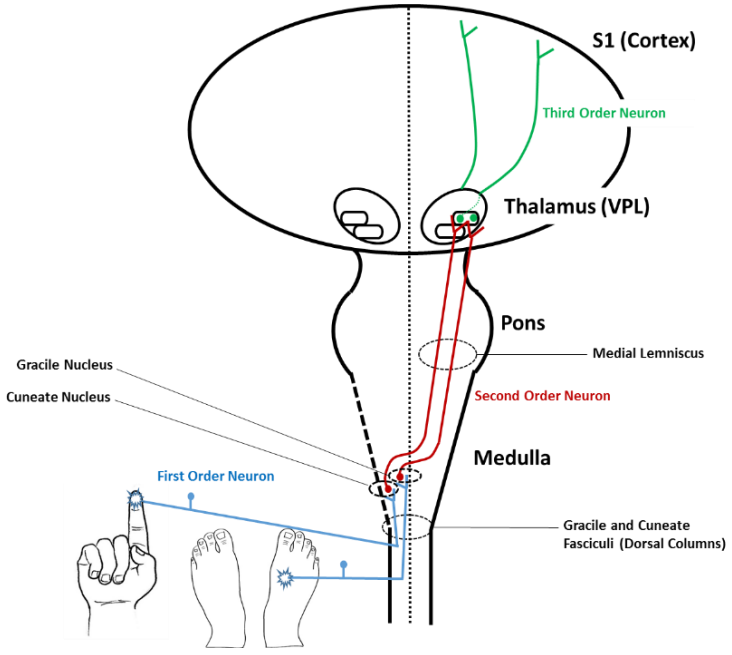

Figure 1.2 Basic pathways for discriminative touch and pressure in regions below the head.

For skin regions of the face and head, the trigeminal cranial nerve serves to innervate the facial mask, jaw (teeth) and intraoral mucosa and anterior 2/3rds of the tongue surface. Similar to the spinal afferents, the mechanoreceptor tactile units of the face have their cell bodies positioned outside the CNS in the trigeminal (semilunar or Gasserian) ganglion with their proximal processes entering the brainstem at the level of lateral mid-pons. From there, first order fibers enter the ipsilateral main sensory trigeminal nucleus and make synaptic links to second order neurons, which then cross to synapse with third order neurons in the thalamic VPM (ventral posteromedial nucleus) (Capra & Dessam, 1992; Tomita, 2012).

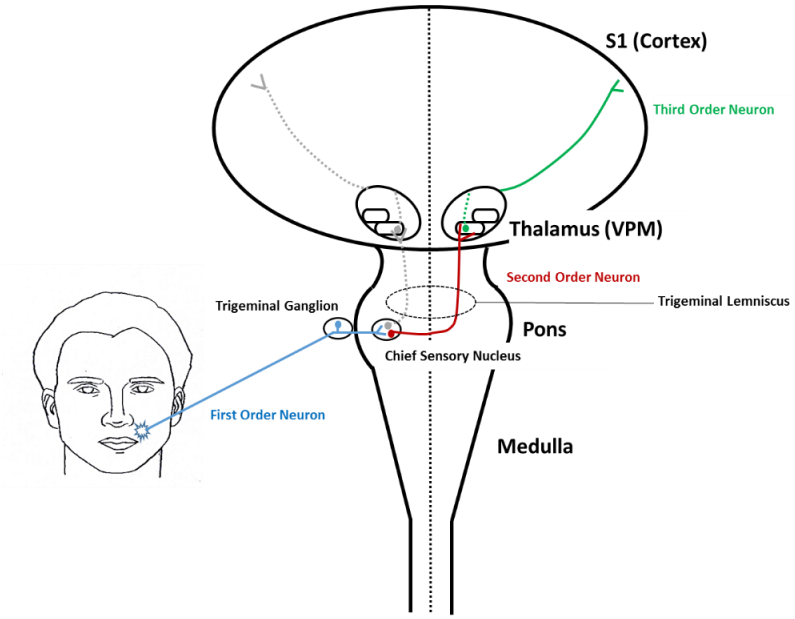

Figure 1.3 Basic pathways for discriminative touch and pressure in the face.

Thalamic Modulation

Before ascending to cortex, somatosensory information passes through a critical region of subcortex, the thalamus. In much of the literature describing velocity and direction encoding in the central nervous system, a considerable portion is often reserved for discussions of relay, driving, and feedback associated with thalamic modulation.

The thalamus has extensive interconnectivity with deep layers 4 through 6 of cortex, where interneurons distribute afferent information to other cortical layers. This allows for signal spread throughout higher cortical sensory and motor regions (Mountcastle, 1978; Jones, 1981; DeFelipe, 1992, Ahmed et al., 1994). Additionally, thalamic connections extend to motion regulating portions of the cerebellum and basal ganglia, as well as limbic regions including the hippocampus and amygdala (Parent & Parent, 2005; Kamishina et al., 2008).

Nearly all thalamic nuclei project to cerebral cortex to some extent, and in turn receive reciprocal inputs from cortex that modify thalamic output in a continuous feedback circuit (Guillery & Sherman, 2002; Lee & Imaizumi, 2013). In this way, the thalamus serves as both a driver and modulator of most sensory processing. There is tight thalamic regulation of visual percepts of direction, object velocity, and head movement (LaCara & Ursino, 2007; Arleo et al., 2013). Several studies have shown plastic connections associated with thalamic gating of somatosensation (Wang et al., 2010; Diaz-Qesada et al., 2014), both in the realms of touch (Staines et al., 2002; Yu et al., 2013; Cerkevich et al., 2013), and limb proprioception (Fasano et al., 2010; Lee et al., 2012).

In thalamic gating, extraction of key sensory information is done through selective mechanisms that both inhibit behavior-irrelevant, and facilitation behavior-

relevant afferent signals (McCormick & Bal, 1994; Staines et al., 2000; Mayer et al., 2006). Rather than solely relaying information to cortex, thalamic processing neurons shift coding properties of the incoming afferent signals to detect salient features of the sensory environment (Ahissar et al., 2002; Chung et al., 2002). High-frequency thalamic bursting in response to relevant changes in the environment can cause cortical neuronal targets to be more likely to become active in the downstream processing path (Pinto et al., 2000; Swadlow et al., 2000), while in quiet-alert states, steady-rhythmic thalamic activation can lead to an 'adapted' state in cortex characterized by low background firing, higher signal-to-noise ratio and sharpened receptive fields (Steriade et al., 1993; Castro-Alamancos, 2002).

Cerebellar Contributions to Tactile Processing

In addition to thalamic modulation, newer studies have described extensive cerebellar influence on sensory processing and tactile discrimination tasks (Habas, 2010; Valle et al., 2010; Kuber et al., 2011; Van Ede & Maris 2013; Bing et al., 2015). The cerebellum has been considered a predominately motor structure because cerebellar damage leads to overt impairments of motor and postural control, balance, and coordinated voluntary movement. The cerebellum is also a key structure in motor learning through cortical feedback processes and movement network adaptation.

Recent examination of sensorimotor feedback networks however, has unveiled mechanisms of pure somatosensory processing in cerebellar function. In addition to direct afferent pathways from limb and face to cerebellum, tactile information also ascends up through the dorsal column-medial lemniscal tract to somatosensory cortex. These

projections connect back to the cerebellum providing a tactile processing loop that acts primarily to enhance proprioceptive responses (Kennedy et al., 1966; Rowland & Jaeger, 2008). In discriminative touch processing, the dentate nucleus, a main cerebellar output region, has been shown to respond preferentially to sensory discrimination tasks without movement (Gao et al., 1996; Parsons et al., 1997; Kuper et al, 2011), and has extensive connectivity to the midbrain red nucleus which has been hypothesized to play a key role in touch processing (Lui et la., 2000; Gruber & Gould, 2010.

The cerebellum in humans is activated in anticipation of somatosensory events, even when these events do not require overt motor responses. In a study by Tesche & Karhu (2000), a cerebellar sensory response was observed when a tactile stimuli failed to occur at expected points in time. This is consistent with the premise that the cerebellum is specialized for responding to the temporal relationships between events, whether motoric or sensory.

The plasticity of sensory and motor cortices has a well-described role in motor learning, and the cerebellum facilitates these functions using sensory feedback. Classically, the cerebellum is necessary for the execution of adaptively timed motor responses following repeated paired presentations of a stimulus (Hogri et al., 2014). In patients with cerebellar atrophy for example, there is a pronounced difference in cerebellar filtering of time-specific incoming sensory volleys, which negatively influence motor learning and sensorimotor adaptation (Dubbioso et al., 2015).

For the present study evaluating neural networks related to tactile velocity processing, one might hypothesize considerable cerebellar involvement, especially in the rapidly adapting stages of slower velocity presentations. Velocity coding of moving

sensory stimuli heavily incorporates adaptive mechanisms such as long-term potentiation (LTP) and long-term depression (LTD), both of which have been attributed to thalamic and cerebellar feedback control (Hamada et al., 2012).

Integrated Cortical Networks

The complexity of incoming sensory signals to cortex, both from the periphery and subcortical modulatory-gating loops, denotes a need for an efficient, yet highly plastic central integrating system. For example, manual object exploration with touch requires the peripheral encoding of 'stick-slip' textural elements of a manipulated object's surface. Vibratory and pressure information dispersed as an object passes over the dermal surface is coded as patterns of discharge intensities and spatial distributions of activated mechanoreceptors. Similarly, the perception of direction and velocity of a *moving* tactile stimulus across the skin requires that receptors are acutely sensitive to skin compression, indentation and stretch (Essick & Edin, 1995).

Interestingly, in a study by Edin et al. (1995), it was reported that both SA and FA receptors responded systematically to directional skin stimulation, even when the passing stimulus was not in direct contact with the receptive field. This indicates that mechanoreceptors are so sensitive to neighboring distortions by tangential stretch, that true contact with the receptive field is not required for activation. Additionally, many receptors, particularly SAII-type, discharge in a highly consistent manner to directional stimulation, and show replicable differences in discharge patterning even when the velocity of the stimulus is varied (Edin et al., 1995). In imaging studies of central activations, the standard description of touch processing in primate cortex is that it first

occurs over several subdivided regions of interest: the primary somatosensory cortex (SI) and its major sub-areas 3a, 3b, 1, and 2; the secondary somatosensory cortex (SII) positioned along the superior ridge of the lateral sulcus; the deeper, insular somatosensory cortex; and the posterior parietal cortex (PPC), designated Brodmann's areas 5 and 7b. The primary sensory cortical subdivisions (3a, 3b, 1, 2) constitute distinct architectonic and functional fields, and each contains discrete representations of body receptors (Merzenich et al., 1978; Kaas, 2004). Area 3b corresponds to 'classic' primary sensory cortex, as it receives somatic-mechanoreceptive input from thalamic nuclei and relays signal to adjoining regions. Area 3a receives predominately kinesthetic/proprioceptive information from thalamus, and areas 1 and 2 receive most input from 3b and serve as second level discriminative touch processors of cutaneous, rapidly adapting reception (Krubitzer et al., 1990; Kaas et al., 2006). While each region is distinct, there is considerable interconnectivity between regions, as well as adjoining regions of ipsilateral and contralateral cortex (Petreanu et al., 2007; Aronoff et al., 2010), subcortex (Jacquin et al., 1990; Pereira et al., 2007; Cohen et al., 2008; Strick et al., 2009) and thalamus (Diamond et al., 1992; Sherman & Guillery, 1998; Groh et al, 2008; Cruikshank et al., 2010).

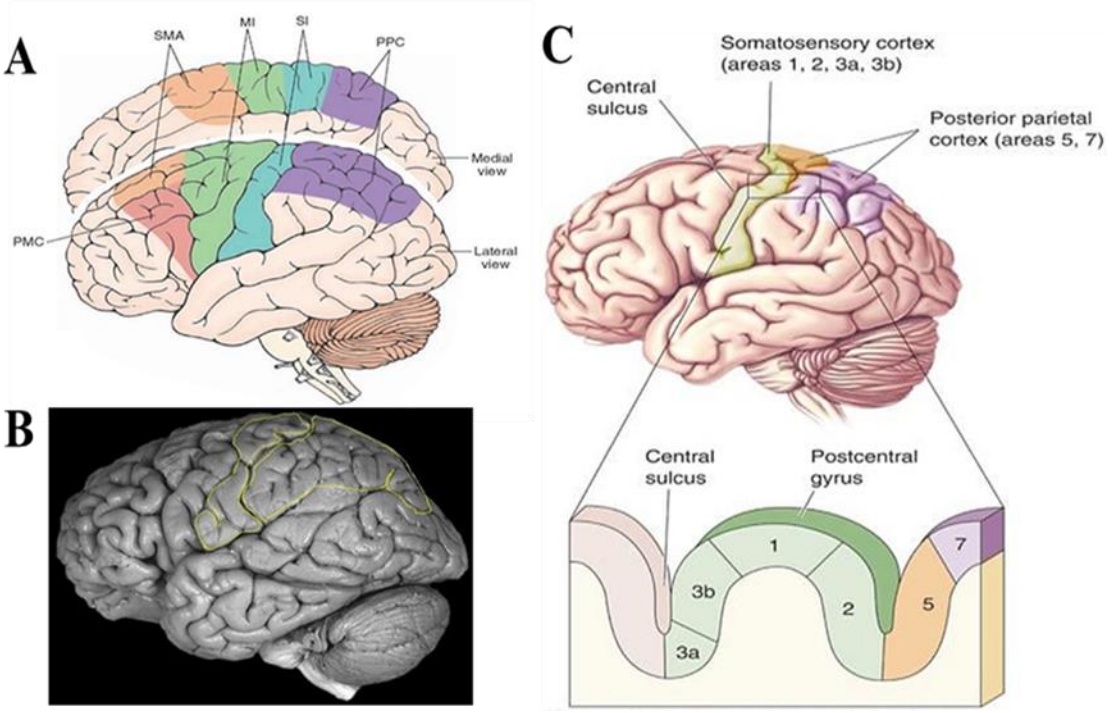

Figure 1.4 Human somatosensory cortical arrangement. Cartoon illustration (A) indicates cytoarchitechtonics; MI= primary motor cortex, PMC= premotor cortex, SI= primary somatosensory cortex, SMA= supplementary motor area, PPC= posterior parietal cortex (retrieved from http://what-when-how.com/neuroscience/the-upper-motor-neurons-motor-systems-part-1/), (B) shows an overlay of the sensory regions on a photograph of a human brain (retrieved from http://www.opt.uab.edu-class2011/1st-20year/NeuroAnatomyNBL120-VirtualLab.htm) and, (C) shows details of somatosensory cortical arrangement on post-central sulcus (retrieved from (https://www.studyblue.com/notes/note/n/somatic-sensory-system/deck/6227652).

To process trigeminal ‘facial’ touch, functional mapping studies of rodent whisker-barrel cortex have revealed a remarkable spread of signal across many integrating brain areas (Aronoff & Peterson, 2007). The earliest cortical response to tactile stimulation (~10 ms) arises in the somatotopic representation of the contacted region in the contralateral hemisphere. Depending upon behavioral state and strength of stimulus, the signal can spread rapidly across a large cortical region (Ferezou et al., 2006, 2007; Berger et al., 2007). During quite-alert states, the highly consolidated evoked response in SI spreads to neighboring regions of SI, then to SII. Interestingly, within ~8 ms of the first sensory cortical response, there is often a second localized response in primary motor cortex, which spreads to local motor regions. This may be due to recently described monosynaptic excitatory connections between SI and MI that run through deeper layers of pyramidal neurons (Farkas et al, 1999; Alloway et al., 2004; Chakrabarti et al., 2008; Johnson & Frostig, 2015). Later in the response, neural activity can propagate via long-range axons to cortex ipsilateral to the stimulus, often appearing first in regions of frontal cortex, then MI, SII and lastly bilateral PPC. A facial-trigeminal sensory stimulus therefore, results in propagating waves of activity which spread across many sensorimotor regions within a 100 ms timescale (Trulsson et al, 2000; McGlone et al., 2002; Aronoff et al., 2010, Lundblad et al., 2011).

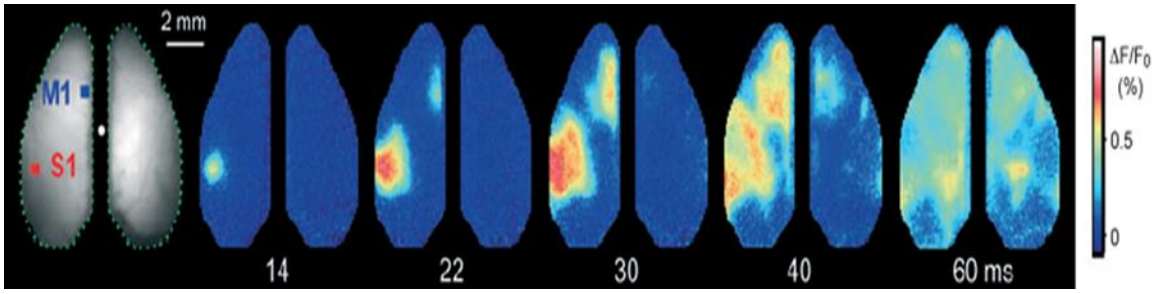

Figure 1.5 Long-range connectivity of mouse somatosensory barrel cortex. Activation is shown (blood flow change) on a millisecond timescale following a single stimulation of a whisker on the right face (Aronoff et al., 2010).

Direction and Velocity Discrimination

In the more detailed coding of direction and velocity of transitional touch, three dimensional information about motion is extrapolated from a spatiotemporal pattern of activation across an essentially two dimensional medium, the skin. To elucidate this mechanism, several early studies of motion processing in SI cortex (areas 3b, 1, 2) have described a population of neurons whose responses are directionally sensitive (Whitsel et al., 1972; Costanzo & Gardner, 1980). Many of the early single unit recordings from SI neurons in primates pinpointed motion- and direction-sensing neurons in all three major sensory cytoarchitectonic regions, with a predominance of motion-sensitive neurons in area 3b (Gardner & Costanzo, 1980; Warren et al., 1986).

Recent findings in non-human primate suggests that the *orientation* of a tactile stimulus was represented by a population of neurons in both areas 3b and 1, and that those neurons were mostly insensitive to amplitude and speed of stimulation (Bensmaia

et al., 2008). Interestingly, the orientation-selective neurons responded more like slowly-adapting rather than rapidly-adapting mechanisms, in that the strength of the orientation signal was greatest during sustained, static presentations of the stimulus.

For velocity scaling, a similar coding of peripheral afferent signals seems probable. Early work by Essick & Whitsel et al. (1986, 1988) suggested that the central nervous system uses information about spatial periodicity and temporal features of contact to estimate skin traversing velocities, most likely by approximating a ratio of RA type I and RA type II (Pacinian-type) population responses as found by Goodwin and Morley (1987). This notion is consistent with the observation that speed-sensitive SI neurons (primarily located in BA 1 and 2) appeared to process tactile motion using a *mean rate* code and not a direct spike count of mechanoreceptor discharge for estimation of stimulus velocity (Depeault et al., 2013).

Mounting evidence suggests that the central coding of moving tactile stimulation involves a decomposition of the mostly isomorphic representation of the stimulus at the periphery, into a complex signal of direction and velocity contours that are managed by neurons throughout progressive circuits of cortex. This process occurs through a relay of increasingly refined and filtered neuronal signals throughout select somatosensory regions. As such, regions of interest (ROI) for this study will include the major cortical regions of the somatosensory network; SI cortex (sub-areas 2, 1, 3a, 3b); SII cortex, insular somatosensory cortex; PPC, and cerebellum.

Somatosensory Network Plasticity

Apart from its impressive algorithmic processing of vastly multifarious signals, the nervous system is composed of living tissue, which makes it capable of equally impressive plasticity. In fact in touch processing, both cortical representations of stimuli and the functional connections required to process stimulation are not 'hard-wired', but fluctuate through competitive interactions at multiple levels of the nervous networks (Tommerdahl et al., 2010).

To manage the continuous flow of incoming signals, the 6-layered somatosensory neocortex is organized into a vertical minicolumnar/macrocolumnar architecture. Each minicolumn contains a radial clustering of the apical dendrites of pyramidal cells and accompanying spiny-stellate and GABAergic double-bouquet interneurons. In somatosensory processing, it is the excitatory spiny stellate cells that are abundant in deep cortex, and receive a bulk of thalamic signals which they then distribute radially to cells in other layers. Alternately, the double-bouquet interneurons tend to inhibit cells in adjacent minicolumns.

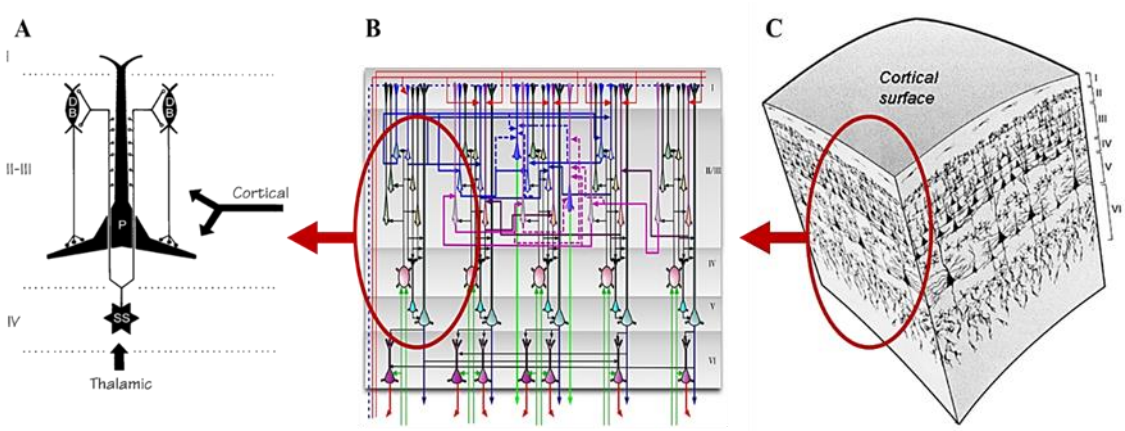

Figure 1.6 Arrangement of the (A) somatosensory cortical minicolumn and (B, C) macrocolumn. P=pyramidal neuron, DB= double-bouquet neuron, SS= spiny stellate neuron (A, from Whitsel et al., 1999; B from Dileep & Hawkins, 2009; C retrieved from http://imgbuddy.com/cerebral-cortex-layers.asp).

This unique arrangement allows for a spatially complex pattern of radial activity through several layers of cortex, but keeps signal propagation fairly modular from a horizontal, macrocolumnar aspect. This presents a further potential mechanism for somatosensory coding and stimulus feature extraction via signal propagation and signal constraint, in that cells which occupy the same radially oriented minicolumn have similar receptive properties, while cells in neighboring minicolumns (in essentially the same somatotopic brain area) do not (Mountcastle, 1978; Favorov & Diamond, 1990).

Similar touch signal refining interactions also appear to take place in high processing circuits between SI, SII and PPC (Rowe et al., 1985; Popescu et al., 2012; Hu et al., 2012). In a series of Optical Intrinsic Imaging (OIS) studies in cat cortex, evoked

responses of contralateral SI and SII were monitored during forepaw pad stimulation with either a flutter (25 Hz) or vibratory (200 Hz) touch stimulus. They found that although the same region of forepaw pad was stimulated, the 25 Hz stimulation evoked vigorous and spatially localized activation in both contralateral SI and SII, but the 200 Hz stimulation evoked robust activation in contralateral SII only, and had a primarily inhibitory effect on SI.

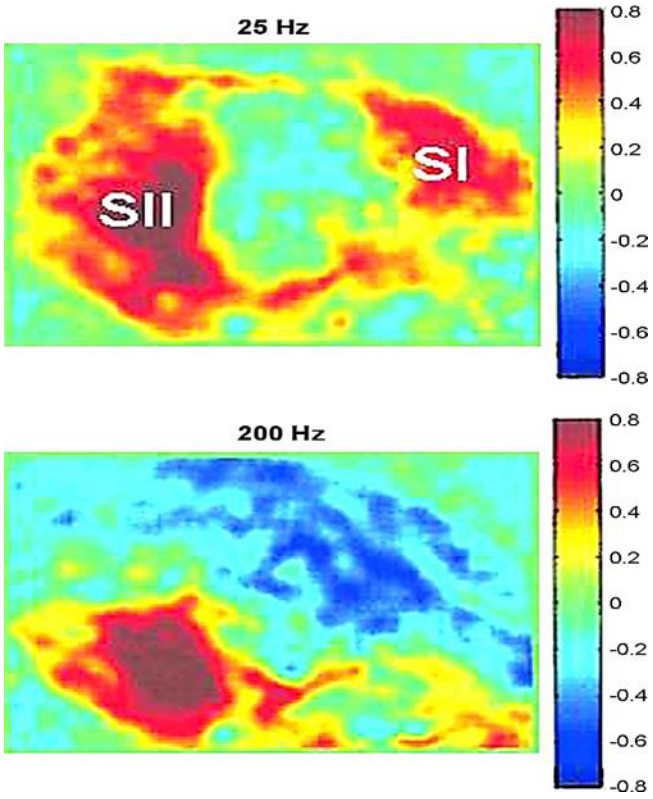

Figure 1.7 Optical intrinsic imaging of cat somatosensory cortex (SI and SII) during 25 Hz (flutter) versus 200 Hz (vibration) stimulation of the forepaw pad (Tommerdahl et al., 2010).

Additionally, simultaneous *bilateral* peripheral stimulation OIS studies have shown that ipsilateral influences effect cortical responses, often changing SI light absorbance through short-latency activations. This frequently results in a muting of SI response when compared to contralateral stimulation alone (Iwamura et al, 2002; Tommerdahl et al., 2005, 2006).

Taken together, this indicates that suprathreshold mechanical touch signals start as widespread, relatively diffuse activity across SI macrocolumns that are driven by the characteristics of the stimulus. Over a time scale of milliseconds, macrocolumn activity fractionates into refined stimulus-specific patterns of distinctly active minicolumns. This allows for a dynamic representation of tactile stimulus through a type of competitive selection of neuron subsets whose feature-tuning properties most closely match those of the stimulus.

Perhaps most importantly, dynamic properties such as those discussed above permit rapid and accurate optimization of touch processing networks. Coding redundancy is lessened by taking into account recent sensory history, since it enables a reduction of neurons that must be recruited to code a recurrent sensory signal. Stimulus-driven dynamics can thusly allow cortical processing networks to be both broadly- and finely-tuned to novel or redundant signal, temporally sensitive, and able to dedicate specific circuits to the management of input which the network has recently experienced (Greenlee & Heitger, 1988; Kohn & Whitsel, 2002; Tommerdahl et al., 2010: Peron et al., 2015).

Adaptation

In sensorimotor physiology, adaptation to repetitive stimulation is another mechanism that allows response tuning throughout changing environmental and internal conditions. Studies across the lifecycle of both animal and human subjects have shown that somatosensory cortex maintains the capacity to apportion neural area in response to redundant stimulation, amputation, and behaviorally relevant experience. Adaptation is also a key mechanism in functional recovery after injury, since it enables the reorganization of spared neural circuitry to accommodate regions of damage.

At a cellular level, repeating tactile stimulation transiently alters the response properties of somatosensory cortical neurons (Lee & Whitsel, 1992; Kelly & Folger, 1999; Whitsel & Kelly, 2000; Kohn & Whitsel, 2002). Even in *ex vivo* conditions, the response of an isolated neuron is dictated by its recent activity. Because of Ca^{++}-activated ion channels along the soma, a stimulated pyramidal neuron that has just undergone a series of stimulus related depolarizations will tend to show a higher spike firing rate upon identical subsequent stimulation. Similarly, recent auto-activity can alter the conductance of dendrites, modifying the process by which patterns of input are converted to somal-generated action potentials (Magee, 1999). This indicates that in individual neurons, the firing capacity and the ability to propagate signal to other neurons is highly dependent upon its preceding history of activation.

In groups of neurons, adaptation results from an overall shift in both excitatory (glutamate-gated NMDA, AMPA and Ca^{++}-dependent) and inhibitory (GABAergic) neurotransmission (Kim, 1995; Kohn & Whitsel, 2002; Rao & Finkbeiner, 2007; Malina et al., 2013), which leads to rapid changes in larger somatosensory processing networks.

Relevant to this study, anatomical tract tracing research has shown an intricate convergence and divergence of somatosensory thalamocortical connections, making vertical tactile pathways in particular, highly plastic and susceptible to associative learning and adaptive reorganization (Jenkins & Merzenich, 1990; Xerri et al., 1998; Aronoff et al., 2010; Zembrzycki et al., 2013; Hubener & Bonhoeffer, 2014). Additionally, there is substantial horizontal connectivity that integrates information across corticocortical zones, and likely plays a pivotal role in short-term somatosensory cortical adaptation either through changes in direct inhibitory transmission or unmasking of previously inhibited excitatory circuitry (Merzenich et al., 1983a, 1983b, 1984; Jacobs & Donoghue, 1991; Heiss, 2008; Carsea & Froemke, 2013; Schnepel et al., 2014).

This phenomenon provides an ideal focus for research looking to evaluate short-term cortical processing changes. Experimental presentations of tactile stimulation varied by velocity, direction, inter-stimulus interval (ISI), or intensity, could capitalize on the nervous systems extraordinary ability to detect change, monitor co-incidence, and adjust networks adaptively.

Orofacial Anatomy and Sensory Function

Although tactile sensory processing anywhere in the body occurs through well-defined pathways, there are some fundamental differences in anatomical layout and function between the processing of inputs that occur in the face, versus those that occur in regions below the neck.

Muscles

Muscles of the facial mask and perioral area responsible for speech, facial expression, and are involved in deglutition, swallowing, sucking and airway protection and are arranged differently than muscles found in limbs. While most perioral muscles originate from the bony structures of the skull or deep fascia, nearly all make insertion into the skin of the facial mask rather than terminating on an adjoining bony structure. These muscles, including the zygomaticus major and orbicularis oris around the mouth, pull on the skin to produce movements required for lip and cheek coordination during speech, infant suck, and food intake.

Sensory Receptors

The afferent processes in the soft tissue of the face are functionally comparable to limb mechanoreceptors (slowly adapting, SA type I and type II, and fast adapting, FA), but there is also some noteworthy specialization in facial receptor type and distribution. For instance, a group of fast adapting receptors that respond best to vibratory stimulation at 250 Hz, the Pacinian corpuscles, are prevalent in both the hairy and glabrous (palmar surface) regions of the hand, but are virtually absent in the face (Barlow, 1987; Johansson et al., 1988, Nordin et al., 1989).

Additionally, because of the variable modes of muscle origins and insertions (bone, semitendonous nodes, integument, skin), there are no muscle spindle receptors and Golgi tendon organs in the face (Stal et al., 1990; Conner et al., 1998). Muscle movement and position sensing is accomplished by specialized Ruffini-type receptors that are highly sensitive to stretch and skin deformation (Nordin et al., 1989; Andreatta et al., 1996;

Barlow, 1998). Afferents in the facial skin, lips and mucosa therefore respond not only to contact with environmental objects, but are exquisitely tuned for facial proprioception such as lip-to-lip contact, changes in intraoral air pressure, jaw motion and perioral stretch (Trulsson & Johansson, 2002).

Perspectives from Orofacial Pneumotactile Research

Much of the neurophysiological information about neural networks involved in sustained tactile stimulation in humans comes from research using electrical stimulation, usually applied to a limb with either biphasic or monophasic current pulses delivered at select frequency and intensity settings (Hamada et al., 2002; Peurala et al., 2002; Wu et al., 2006; Celnik et al., 2007; Conforto et al., 2010). Comparatively little is known about the trigeminal somatosensory networks responsible for processing cutaneous afferent information associated with facial sensation and proprioception. Similarly, research evaluating non-electrical tactile stimulation as a potential neurotherapeutic application is rare, except in preterm infants in the neonatal intensive care setting learning to orally feed (Barlow et al., 2008; Barlow et al., 2014a, 2014b, 2014c; Fucile et al., 2010, 2012).

Recently, research utilizing pneumotactile prototypes of the device described in this project have shown there are distinctly different response adaptation patterns to repetitive stimulation between the face and limb (Popescu et al., 2010). In regions of the perioral area, there are characteristically different cortical short-term recovery functions with different timescales of tactile information integration.

Early MEG studies comparing responses of the face (trigeminal) and hand (median nerve) to repeating trains of pneumotactile stimuli revealed not only differences

in peak latencies of cortical responses due to variations in axon length and conduction time, but also significantly different patterns of evoked neuromagnetic amplitude modulation during *short-term* cortical adaptation. In that case, results showed that primary somatosensory cortex (SI) adaptation was greater for the face when compared to the hand (Venkatesan et al., 2010).

Related pneumotactile-MEG studies have shown that *long-term* adaption (reflected as changes in the SI response amplitude to the first pulse in repeating trains as a function of stimulus rate/frequency) is present only for finger stimulation, and there are overall shorter recovery lifetimes for the fingers following repeating stimulation in comparison to the face (Popescu et al., 2010). Similar variable responses in cortical processing *networks* (SI, S2, and PPC) associated with face and upper extremity stimulation were shown in the most recent adaptation paradigms, reiterating significant differences between face and limb structure and function.

These differences likely due to variations in mechanoreceptor receptive field size, signal integration, central-hierarchical processing, and role in motion sense and proprioception (Popescu et al., 2013; Venkatesan et al., 2014). Overall, it follows that studies evaluating trigeminal network tactile processing will show profoundly different response profiles than those evaluating tactile processing in the limbs.

Rationale for Perioral Stimulator Placement

Historically for sensory stimulation studies, tactile discrimination of the physical attributes (size, force, direction and velocity) of a moving stimulus has been found to improve as more receptive fields are activated by the stimulus (Essick, 1998). Also in

most cases, stimulation of areas with denser innervation results in a more intense electrophysiological or hemodynamic response in cortical networks, which fits agreeably with the somatotopic arrangement of the central nervous system, including the brain. In humans, areas dense with mechanoreceptors such as the face, tongue, larynx, hand and fingers, are represented with disproportionately large areas in both the sensory and motor cortices, and are acutely sensitive to touch, stretch and pressure stimuli.

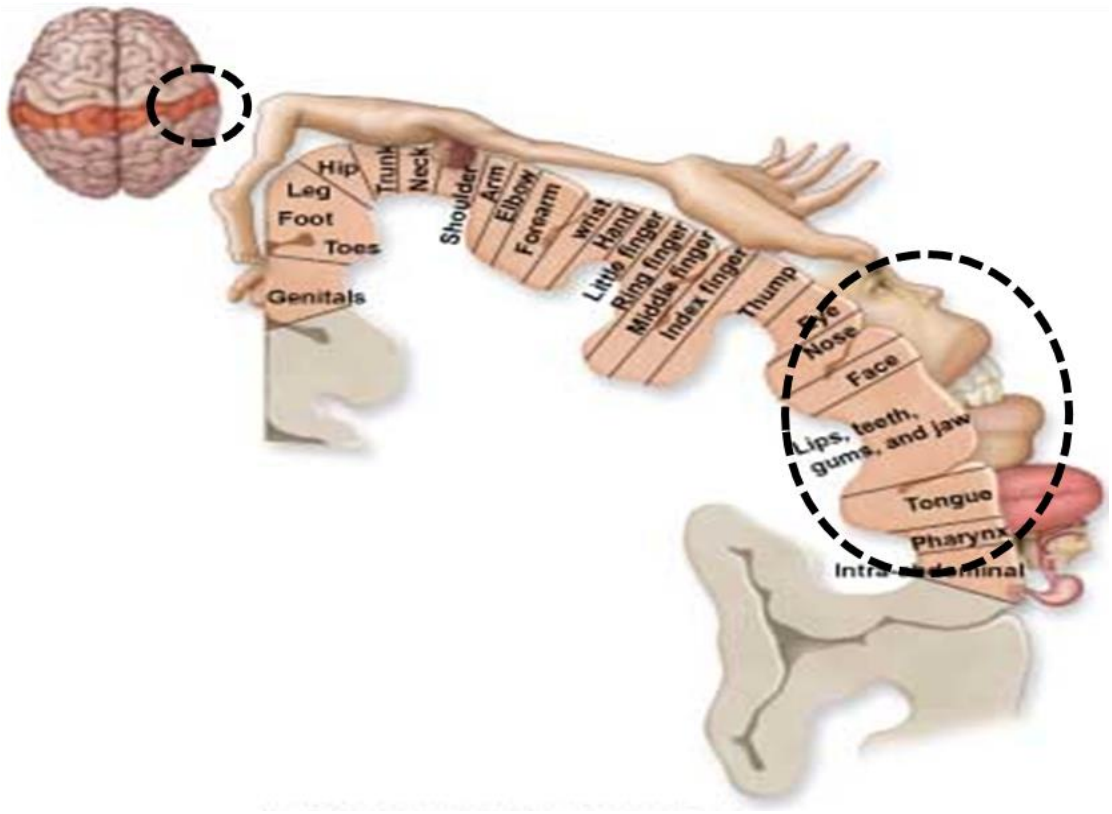

Figure 1.8 Homuncular arrangement of the human somatosensory cortex. Note the large region dedicated to face and perioral mechanisms (retrieved from http://imgarcade.com/1/cortical-homunculus/).

As described in the previous sections, the perioral region contains a dense array of highly specialized mechanoreceptors that are somatotopically mapped to a disproportionately large region of cortex. The trigeminal nerve, which innervates the lower two-thirds of the face, serves as the major pathway for transduction of sensory inputs associated with all realms of touch, pain and temperature, and plays an integrative role in oromotor control in the perioral region (Capra & Dessem, 1992; Tomita et al., 2012).

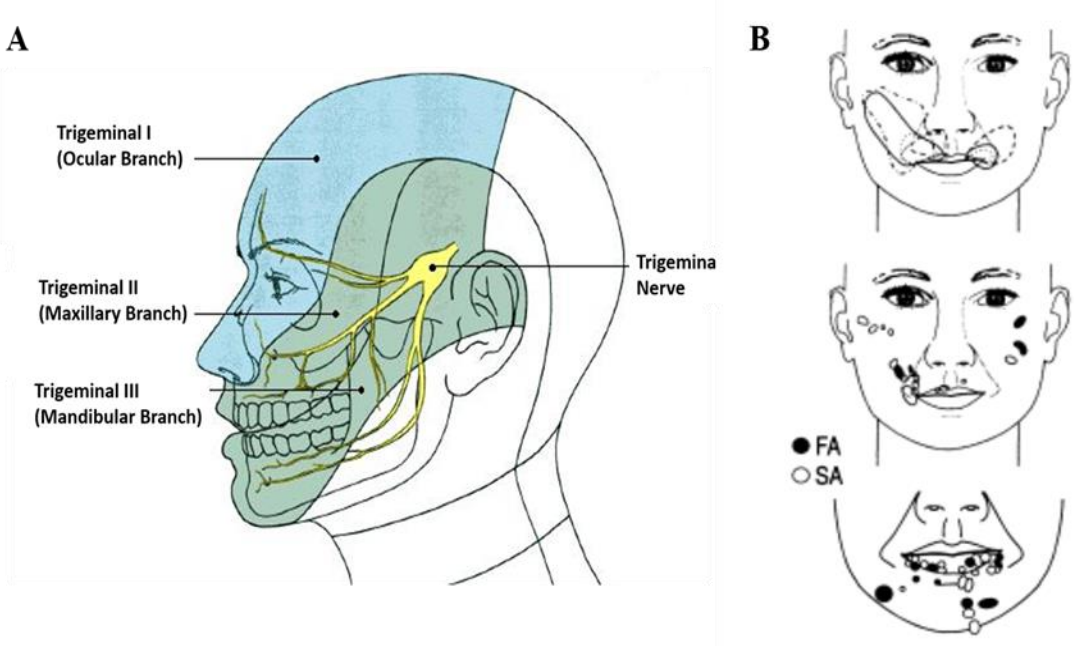

Figure 1.9 The human trigeminal nerve with its three subdivisions. (B) Receptive fields of nerve fascicles (top) and single tactile fast-adapting and slowly-adapting afferents (middle and bottom) established using microneurography [(A) retrieved from http://www.ninds.nih.gov/disorders/trigeminal-neuralgia/detail-trigeminal-neuralgia.htm, (B) from Trulsson & Johansson, 2002).

The trigeminal-sensory system is also ideally suited for study when considering future directions for diagnostic and therapeutic applications of pneumotactile stimulus arrays. The predominantly crossed representation of efferents and afferents for the lower 2/3rds of the face often manifests with contralateral loss in motor and sensory function following a unilateral MCA stroke that infarcts sensorimotor cortex. More than half of human strokes occur in a unilateral middle cerebral artery (MCA) that supplies blood to the trigeminal-sensorimotor integrating and control portions of the brain (Bogousslavsky et al., 1988; Eastwood et al., 2002). Moreover, the corticobulbar tract which connects motor cortex to the facial motor nucleus controlling movement of the face, is usually disrupted in MCA lesions. The neurons in the dorsal region of the facial nucleus (controlling upper face) receive cortical input from both right and left cortices, while ventral regions of the facial nucleus (controlling lower face) receive input from only the contralateral cortex (Jenny & Saper, 1987; Morecraft et al., 2004; Yildiz et al., 2007). For this reason, many stroke survivors are left with pyramidal-facial paresis or 'droop' on the side of the lower face effected by cortical damage. This can lead to profound and long-lasting changes in speech intelligibility, expression and facial gesture, feeding-oral intake management and even airway protection.

Rationale for Stimulus Velocity Selection

For velocity selection, an extensive review of tactile psychophysical literature led to the three velocities used in this experimental paradigm. In a series of early

psychophysical studies using continuous brushing along a linear path of skin, it was determined that in the forearm, the human capacity to identify the *direction* of a moving tactile stimulus was directly related to the traverse length of the stimulus (Whitsel et al., 1986). Judgements about the velocity and speed of the stimulus were most accurate when the traverse length was long, likely because more mechanoreceptors were activated and provided greater perceptual information to higher processing networks.

Similarly it has been shown that for tactile acuity, the optimal range for skin traverse *velocity* is between 3 and 30 cm/s (Dreyer et al., 1978; Whitsel et al., 1979, Lamb 1983; 1986; Essick et al., 1988a, 1991; Luken et al., 2011; Ackerley et al, 2014). Although subjects are still able to discern characteristics of moving stimuli presented at higher velocities, performance on velocity discrimination tasks falls off rapidly at presentation speeds exceeding 50 cm/s. From a central processing standpoint, this may indicate that for stimulus velocities greater than 50cm/s, neural circuits are processing inputs through different, perhaps "periodicity consolidating" networks in higher levels of cortex (Darrian-Smith et al., 1984). Conversely, it could be that as stimulus velocity increases, there is enough loss of temporal and spatial detail that discrimination accuracy is reduced (Johnson & Lamb, 1981).

Research has shown that perioral skin regions on the face are equally well-tuned for tactile velocity discrimination (Essick et al., 1988b, 1992; Szaniszlo et al., 1998; Todd 2012). Because of previously described differences in mechanoreceptor type and distribution, the face is in fact, highly sensitive to moving tactile stimulation, particularly around the lips and oral interangle (Nordin & Thomander, 1989; Barlow et al., 1996, 1998; Ito & Gomi, 2007). Psychophysical methods designed to assess a patient's ability

to distinguish onset, direction, and velocity of continuous stimulation applied to the face have shown to be more reliable and sensitive to mild sensory impairment than many standardized neurological assessments of orofacial sensory competence. Like the forearm, discriminative sensitivity to brushing or linear contactor stimulation seems to be most acute in the 3 cm/s to 30cm/s range (Essick et al., 1988b, 1992).

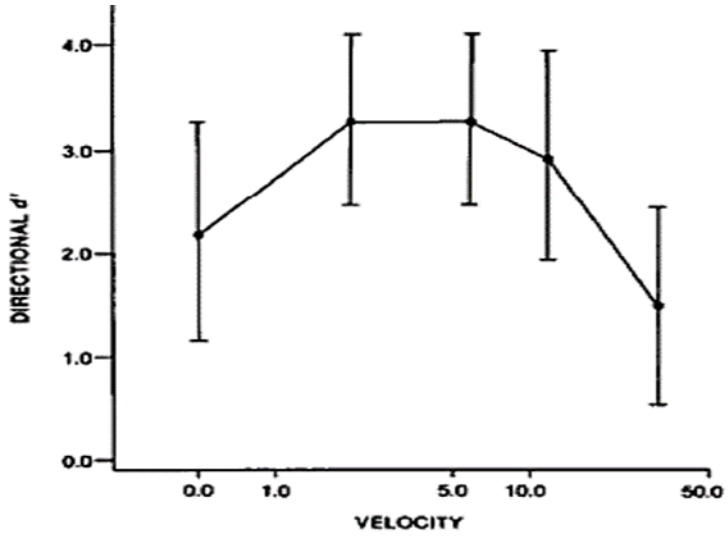

Figure 1.10 Mean directional sensitivity (d^2) of the perioral region as a function of tactile (brushing) stimulus velocity (Essick et al., 1988b).

Interestingly, in both limb and face studies of continuous motion (either brushing or linear rolling) discrimination, moving tactile stimulation presented slower than 3-5cm/s appeared to be processed in cortical networks as discrete stimuli, rather than a constant motion across the skin. It seems probable that at some velocity threshold, networks of somatosensory cortical neurons switch from processing individual stimuli to

processing temporal cues corresponding to consecutive, directional stimulation (Phillips & Johnson, 1985; Wacker et al., 2011; Depeault et al., 2013; Pei & Bensmaia, 2014).

It has also been reported that in instances of discontinuous, punctate stimulation, perception of the stimulus can be affected by differing inter-stimulus timing intervals. In some cases, tactile input, stimulus timing and spatial position are integrated in a process known as 'fusion,' or tactile 'funneling' (Chen et al., 2003; Warren et al., 2011; Kitazawa, 2013). When humans are asked to judge the distance between two punctate taps delivered in rapid succession to the skin, they consistently underestimate the distance of the taps (Goldreich et al., 2007). Oddly, the perceived distance between taps shortens as the time interval between taps is reduced. In a stimulus involving multiple punctate taps in rapid succession to neighboring skin sites, perceived locations are shifted toward the subsequent stimuli (Geldard & Sherrick, 1983; Goldreich & Tong, 2013). As an example, in the 'cutaneous rabbit' response, when several taps are presented close to the wrist, followed by several taps to mid-forearm, then several taps close to the elbow, they are perceived to be uniformly distributed, as if a 'rabbit' were hopping along the arm (Geldard & Sherrick, 1972; Eimer et al., 2005; Miyazaki et al., 2010). Optical imaging of somatosensory cortex has shown that similar fusion of topographic representation is occurring during tactile funneling. Simultaneous stimulation of two skin sites results in activation of a single focal region of cortex between the two topographic representations (Chen et al., 2003).

Because of these unique perceptual phenomenon, in this study it is hypothesized that the spatial organization and centroid of neural activation will vary as a function of tactile saltatory velocity. Specifically, there may be an inverse relation between velocity

and activation, with lower velocities of tactile saltatory stimulation showing greater regions of BOLD activation and higher velocities producing reduced regions of BOLD activation. Also, based on recent somatosensory integration and adaptation literature, it seems likely that our stimulus at the lowest velocity (5 cm/s) will result in substantially different processing and adaptation characteristics over time than network responses to stimuli presented at the two higher velocities; 25cm/s and 65 cm/s (Spackman et al., 2006; Pita-Almenar et al., 2011; Yamashiro et al., 2011; Johnson & Frostig, 2015).

Impact of Stroke and Neurological Disease on Sensorimotor Function

In neurological disease, particularly in stroke, vascular pathology associated with trauma, and hypoxic ischemia, cerebrovascular disruption has enormous impact on brain function and sensory processing circuits. During acute injury, some regions of brain sustain immediate hypovolemic damage, while other areas remain viable and capable of plastic reorganization due to collateral blood flow through pre-existing microcirculation anastomoses. It is this collateral microcirculation that seems to be key to minimizing damage and offset adverse outcomes throughout the prolonged period of recovery (Shuaib et al., 2011; Lay et al., 2011, 2012; Liebeskind, 2012; Lay & Frostig, 2014).

Interestingly, after abrupt hypoxic events such as focal, single hemisphere stroke, restorative plasticity mechanisms have been shown to occur immediately in many regions of the brain. Even before inflammation resolution, the peri-infarct regions (penumbra) of the affected hemisphere exhibit early gene expression changes which can lead to axonal re-sprouting, dendritic spine plasticity, and ultimately regional map shifts associated with functional improvement (Luhmann et al., 1995; Carmicheal et al., 2005). Plasticity also

occurs in the spared hemisphere, in both sensory and motor cortices, and in the brain stem and spinal cord (Lapash-Daniels et al., 2009; Brown et al., 2009). These findings suggest that the very processes involved in acute damage may trigger neural circuit reorganization, making the damaged brain 'primed' for regenerating new processing pathways in response to post-damage stimulation.

As with other aspects of central nervous system rescue after injury, somatosensory recovery is highly dependent on both the activation of existing connections, and the development of new connections (Moskowitz et al., 2010, Nudo & McNeal, 2013). Physiologically, reorganization into adjacent, undamaged cortex allows for expansion into alternate representation sites. For somatosensory cortex, this possibly occurs due to an overlap of somatotopy between SI and SII, structural links to PPC, and thalamic connections to supplemental motor regions which are key elements in the tactile processing stream, and likely highly responsive to post-injury stimulation (Blatow et al., 2007; Frostig et al., 2009, 2012).

Functional Neuroimaging of Tactile Networks

fMRI

Functional magnetic resonance imaging (fMRI) is a non-invasive neuroimaging technique that can be used to evaluate neural substrates of somatosensory networks in the brain. FMRI measures BOLD (Blood Oxygenation Level Dependent) signal change that is due to the hemodynamic sequelae of neuronal activity (Kwong et al., 1992; Fox et al., 2007).

During neurovascular gas exchange, hemoglobin (Hb) transfers its oxygen load at the capillary level to supply active neurons. Once unbound from oxygen molecules, deoxyhemoglobin (deoxyHb) becomes paramagnetic due to the higher spin rate of the remaining heme iron. Under the large, mostly homogenous magnetic fields generated by the MRI scanner, the change in the magnetic susceptibility of the deoxyHb causes small, local field distortions that ultimately allow for image differentiation of blood, surrounding tissue and cerebral spinal fluid (CSF) (Pauling & Coryell, 1936; Ogawa et al., 1990, 1992).

During imaging, the local extravascular water protons (hydrogen) are sensitive to magnetic field distortions caused by radio frequency (RF) pulses from the MR scanner. With each RF pulse, the hydrogen atoms align with the induced magnetic field (flip angle), then relax back to a low energy state releasing energy into the surrounding environment. A receiving head coil detects this energy (signal decay) which is characterized as T2 (spin echo) or T2*(gradient echo) relaxation depending on the phase of atom spin disruption (Thulborn et al., 1982). Thus, when the blood content of deoxyhemoglobin changes, the relaxation process of water protons is altered and can be seen as changes in resultant MR image.

BOLD and HRF

The tight coupling between the neurovascular system and active neurons allows for a predictable hemodynamic response function (HRF) utilized in fMRI BOLD research. Although less temporally acute than EEG or MEG due to the delay between

neuronal demand and vascular supply, the HRF can give excellent spatial information about regions of activity associated with stimulus responses.

In a stimulus response curve, there is an initial dip in the HRF due to a lag between oxygen consumption and cerebral blood flow (CBF) increase, which is small, comprising only about 0.1% of signal change (Hu et al., 1997). This is followed by a steep rise (main response, hyperoxic phase) resulting from incoming CBF and local vasodilation of feeding arterioles. In this main response phase, the HRF peak will saturate after ~10s in single stimulus conditions, but can be sustained at a steady intensity during repeating stimulus block designs. Finally, there is an undershoot in the HRF associated with the increased blood flow in excess of neuronal demand, which is also longer and more pronounced in stimulus block designs.

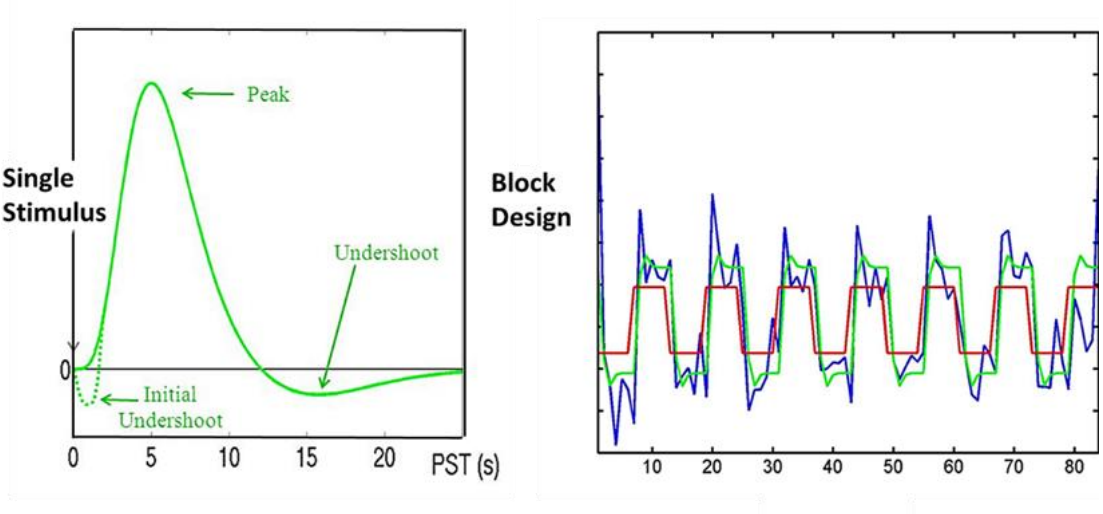

Figure 1. 11 The hemodynamic response function curve for single stimulus response and repeating stimulus presentations in a block design (Retrieved from https://theclevermachine.wordpress.com).

BOLD and Adaptive Networks

The neuronal processes causing BOLD signal changes is most directly associated with synaptic exchange at the site of activation, not with the firing level of the neurons receiving synaptic inputs (Logothetis et al., 2001). This means that fMRI reflects the synaptic activity driving neuronal assemblies, but does not provide information about the content of the neuronal firing patterns produced by the neurons.

As such, the BOLD signal change corresponds to local populations of neuronal activation, but the activated neurons can be either excitatory (EPSP) or inhibitory in nature (EPSP). For evaluations of neural networks in tactile processing, particularly involving changes related to connectivity restructuring or adaptation, it is important to consider which active mechanism is occurring. It may that during adaptive phenomena associated with velocity changes, local inhibitory or masking networks become increasingly active.

Summary

This project was designed to delineate the neural networks involved in the processing of saltatory tactile impulses at three different velocities presented through a spatial array of TAC-Cells placed over perioral and buccal hairy skin. A key feature for orofacial motor control (speech, gesture, safe oral intake, and airway protection), the encoding of afferent information associated with facial sensation using high resolution neuroimaging methods is expected to contribute new knowledge on the neural

representation and modulation of such activity in response to highly controlled dynamic somatosensory fields. Research studies often cite orofacial dysfunction due to diminished sensory feedback as a major issue that may hinder motor recovery in many disease states. Additionally, there is significant interconnectivity between sensory and motor systems that may provide avenues for neurotherapeutic intervention, particularly in individuals who cannot participate in standard motor rehabilitation. The knowledge gained in this study of neurotypical responses could be readily adapted to research projects that investigate disrupted sensorimotor processing occurring in brain injury, cerebrovascular accident or congenital anomaly.

CHAPTER TWO: METHODS

Hypotheses

Hypothesis 1:

H_0: The spatiotemporal organization of the cortical and subcortical network of BOLD responses to saltatory pneumotactile inputs presented to the lower face will manifest an underlying, shared neural substrate dedicated to processing moving sensory stimuli.

H_A: The spatiotemporal organization of the cortical and subcortical network of BOLD responses to saltatory pneumotactile inputs presented to the lower face will not manifest an underlying, shared neural substrate dedicated to processing sensory moving stimuli.

Hypothesis 2:

H_0: The spatiotemporal organization of the cortical and subcortical network response to saltatory pneumotactile inputs to the lower face will manifest a differential pattern of BOLD responses as a main effect of velocity.

H_A: The spatiotemporal organization of the cortical and subcortical network response to saltatory pneumotactile inputs to the lower face will not manifest a differential pattern of BOLD responses as a main effect of velocity.

Hypothesis 3:

H_0: The spatiotemporal organization of the cortical and subcortical network response to saltatory pneumotactile inputs to the lower face will manifest a differential pattern of BOLD responses as a function of individual velocities (5cm/s vs. 25cm/s vs. 65cm/s).

H_A: The spatiotemporal organization of cortical and subcortical network response to saltatory pneumotactile inputs to the lower face will not manifest a differential pattern of BOLD responses as a function of individual velocities (5cm/s vs. 25cm/s vs. 65cm/s).

Hypothesis 4:

H_0: The spatiotemporal organization of the cortical and subcortical network of BOLD responses to saltatory pneumotactile inputs presented to the lower face will include activations of neural regions associated with motion perception, processing and planning.

H_A: The spatiotemporal organization of the cortical and subcortical network of BOLD responses to saltatory pneumotactile inputs presented to the lower face will not include activations of neural regions associated with motion perception, processing and planning.

Study Design

Salient Measures

Cortical and subcortical neural activation was quantified by BOLD signal intensity changes based on the HRF function over time. Specifically, regional differences in brain activity (size and distribution) between saltatory pneumotactile velocity presentations were assessed. Regions of shared BOLD activation across velocities (5, 25 and 65 cm/s), and velocity-specific differences in temporal correlation of activation were measured.

Power Analysis

The sample size for this study was based on an *a priori* power analysis using G*Power statistical software (Erdfelder et al., 1996). A sample size of 20 will yield statistical power greater than 0.80 and a medium-large effects size (T-test estimates of voxel BOLD intensity, $p < .05$).

Participants

Participants selected for study were 20 neurotypical adults (15 females), aged 18–30 (mean age=22.3, SD= 1.67), and right-hand dominant per self-report. All participants had no history of chronic illness or scheduled medications, and each was consented in accordance with the University of Nebraska human subjects' institutional review board approval.

Table 2.1 Subject Information

Subject ID	Age	Gender
01	24	Male
02	27	Female
03	26	Female
04	23	Female
05	20	Female
06	23	Female
07	20	Female
08	20	Female
09	23	Female
10	21	Female
11	21	Female
12	21	Female
13	21	Male
14	21	Female
15	24	Male
16	22	Female
17	23	Male
18	24	Female
19	21	Female
20	20	Male
Mean	22.25	
SD	1.67	

Design Overview

In this study, five stimulus conditions (5cm/s, 25cm/s, 65cm/s, 'All-ON,' and 'All-OFF') were presented in a randomized block design. The three velocity settings were randomly combined with an 'All-ON' condition (tactile stimulator cells activated simultaneously at 1 Hz, without the velocity variable) and an 'All-OFF' condition (stimulator cells in place on the skin without pneumotactile input) to allow for statistical comparison of the effect of each velocity, and the main effect of velocity alone. Stimulus

conditions were presented over 20 seconds continuously, and followed by 20 seconds of rest to allow for HRF decay and neurocapillary recovery.

Neuroimaging was performed using a 3T Siemens Skyra MRI scanner fitted with a 32-channel receiving head coil. A single imaging session consisted of an anatomical scan (T1-weighted MPRAGE, 0.9mm isotropic, TE=3.37ms, TR=2400ms) lasting approximately 6 minutes, followed by three functional (BOLD) data sets lasting 13.3 minutes each. The functional image (T2*-weighted EPI) brain volumes consisted of 41 interleaved slices (2.5x2.5x2.5 mm^3, TE=30ms, TR=2500ms) with a 220mm field of view oriented to include orofacial sensorimotor cortex and cerebellum.

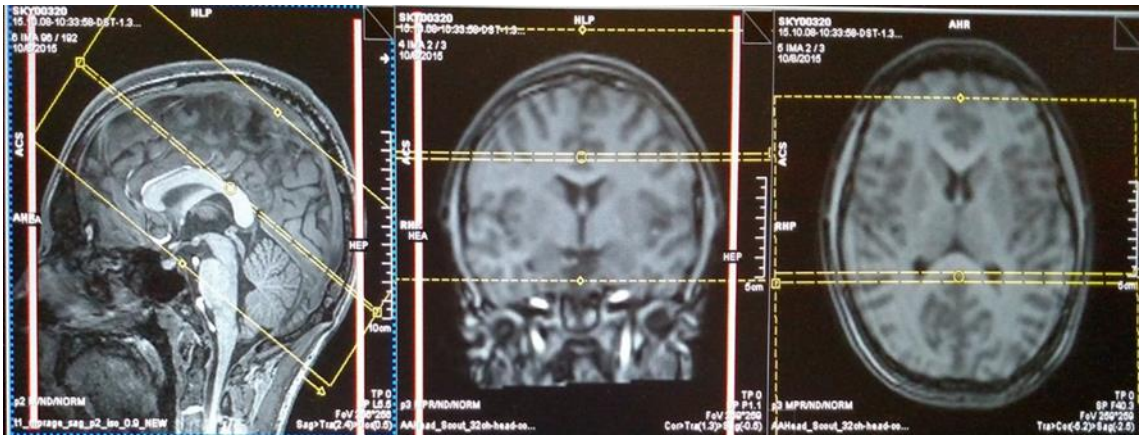

Figure 2.1 MRI field of view orientation

In each BOLD acquisition, 8 brain volumes were recorded every 20 seconds (8 volumes during the 20s block of velocity stimulation, 8 volumes during the following 20s recovery block of no stimulation), for a total of 330 volumes collected per BOLD [8 volumes x 2.5s (TR) x 40s (20s stimulation/20s no stimulation) blocks = 800 seconds, or

13.3 minutes]. Thus the full scan time averaged about 46 minutes (MPRAGE + 3 BOLDs). During scanning, participants were asked to lie quietly without motion, and watch for the E-Prime coded visual stimulus (numeric countdown) described in following sections.

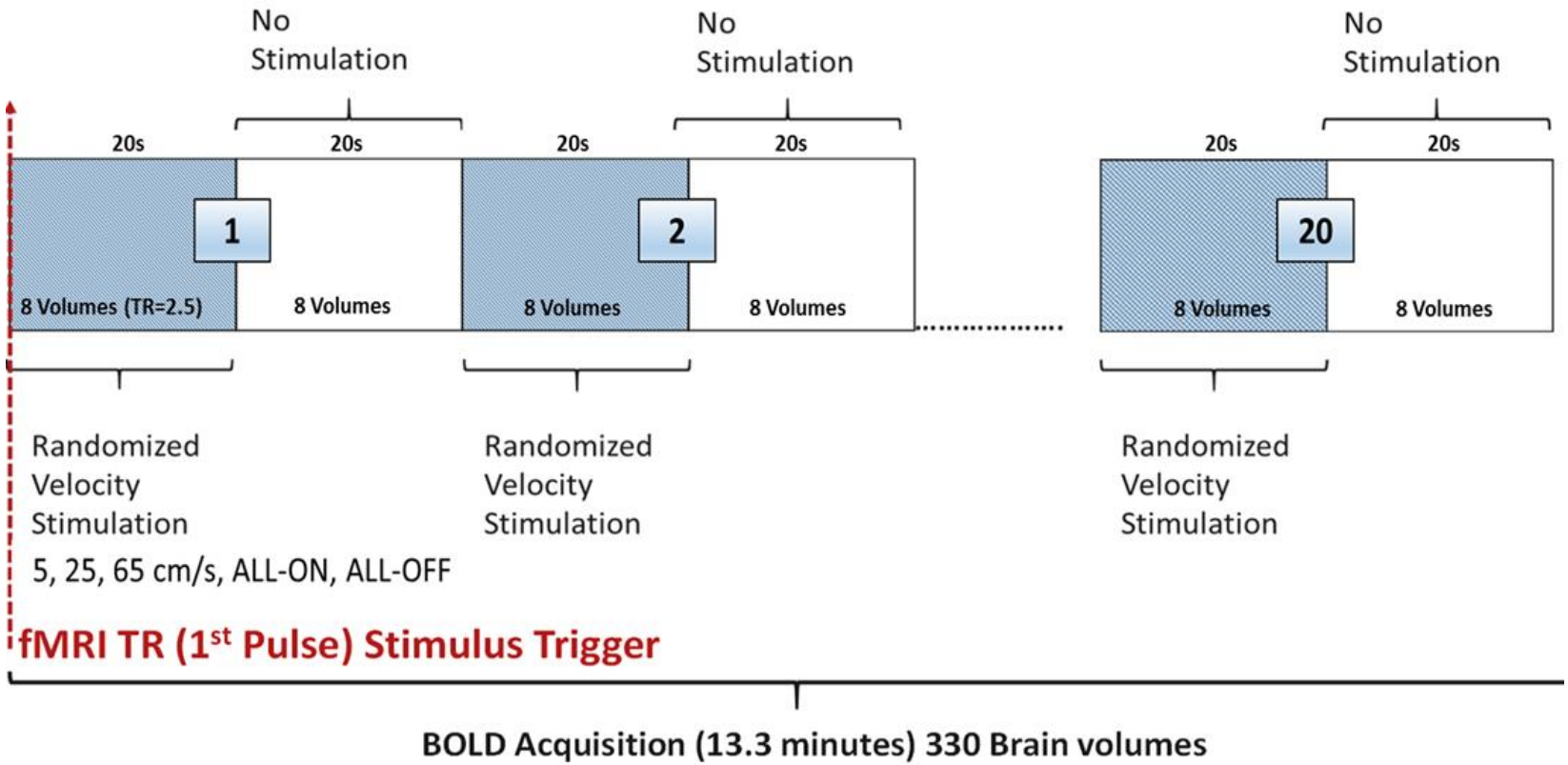

Figure 2.2 Randomized block design for stimulus presentation and scan acquisition.

The somatosensory stimulation array used for this protocol consisted of 7 small, pneumatic capsules that were adhered to the hairy skin of the right lower face. Each capsule (TAC-Cell) was machined from Delrin® acetal thermoplastic [6 mm inside diameter, 15 mm outside diameter, 6 mm height. The top of each cell was ported to a barb-fitting which was connected to a 5.18 meter, (1.6 mm internal diameter) polyurethane and silicone rubber pneumatic line attached to the Galileo tactile stimulation generator. The flanged surface of each cell was secured to the skin using double adhesive tape collars following skin preparation with tincture of benzoin to improve adhesion.

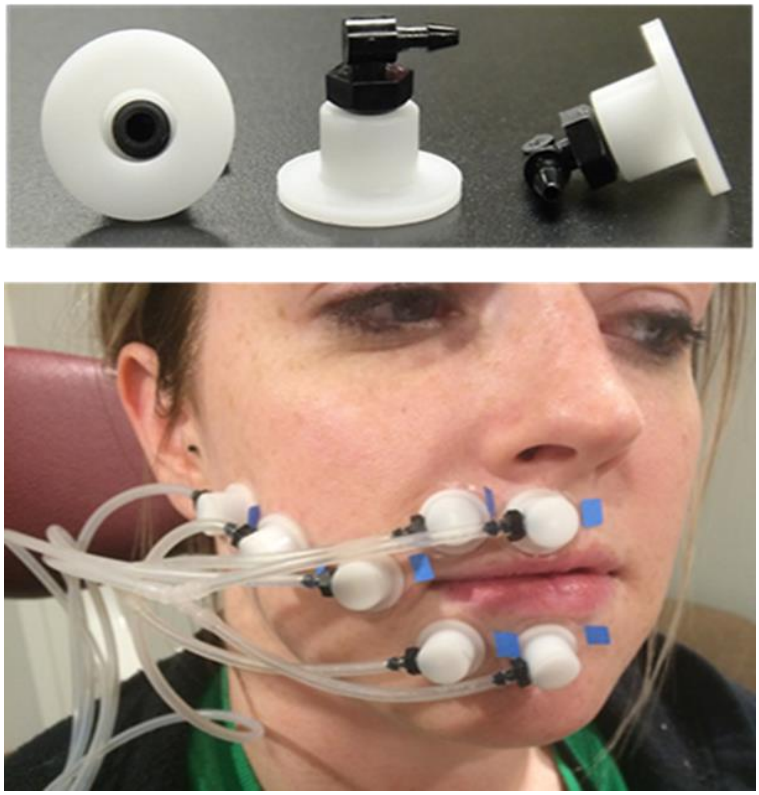

Figure 2.3 Pneumatic cells and array configuration

The first two pairs of cells in the array [channel 1 (red) = the top cell placed at the philtral column, and the cell directly inferior to it below the lower lip; channel 2 (orange) = the next lateral cell over, and the cell directly inferior to it below the lower lip] were adjoined with bifurcated tubing to allow for synchronous activation.

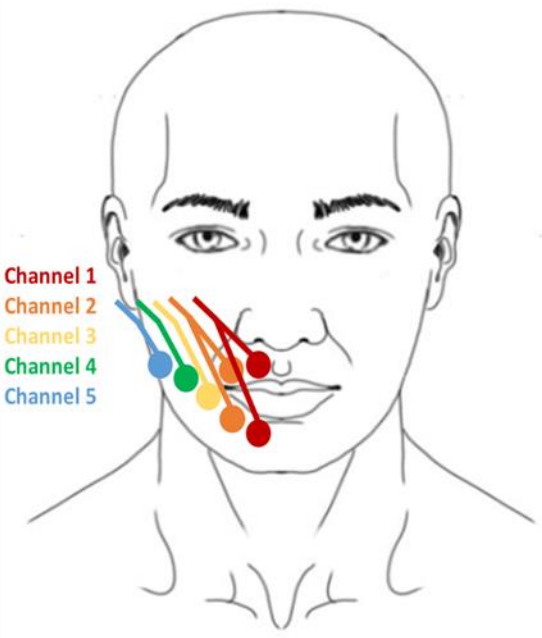

Figure 2.4 Arrangement of pneumatic cells and feed lines. Note channels 1 and 2 are configured as paired TAC-Cells, using a bifurcated Y-manifold to achieve synchronous activation.

Pneumotactile velocity stimuli were delivered to the facial skin by a multichannel pneumatic amplifier (the Galileo Somatosensory™, Epic Medical Concepts &

Innovations, Shawnee Mission, KS), which was programmed to generate saltatory biphasic pulses [duration=60 ms, 10 ms rise-fall time (10 -90% intercepts), biphasic amplitude from -50 to 140 cmH_2O].

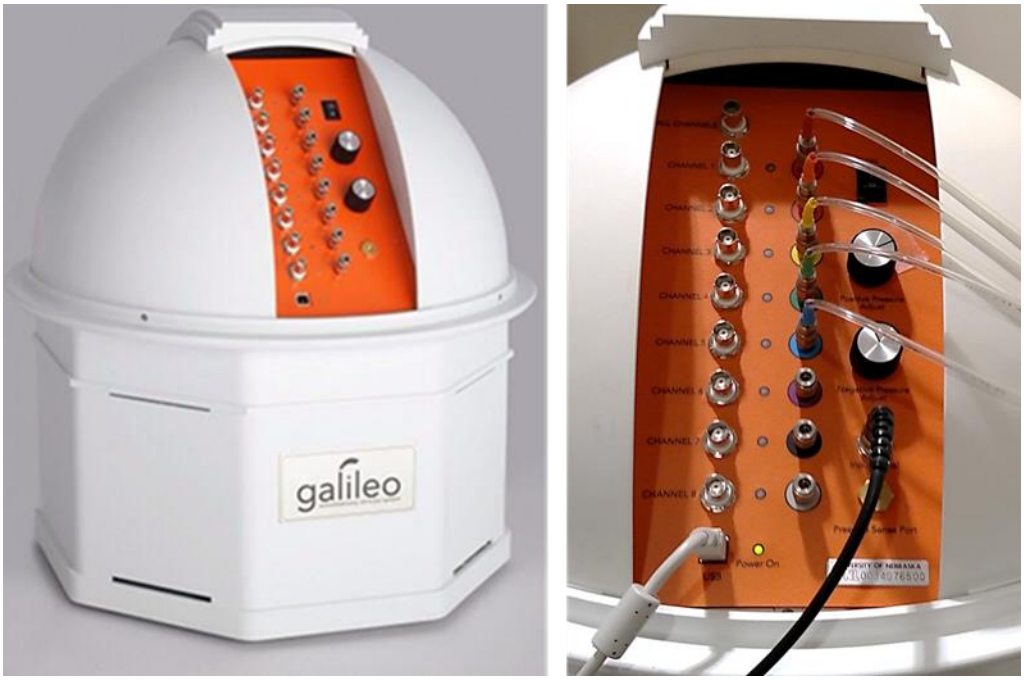

Figure 2.5 The Galileo Somatosensory stimulator with magnified view of hardware interface panel.

Pneumotactile Velocity Stimulus Control and Software

A laptop (MS WIN8.1) ran the graphical user interface to control the Galileo via a USB port for sequential activation of output channels 1 through 5 with a custom-written saltatory velocity program coded in *.xml (Appendix A) individualized to each

participant based on perioral morphometrics. After consent and a verbal description of the paradigm, pneumatic cells were aligned on the participant from the right philtral column to the right (buccal) face. Once in place, the array length was calculated based on the distance between cells (each length measured from the center of one cell to center of the next). Because of bifurcation of the first two channels, *both* the upper and lower cells of those channels were considered 'first' and 'second' in the array. The measurement values of array length were used to designate on/off times for velocity sequences (traverse speed in cm/s). Thus, velocity protocols were consistent across all participants, regardless of orofacial size (Appendix B).

The programmed on/off times produced a pneumotactile 'saltatory' (jumping) stimulation that traversed the skin in a repeating medial-to-lateral direction at three velocities (5cm/s, 25 cm/s, 65 cm/s) and also provided the 'All-ON' and 'All-OFF' conditions.

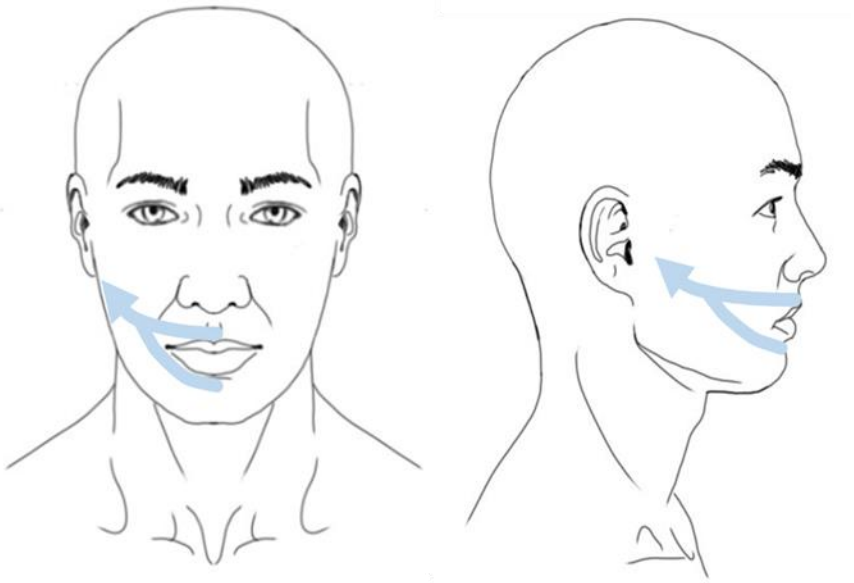

Figure 2.6 Sequential activation pattern of pneumatic stimulator cells. Blue arrow indicates direction of saltatory pneumatic activation.

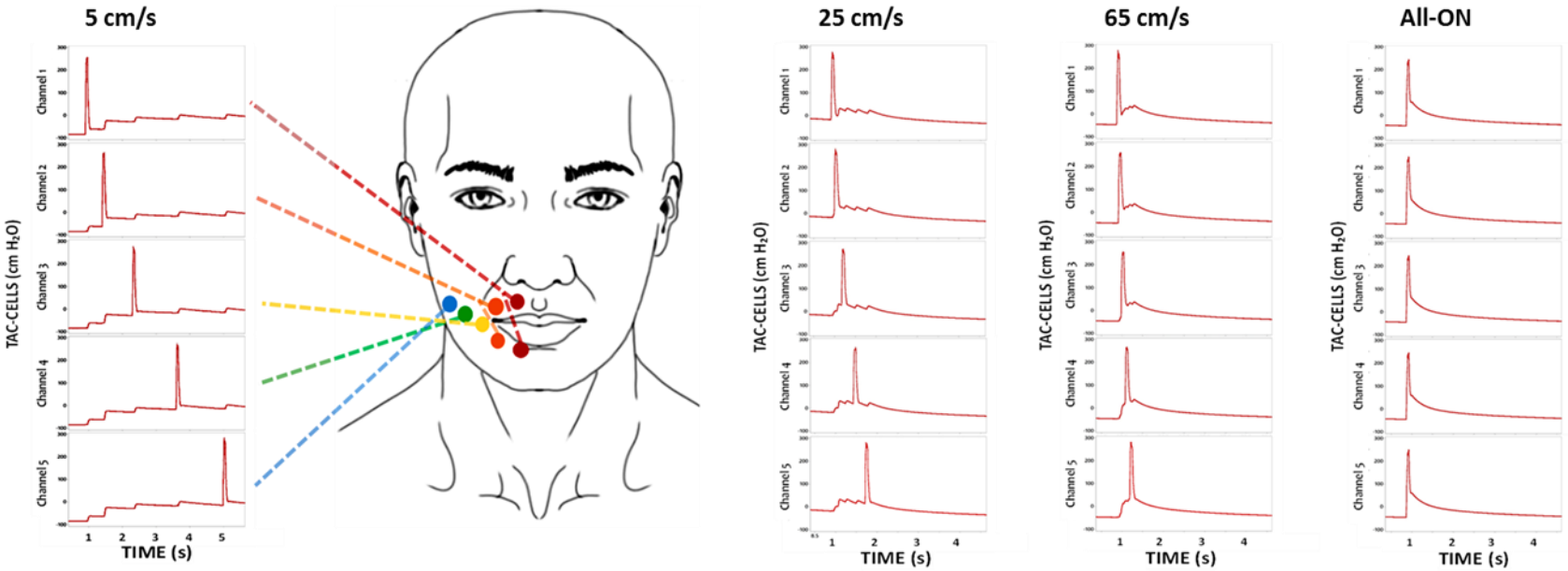

Figure 2.7 Stimulus velocity pressure waveforms. Programmed time delays between pressure pulses at each cell resulted in 5 stimulus conditions: 5 cm/s, 25cm/s, 65 cm/s, and All-ON synchronous activation. The All-OFF condition is not shown as pressure waveforms would be at baseline.

Neuroimaging Data Acquisition and Stimulus Co-Registration

A single imaging session started with the 6-minute anatomical MPRAGE scan, during which participants lay quietly with the TAC-Cell array on the facial skin, but no active stimulus was provided.

Figure 2.8 Participant preparation for data acquisition. The TAC-Cell array is positioned on the lower face prior to placement of the 32-channel head coil.

During functional image acquisition, the program of saltatory pneumotactile stimulus generation was synchronized to the Siemens scanner using the first optical TR TTL pulse from the NetStation control box. The first TR pulse at the onset of each BOLD acquisition was input to a Berkeley Nucleonics (Model 645) programmable pulse generator connected to the Galileo stimulator, and also simultaneously activated the visual countdown of the E-Prime paradigm described in the next section. In order for the Galileo to initiate the velocity sequence, the TR signal was inverted to change the TTL logic (5V to 0V) by the pulse generator into signal that could be recognized by the Galileo software. The BNC pulse generator also served as a timing mechanism via external trigger for the velocity sequences, providing a single pulse to the Galileo stimulator every 40 seconds. Thus, the Galileo would present a velocity condition for 20 seconds, then wait for the external trigger to initiate the next random velocity sequence at 40s, providing a 20s 'off' condition between velocity blocks to permit HRF decay. Each velocity protocol (5 cm/s, 25 cm/s 65 cm/s, All-ON, All-OFF) was randomly presented and repeated 4 times (5 conditions (20s on/20s off) x 4 = 800s = 13.3 minutes).

Three 13.3 minute BOLD acquisitions were obtained in succession, allowing participants 1-2 minutes between acquisitions to move about as needed and allow for a quick check of the integrity and adherence of the TAC-Cell array. For each BOLD acquisition, only the initial TR pulse was used to start E-Prime, and trigger the full 13.3 minute stimulus sequence that was preprogrammed into the Berkeley Nucleonics arbitrary function generator to time the 20 blocks of saltatory cutaneous stimulation produced by the Galileo.

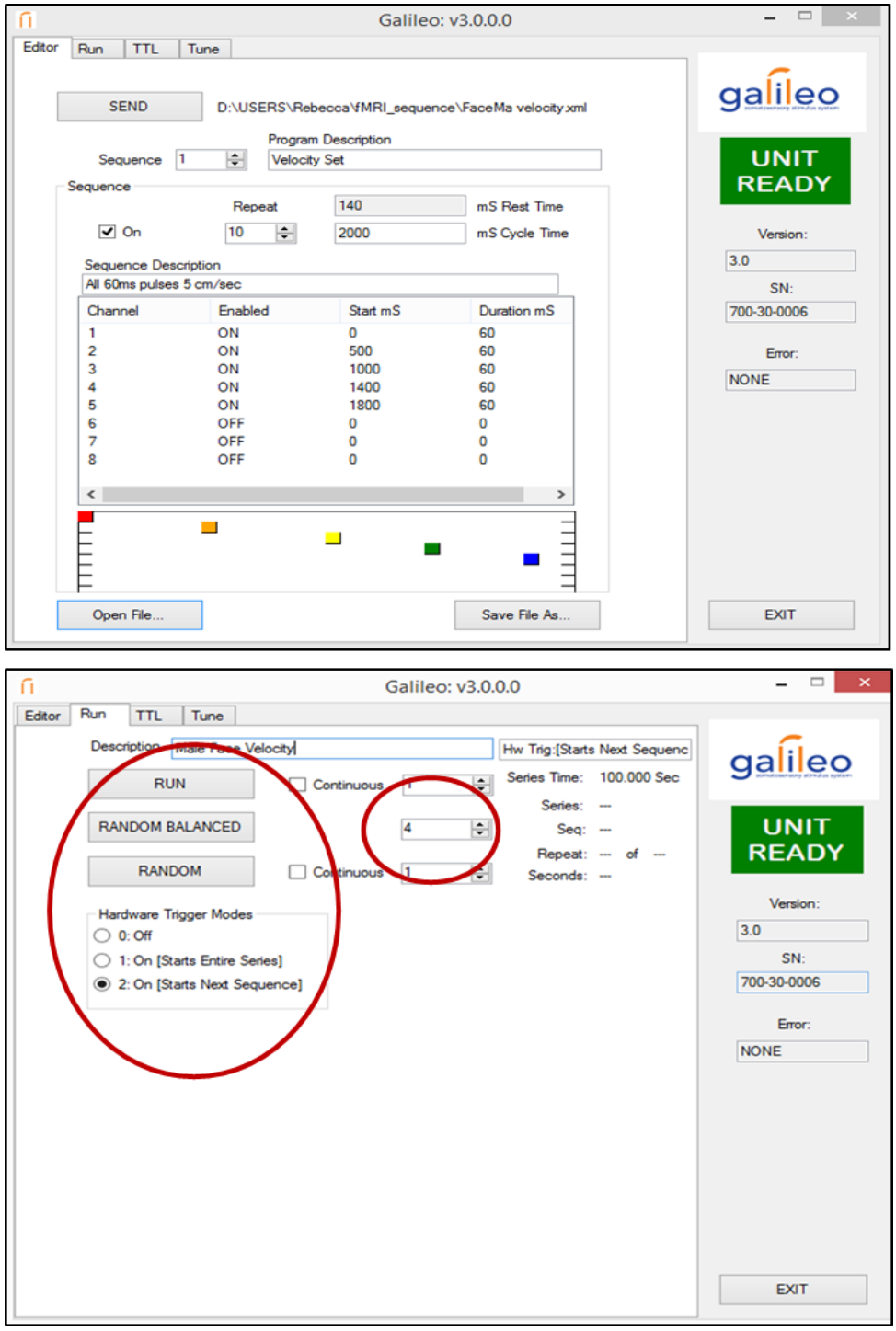

Figure 2.9 Software screenshot for Galileo control of velocity stimulus. Loaded velocity .xml files of 5 conditions (20s each) were presented randomly, repeated 4 times, and set to wait for external hardware trigger.

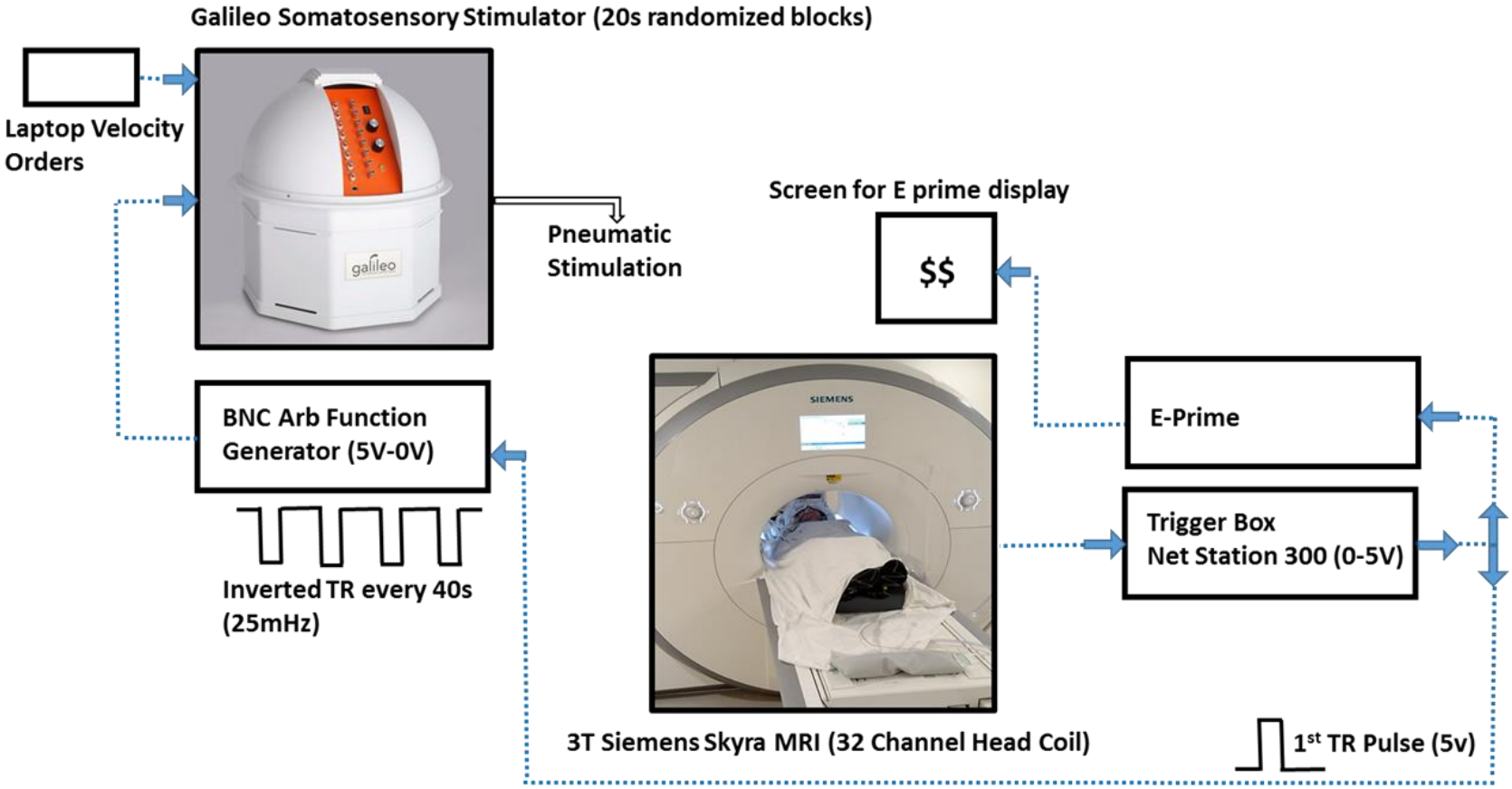

Figure 2.10 Data acquisition and stimulus configuration

E-Prime

To help maintain participant vigilance, during saltatory facial cutaneous stimulus presentation, a visual countdown image was projected briefly in the participants' field of view using E-Prime® (v2.0 Professional, Science Plus Group, Netherlands) software. The countdown also provided the participant with a means of knowing approximately how much time remained in each BOLD acquisition.

The visual countdown ran through the numbers 1-20 serially, with each number cue presented every 40 seconds, corresponding to the completion of each 20s stimulation/20s no stimulation block. To avoid fixation on the screen that might cause visual stimulation and activity in visual processing areas, number presentations were brief, lasting 500ms. As an additional incentive to promote vigilance, '$$' symbols were inserted randomly into the countdown, and participants were asked to keep track of how many dollar symbols they saw, and report that amount to the researcher at the end of each BOLD acquisition.

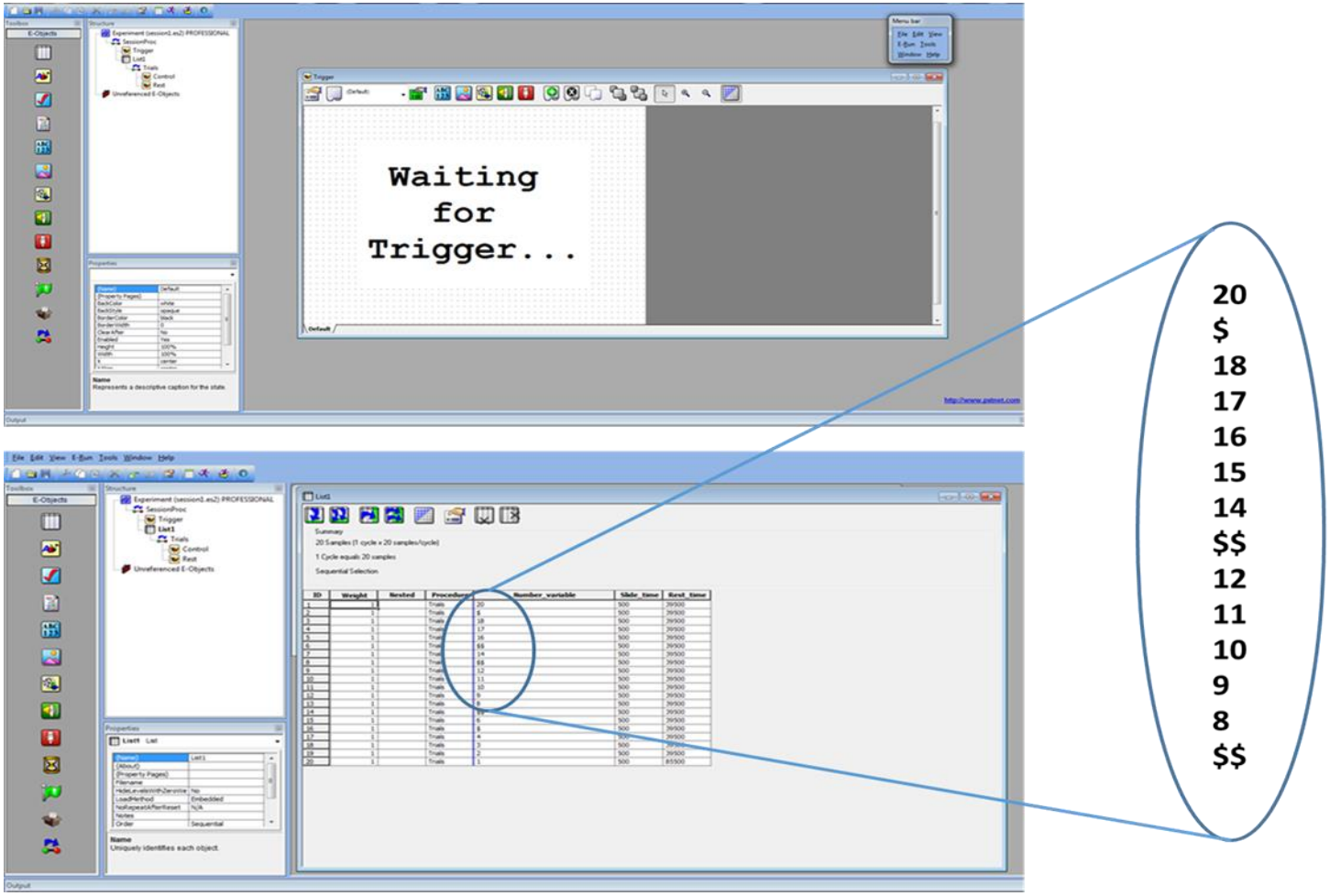

Figure 2.11 E-Prime screen shots. Image shows initiation screen waiting for the Siemens scanner first optical TR TTL pulse, and the visual countdown seen by participants.

Neuroimaging Data Analysis: Primary Matrix Build

Analysis of the fMRI data was conducted using a general linear model (GLM) to examine regions of cortical and subcortical activation associated with the main effect of velocity. In standard GLM fMRI analysis, signal from the contrast (predictor) condition and signal from a baseline condition are averaged independently, then compared to determine significant differences. The amount of difference between conditions is computed per voxel, and the full image volume is presented as a statistical parametric map (SPM) which is colored according to pre-set threshold criterion. For this experimental paradigm, one-sample t-tests ($P_{unc} < 0.001$) of contrast parameter estimates per voxel (dependent variable) were used to determine the overall pattern and spatial extent of BOLD activation in the presence of moving tactile stimulation presented over five conditions.

A priori ROI of putative facial sensorimotor regions [cortex (SI, SII, MI, SMA, PPC, insula), and cerebellum] were selected based on findings from recent literature (Lin et al., 2010; Grabski et al., 2012; Kedarnath & Shruthi, 2015; Rocchi et al., 2016; Jiang et al., 2016).

Raw (DICOM) files from the Siemens scanner were imported into SPM12 (Statistical Parametric Mapping, v12, FIL Methods Group, 1991) fMRI image processing software. Images were pre-processed [motion corrected, co-registered with the anatomical MPRAGE, segmented by tissue type, normalized to Montreal Neurological Institute (MNI) space, and smoothed using an isotropic Gaussian kernel (FWHM = 8mm)]. Once pre-processed, a design matrix was created for assessment with GLM.

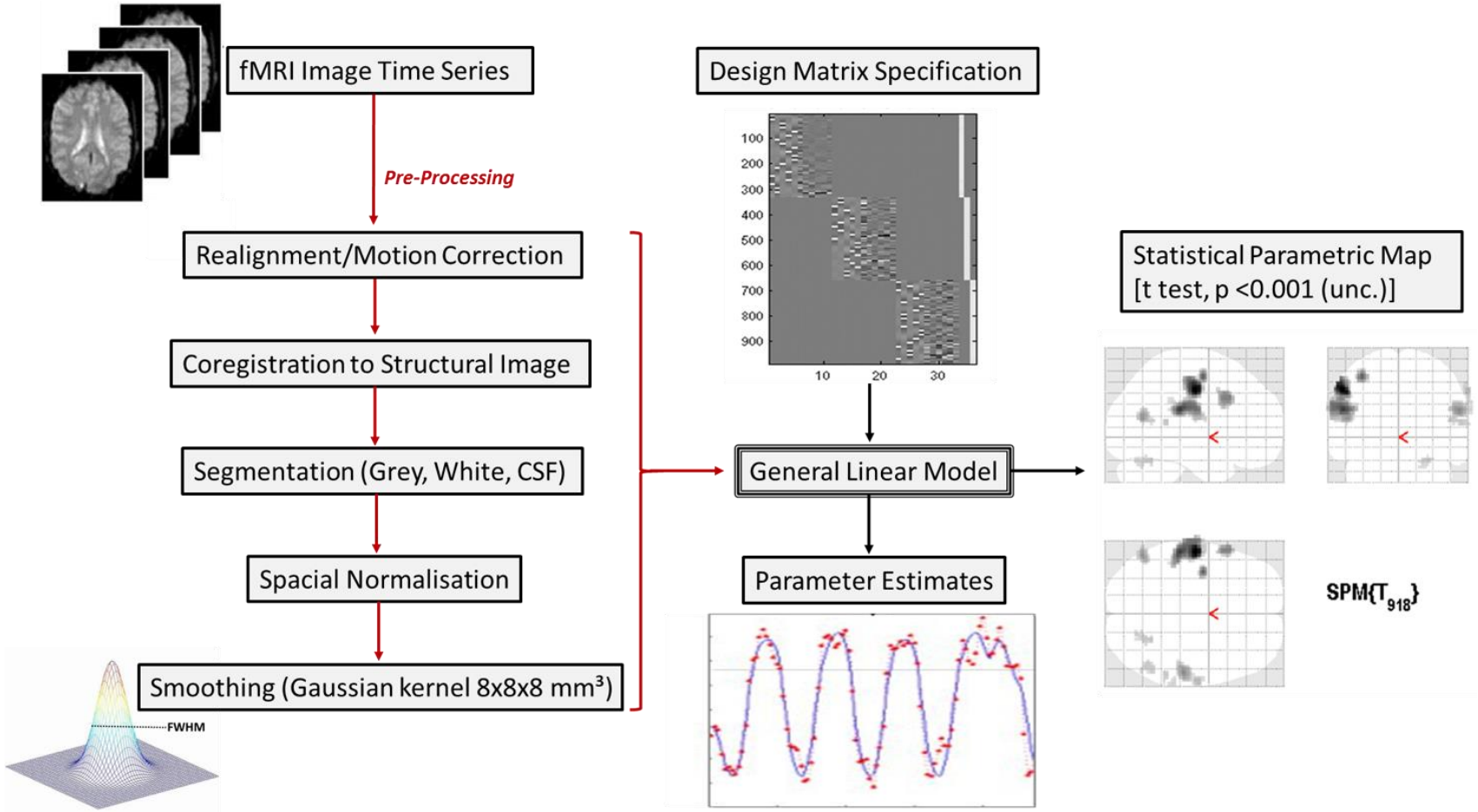

Figure 2.12 SPM12 GLM data pre-processing stream and parametric map

In matrix construction for general linear modeling of BOLD/HRF data, the time course of an individual voxel can be represented by the equation: $Y=X\beta+E$, where Y is the time dependent data per voxel, X is the design matrix that defines experimental contrast, β represents the unknown weights of independent variable(s) in the matrix and their statistical association with Y, and E is residual variance or error (Friston et al., 1994; Beckmann et al., 2003; Monti, 2011). In our paradigm, the set of specified explanatory conditions (5cm/s, 25cm/s, 65cm/s, 'All-ON,' and 'All-OFF') formed the design matrix for the experimental model. First-level specification in SPM (single-subject) was used to build each velocity condition, then the three BOLD data acquisition sessions for each participant were pooled using the FFX (fixed effects, group modeling) estimate function.

A standard box-car method was used to create the analysis matrix for the initial single-subject processing stream, where a value of '1' at a set time point modeled a condition of 'on,' with '0' at all other time points. Time points for the velocity 'on' conditions were obtained from the Galileo output files (Appendix C), and entered into the SPM matrix for each BOLD data set prior to collapse.

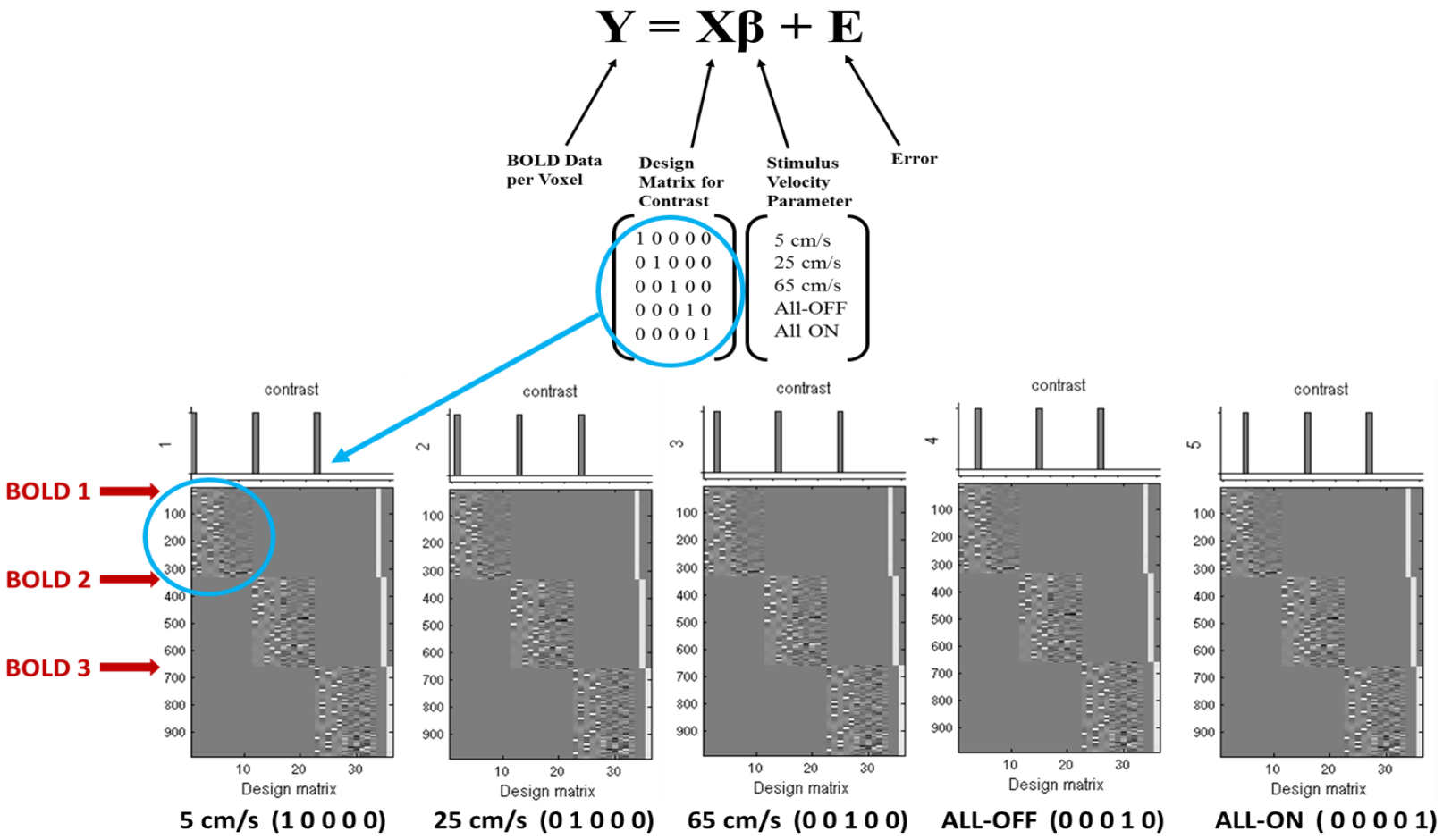

Figure 2.13 GLM model equation with first-level box-car matrix used to set velocity conditions

Neuroimaging Data Analysis: Single Subject by Condition

As a first step to assess *individual* subjects' BOLD response as function of each condition (5 cm/s. 25 cm/s, 65 cm/s, ALL-ON, ALL-OFF), one-sample t-tests ($P_{unc} < 0.001$) of contrast parameter estimates per voxel permitted an overview of the pattern and spatial extent of BOLD activation. The statistical aim of this first-level analysis was to determine the degree of contribution each predictor condition had on the observed values of the dependent variable (Y), and if each scaling parameter (β) was significantly different from zero. The ALL-ON and ALL-OFF conditions were then used in subsequent group analyses (following sections) as comparative baseline conditions for velocity (5, 25, 65 cm/s) estimates.

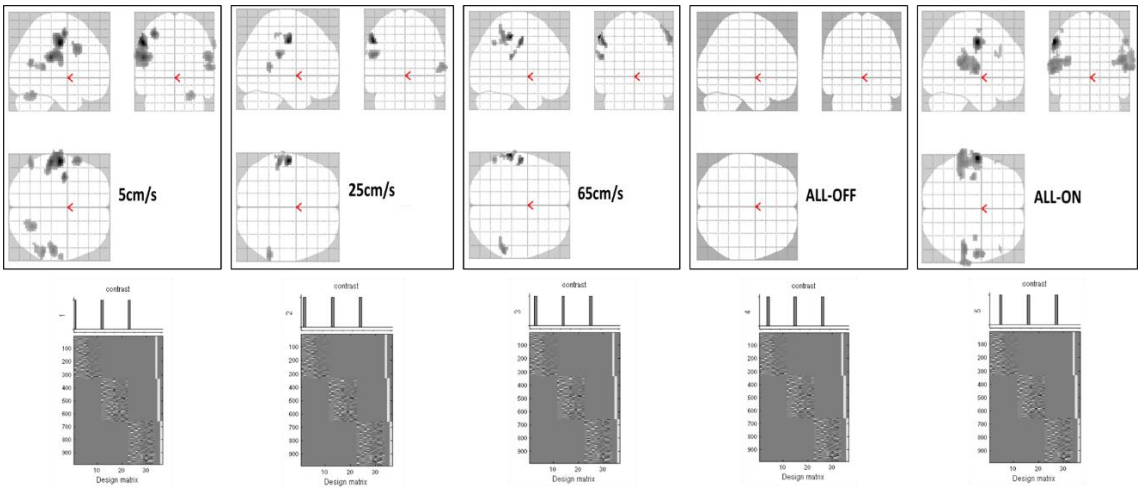

Figure 2.14 Contrast parameter estimates for a single representative subject (01) by condition (first-level)

Neuroimaging Data Analysis: Group Main Effect of Velocity

Group (second-level) analysis, was first performed using a multi-subject matrix constructed using a One-Way ANOVA within-subjects design (F statistic, $P_{unc} < 0.0001$), to estimate the *main effect of velocity*. The matrix incorporated pooled BOLD data from all 20 subjects, where each velocity (5, 25, or 65 cm/s) was contrasted against a control condition (ALL-OFF or ALL-ON). All 'velocity vs. control' conditions were then *combined* into a single ANOVA matrix to show an overall main effect.

In the case of this omnibus test, a box-car matrix was built in which a value of '1' indicated each velocity versus control (5cm/s > ALL-OFF or ALL-ON, 25cm/s > ALL-OFF or ALL-ON, 65 cm/s > ALL-OFF or ALL-ON), and a value of '-1' or '0' was used for other conditions. The resultant BOLD signal transformation resulted in contrast maps representing the individual β weights of all participants against the control condition.

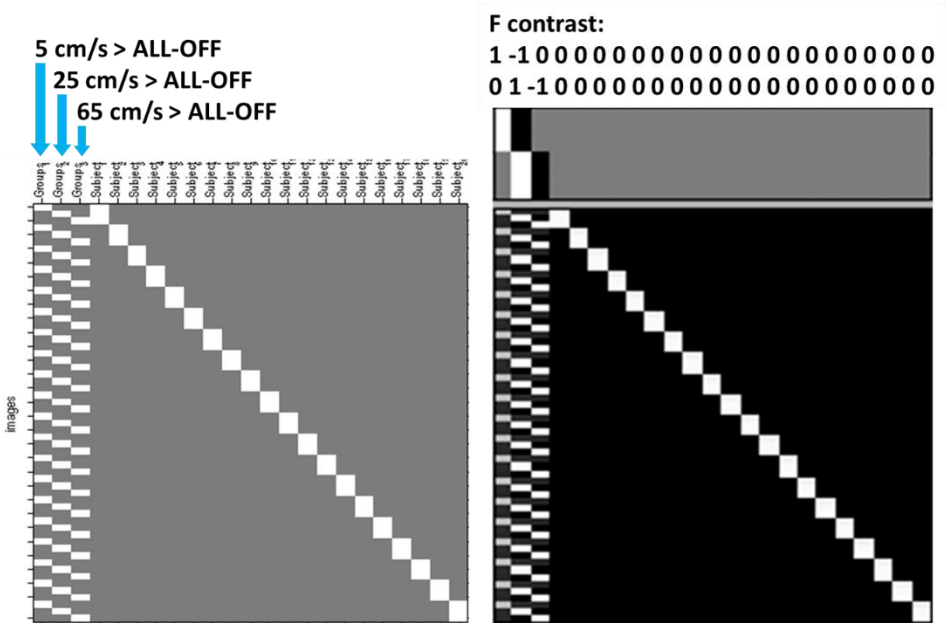

Figure 2.15 Design matrix for group main effect of velocity (second-level).

Neuroimaging Data Analysis: Group Velocities Compared to Control Conditions

For the second step in group analysis, one-sample t-tests ($P_{unc} < 0.001$) were constructed to evaluate the change in BOLD signal associated with *individual velocities* (5, 25, 65 cm/s) when compared to the two control (ALL-OFF, ALL-ON) conditions.

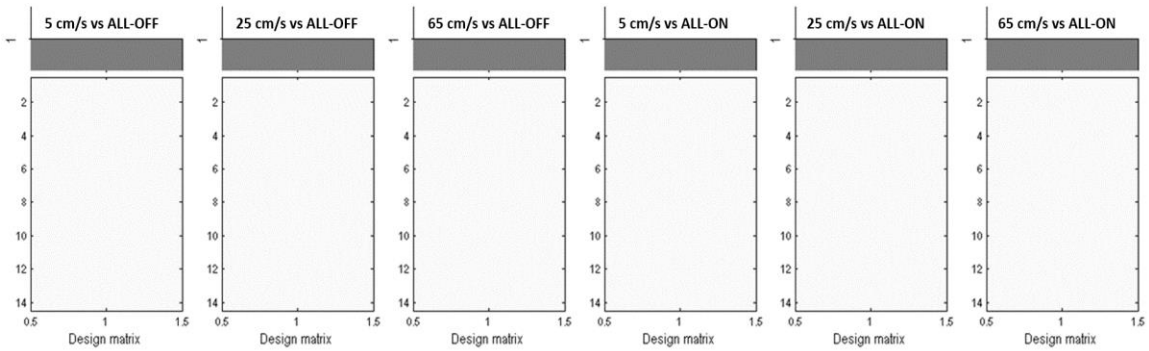

Figure 2.16 Design matrix for group; velocities compared to baseline (second-level t-test).

The statistical aim of this second-level analysis was to determine the degree of contribution each predictor condition had on the observed values of the dependent variable (Y), and if each scaling parameter (β) was significantly different from the *control condition* (ALL-OFF, ALL-ON). In these velocity comparisons, map-wise level of significance was set at an uncorrected value ($p < 0.001$) which was equivalent to $t > 3.10$, with a minimum cluster size (k) of 10 voxels.

CHAPTER THREE: RESULTS

A total of N=20 individuals participated in this preliminary study and were included in the data sample. Three BOLD acquisitions were used in analysis for each participant with the exception of participants 06 and 13 who had only two complete BOLD acquisitions recorded (06 became claustrophobic, and 13 scanning was stopped due to a temporary software glitch).

Neuroimaging Results: Single Subject

Single Subject by Condition: Cortical Activation

The GLM single subject findings pooled across three BOLD acquisitions (first-level analysis) is depicted below in the SPM parametric brain maps in Figures 3.1 (coronal view) and 3.2 (axial view). The BOLD/HRF response shown in the colored regions represents areas that were active above the $P_{unc} < 0.001$ threshold during the five stimulus conditions (5 cm/s, 25cm/s, 65 cm/s, ALL-ON, ALL-OFF).

The overall analysis of activity in these images showed consistent regions of activation across subjects which included *a priori* ROI of facial sensorimotor regions [cortex (SI, SII, MI, SMA, PPC, insula), and cerebellum], with the greatest extent of regional HRF activation seen at the lowest, 5 cm/s velocity. Interestingly, the spatial extent and location of activation varied consistently by velocity in all subjects, with a notable decrease in activation extent as stimulus velocity increased.

In nineteen of the participants, *bilateral* S1 and insular BOLD response was noted, especially during the two slower velocity presentations (5, 25 cm/s). The spatial extent and organization of BOLD signal ipsilateral to the stimulus was also appreciably modulated by condition, with changes in HRF associated closely with changes in velocity.

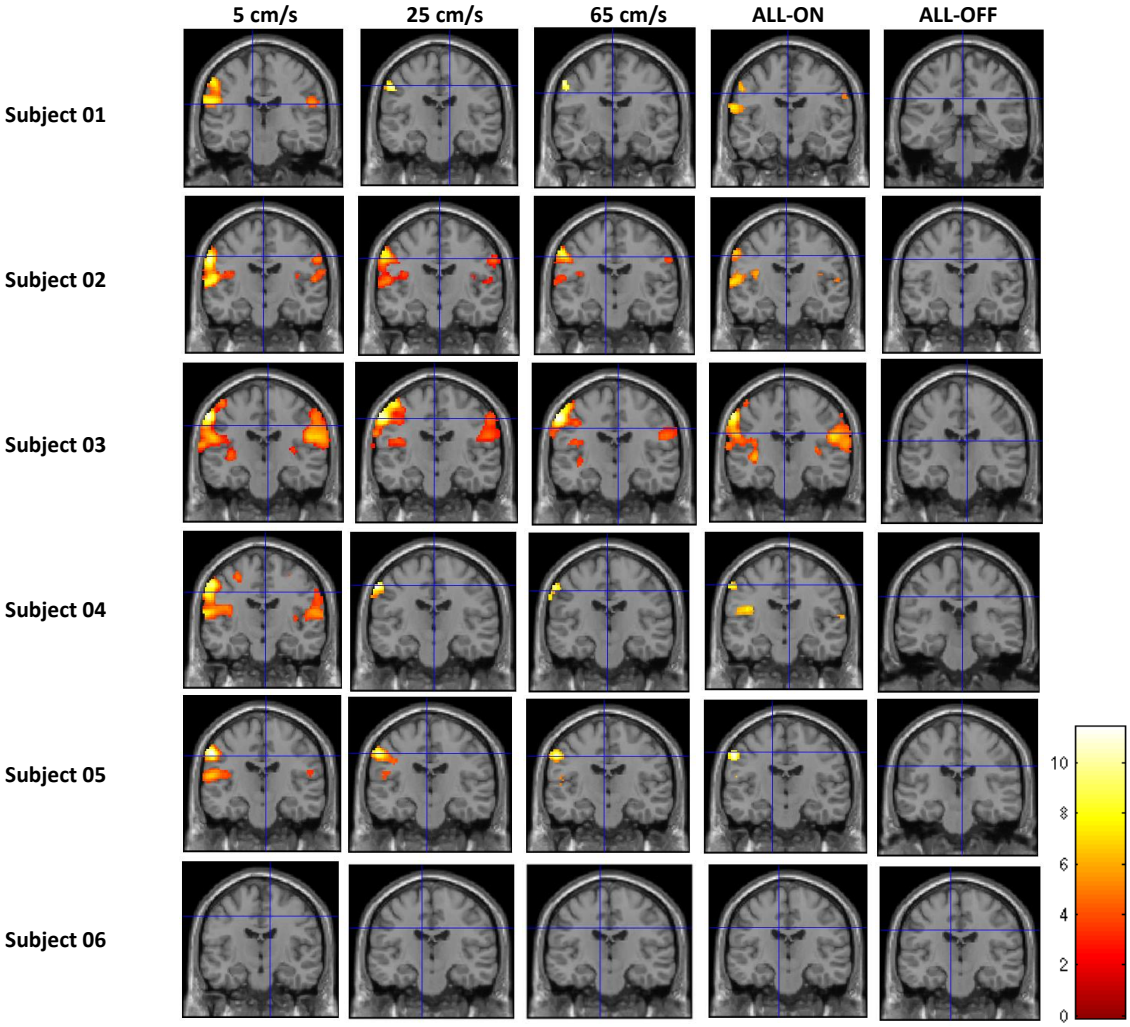

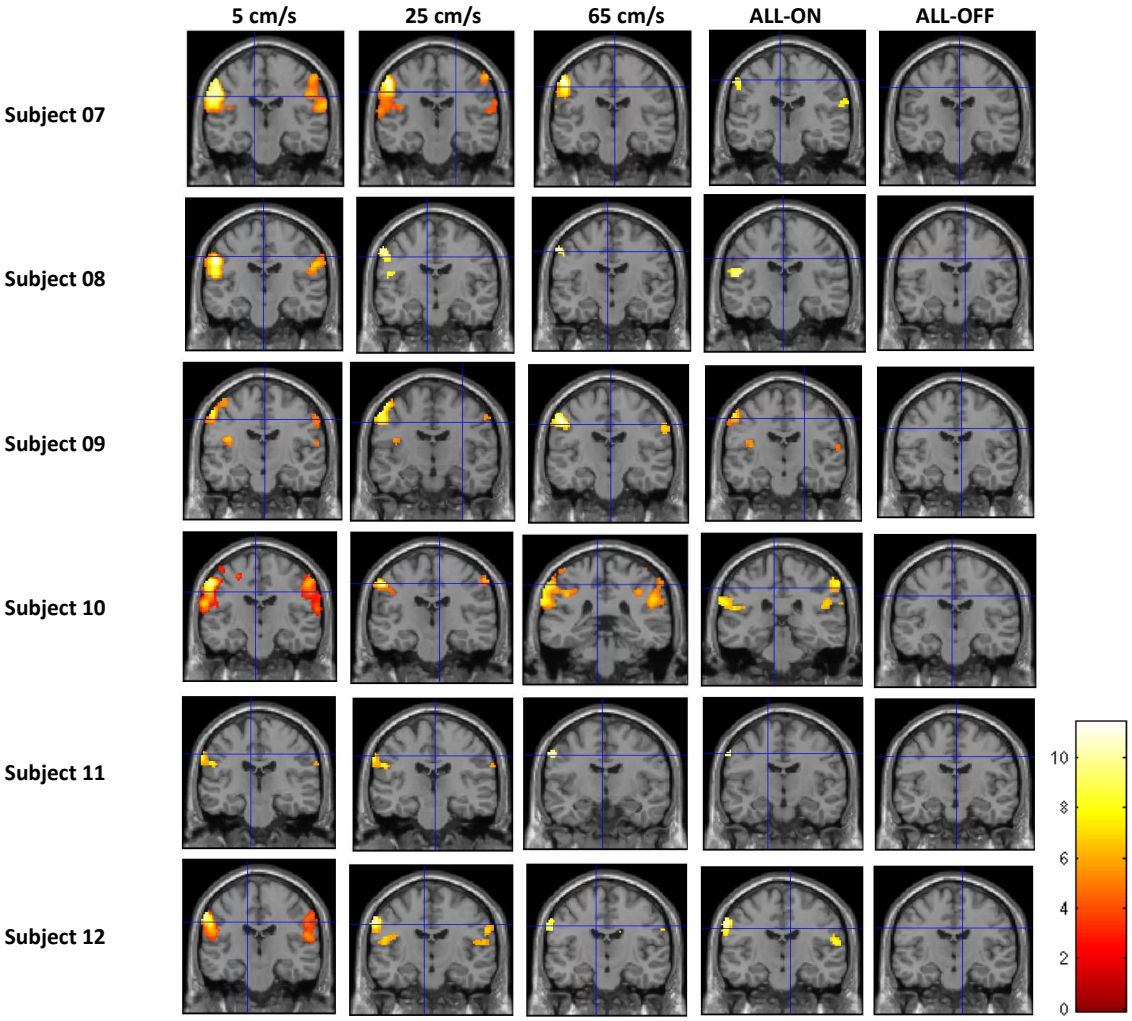
5 cm/s
25 cm/s
65 cm/s
ALL-ON
ALL-OFF
Subject 07
Subject 08
Subject 09
Subject 10
Subject 11
Subject 12
10
8
6
4
2
0

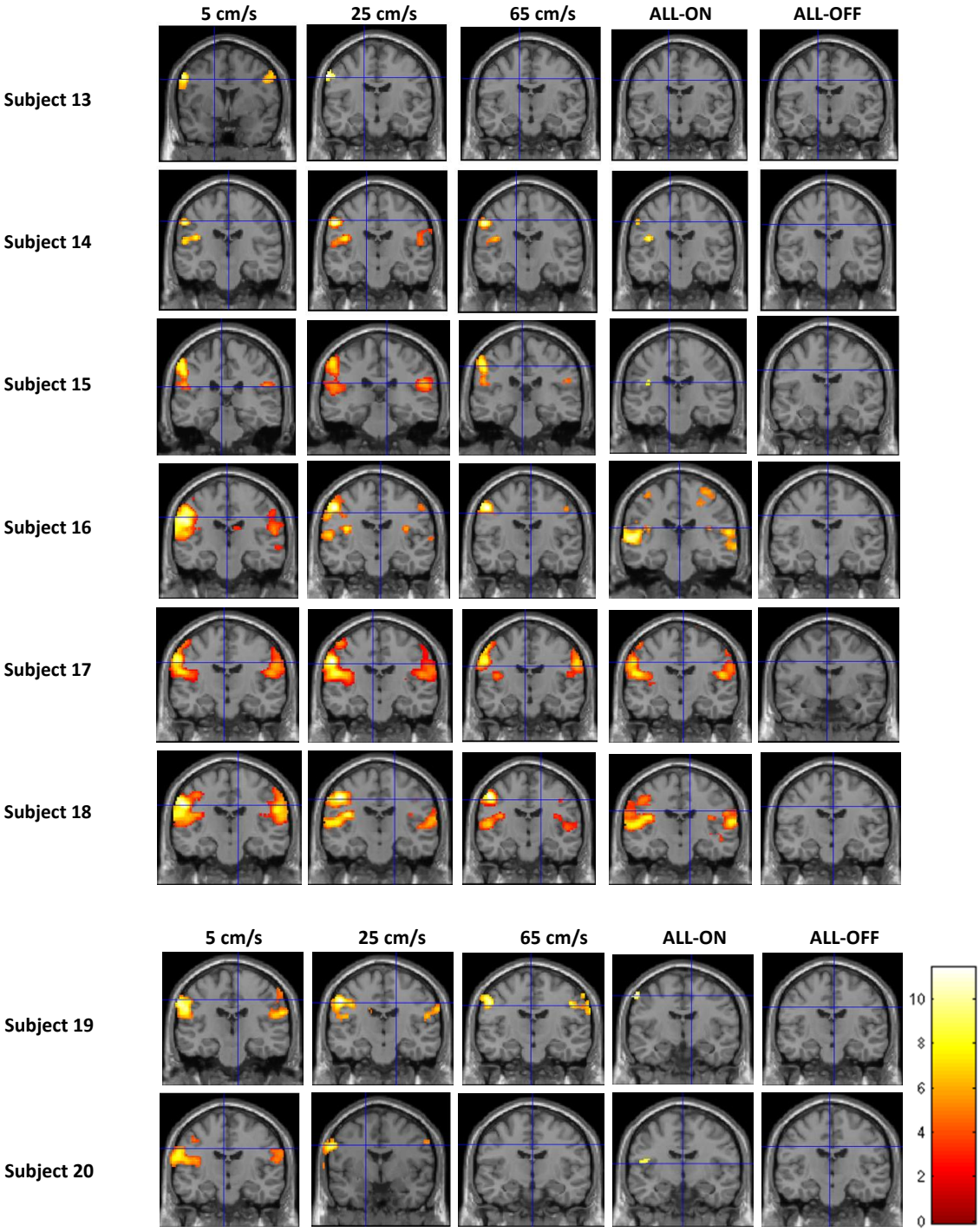

Figure 3.1 Single subject (first-level) cortical BOLD activations by condition (coronal view).

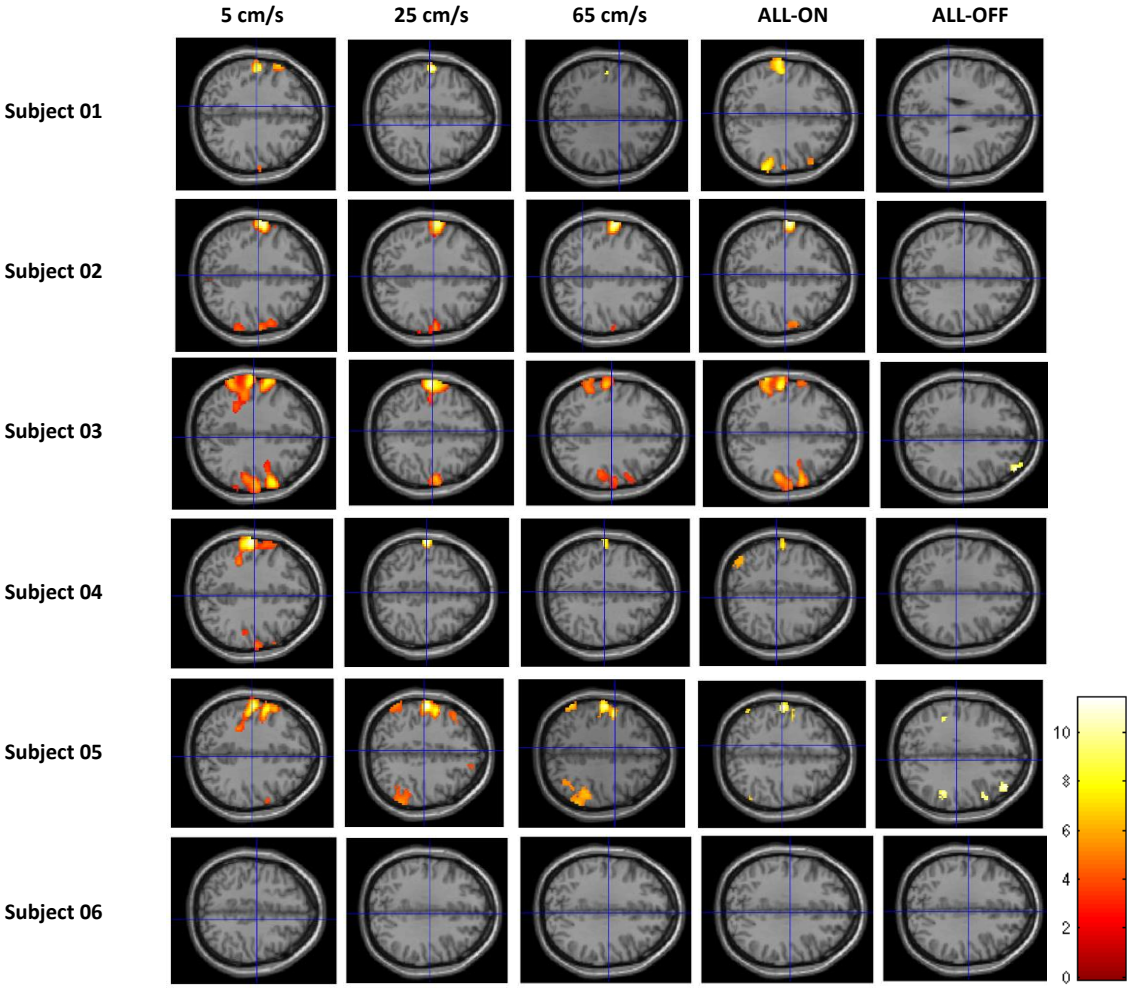
5 cm/s
25 cm/s
65 cm/s
ALL-ON
ALL-OFF
Subject 01
Subject 02
Subject 03
Subject 04
Subject 05
Subject 06
10
8
6
4
2
0

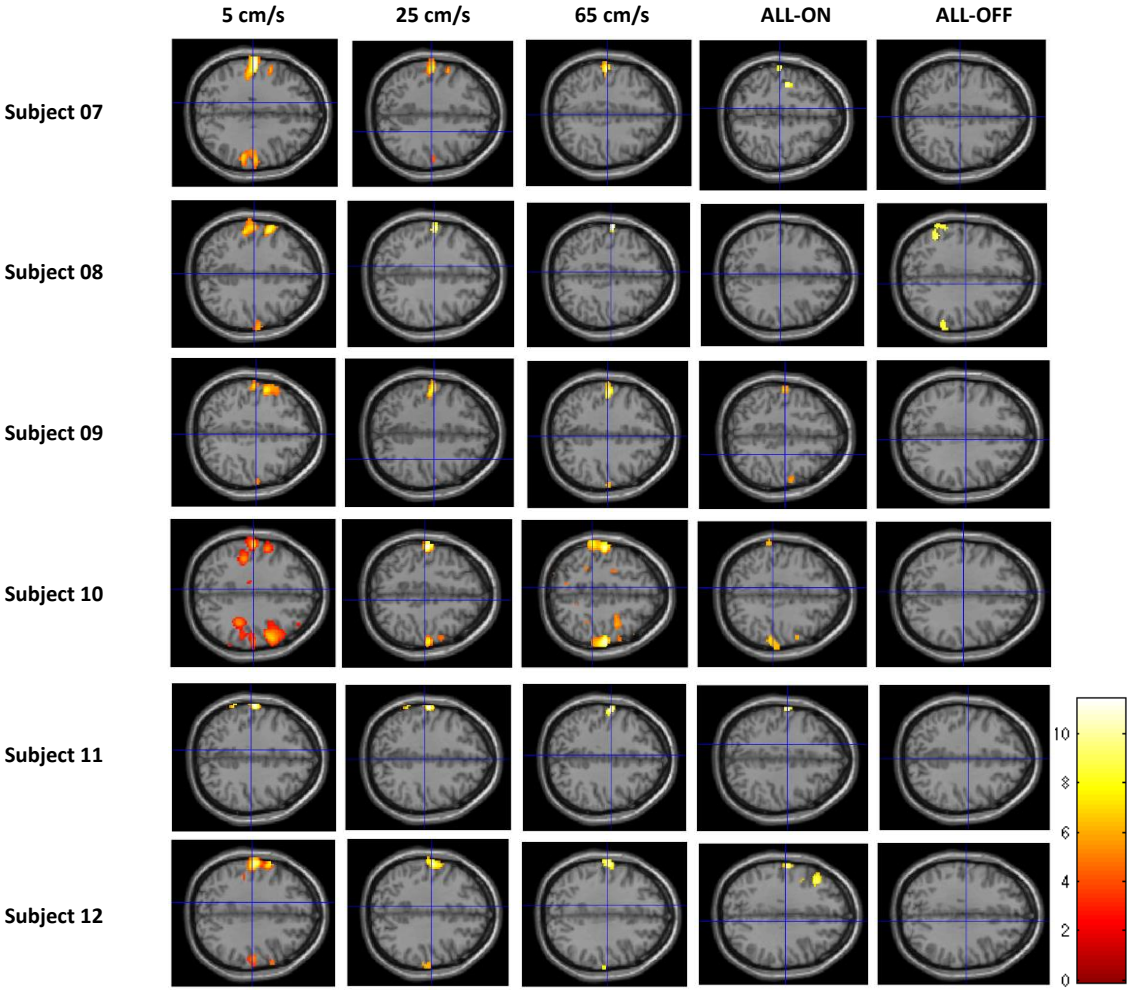
5 cm/s
25 cm/s
65 cm/s
ALL-ON
ALL-OFF
Subject 07
Subject 08
Subject 09
Subject 10
Subject 11
Subject 12
10
8
6
4
2
0

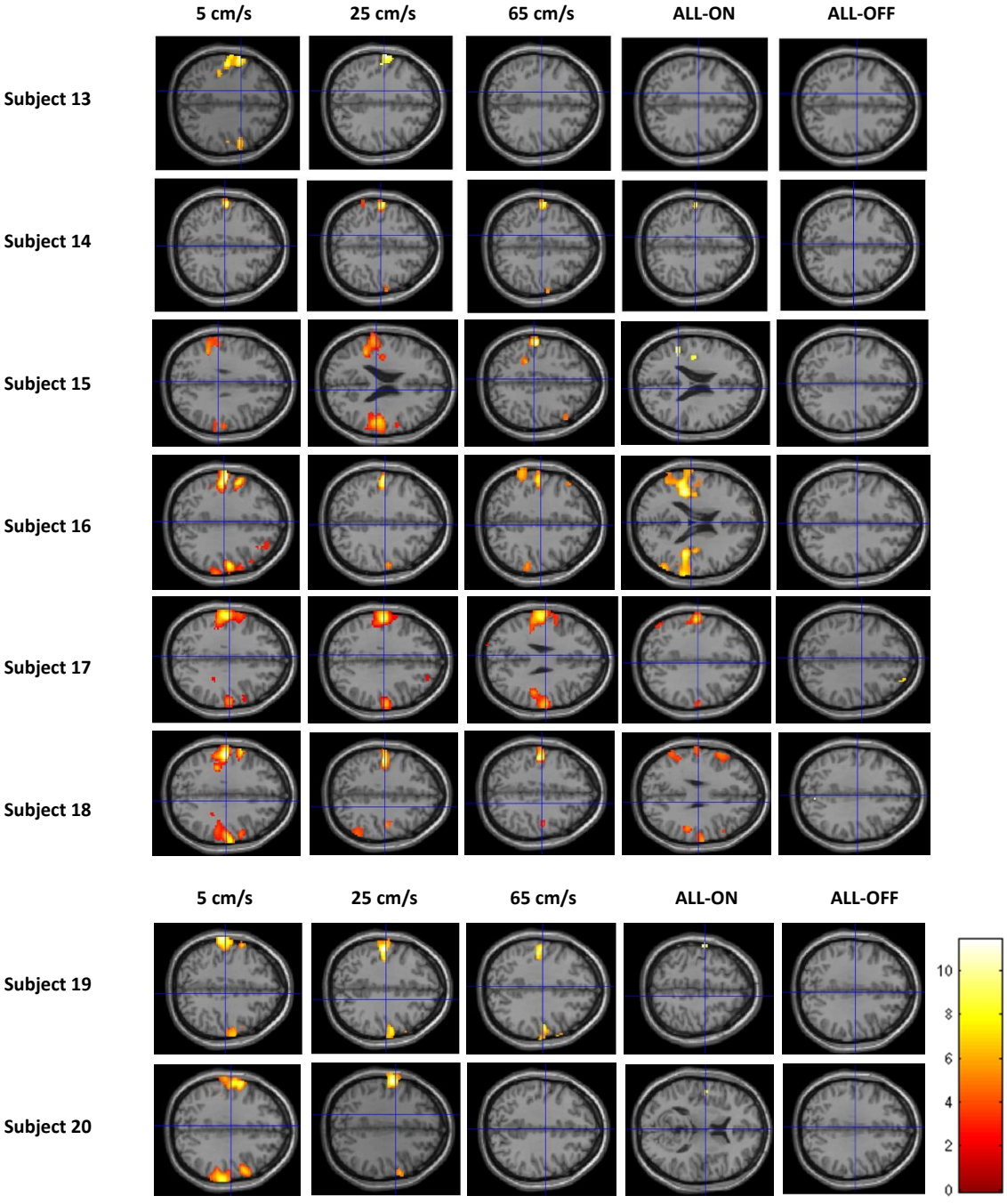

Figure 3.2 Single subject (first-level) cortical BOLD activations by condition (axial view).

Single Subject by Condition: Subcortical Activation

In 70% (14/20) of our participants, a cerebellar BOLD response was observed during the lowest velocity condition (5 cm/s), and also manifest during the 25cm/s, 65 cm/s and ALL-ON conditions in half (10/20) of the participants. Cerebellar activation was predominately ipsilateral to the stimulus side, and consistent with anatomical regions of hilar and capsular (declive) cerebellar dentate nucleus (Dimitrova et al., 2002; Ohmae et al., 2013; Wardman et al., 2014).

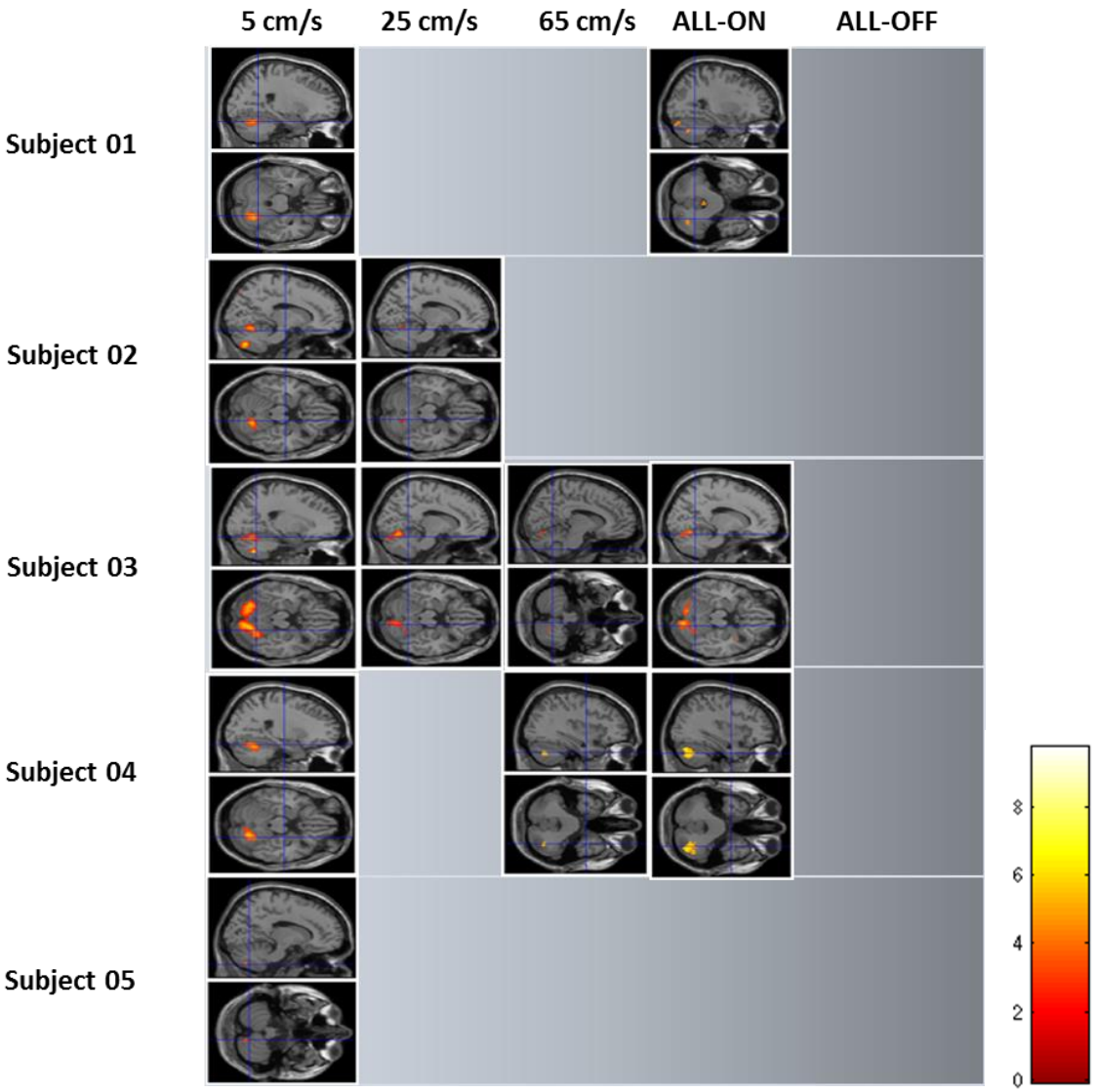
5 cm/s
25 cm/s
65 cm/s
ALL-ON
ALL-OFF
Subject 01
Subject 02
Subject 03
Subject 04
Subject 05
8
6
4
2
0

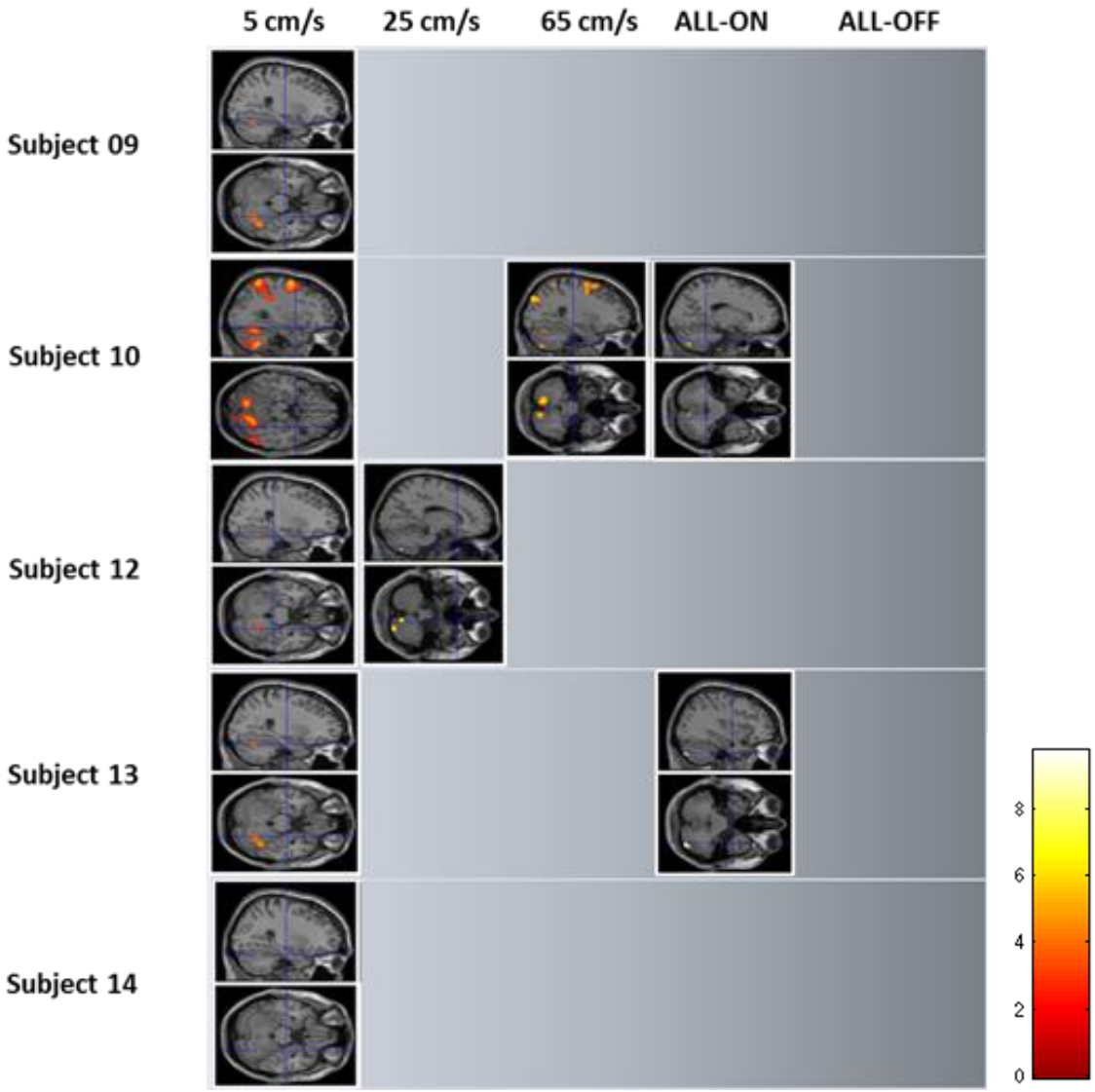
5 cm/s
25 cm/s
65 cm/s
ALL-ON
ALL-OFF
Subject 09
Subject 10
Subject 12
Subject 13
Subject 14
8
6
4
2
0

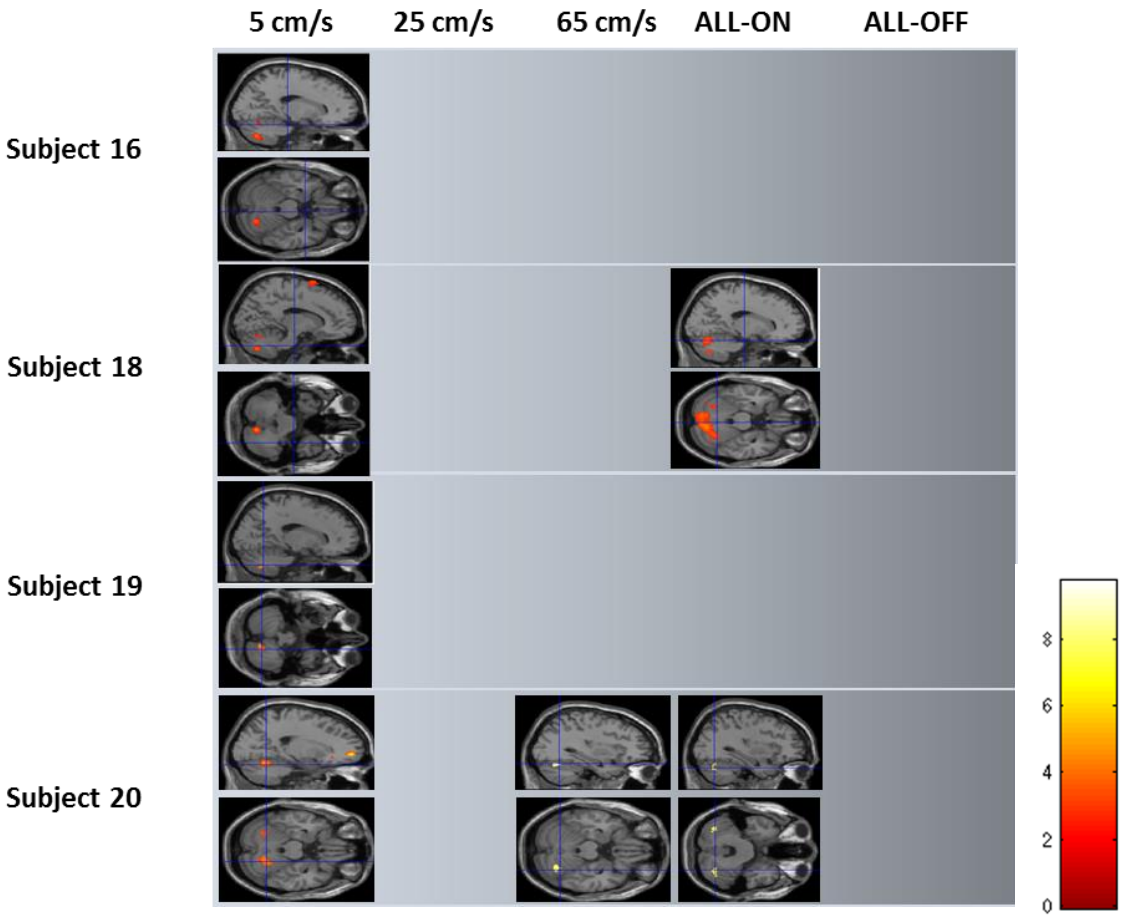

Figure 3.3 Single subject (first-level) cerebellar BOLD activations by condition.

Neuroimaging Results: Group

Main Effect of Velocity

Results from the One-Way ANOVA within-subjects design evaluating the main effect of velocity, showed BOLD responses in predicted *a priori* sensorimotor ROIs including contralateral S1, bilateral cortical S1, S2, M1, and insular regions, and regions of ipsilateral (to the stimulus) deep cerebellum proximal to the dentate nucleus. Voxel maximas associated with major clusters of activation (k=10, mm^3; voxel-wise threshold of $P_{unc} < 0.0001$) and their associated MNI coordinates and brain regions were identified using the SPM12 tool xjView [Neuroimaging Informatics Tools and Resources Clearinghouse (NITRC)], and are listed in Table 3.1. The overall main effect of unilateral, sequential saltatory inputs to the lower right face produced highly localized BOLD responses in facial sensorimotor regions as noted in Figure 3.4.

Table 3.1 Main effect of velocity (second-level) per cluster analysis of BOLD activation

ANOVA Main Effect of Velocity (P_{unc} <0.0001, k>10)

Region	MNI Coordinates			Stat Value (F)	Cluster Size (mm^3)
	X	Y	Z		
L precentral gyrus (BA 6)	-57	3	40	37.81	1540
L postcentral gyrus (BA 3)	-50	-23	23	35.37	
L insula	-45	-37	20	30.34	
R insula	51	-32	20	26.57	278
R inferior temporal gyrus	68	-22	-23	15.66	
R precentral gyrus (BA 9)	58	6	30	23.53	125
R precentral gyrus (BA 6)	53	3	45	19.81	
R precentral gyrus (BA 4)	51	1	53	17.11	
R cerebellum	26	-57	-23	24.78	82

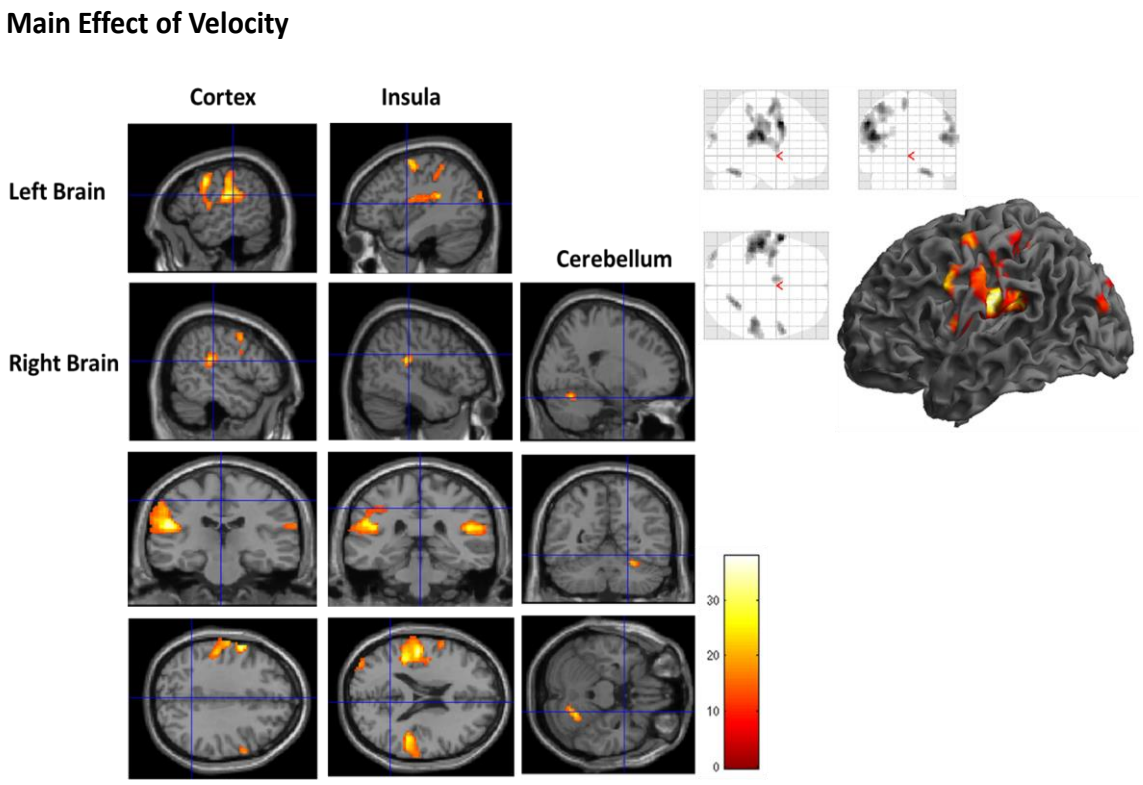

Figure 3.4 Main effect (second-level) of velocity BOLD activation.

Single Subject Compared to Group: ROI

To monitor spatial variability in regional BOLD/HRF activation that might be associated with differences in anatomy and physiological structure across participants, individual (single subject) MNI coordinates of cluster maximas were plotted with the main effect (group) cluster maxima using the SPM12 tool BrainNet [Neuroimaging Informatics Tools and Resources Clearinghouse (NITRC)] by region of interest (Figures 3.5-3.7).

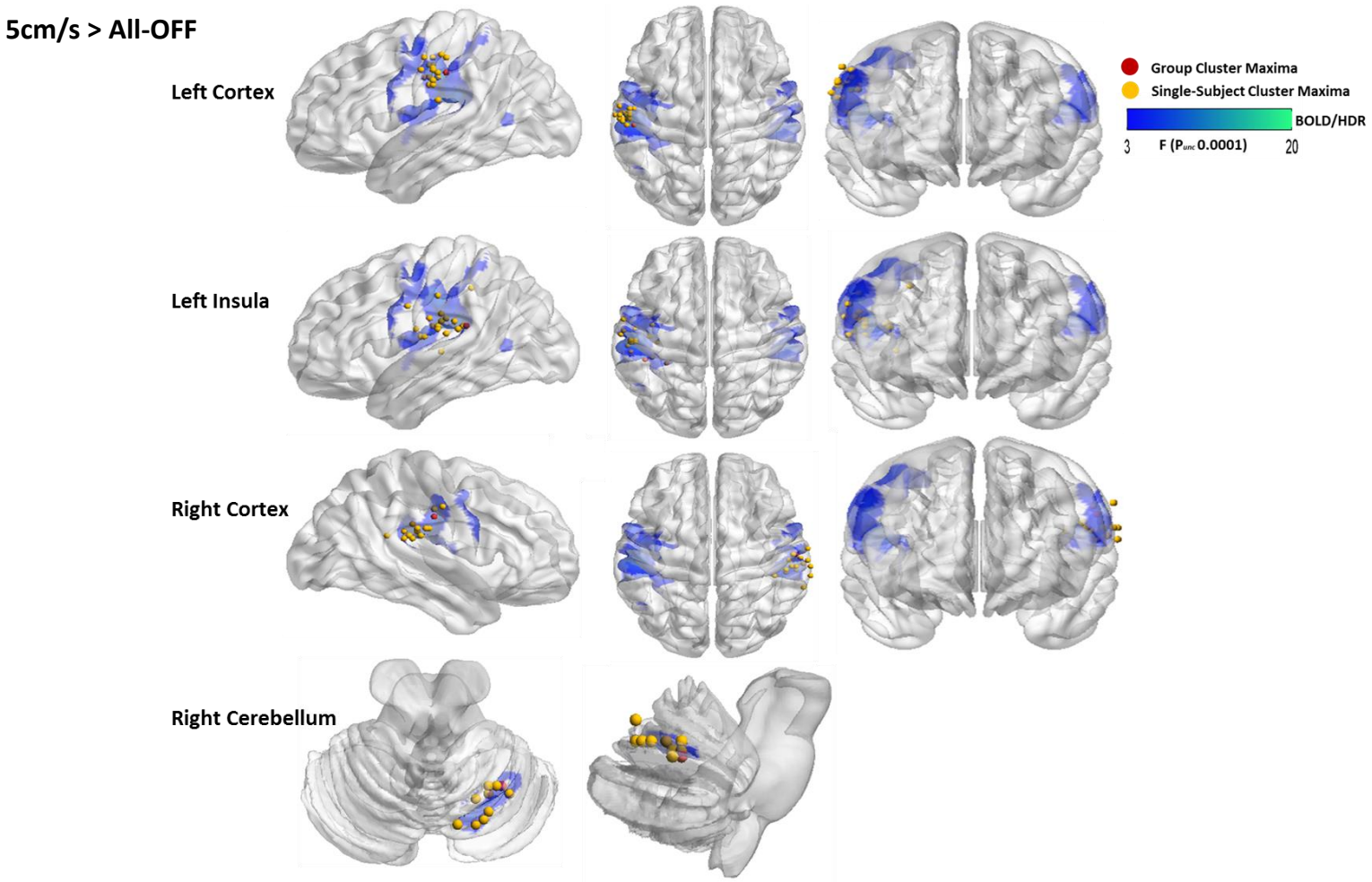

Figure 3.5 Single subject MNI coordinates of cluster maximas (yellow spheres) during 5 cm/s saltatory pneumotactile stimulation plotted with the main effect (group, red sphere) cluster maxima. Blue coloration indicates group BOLD/HRF.

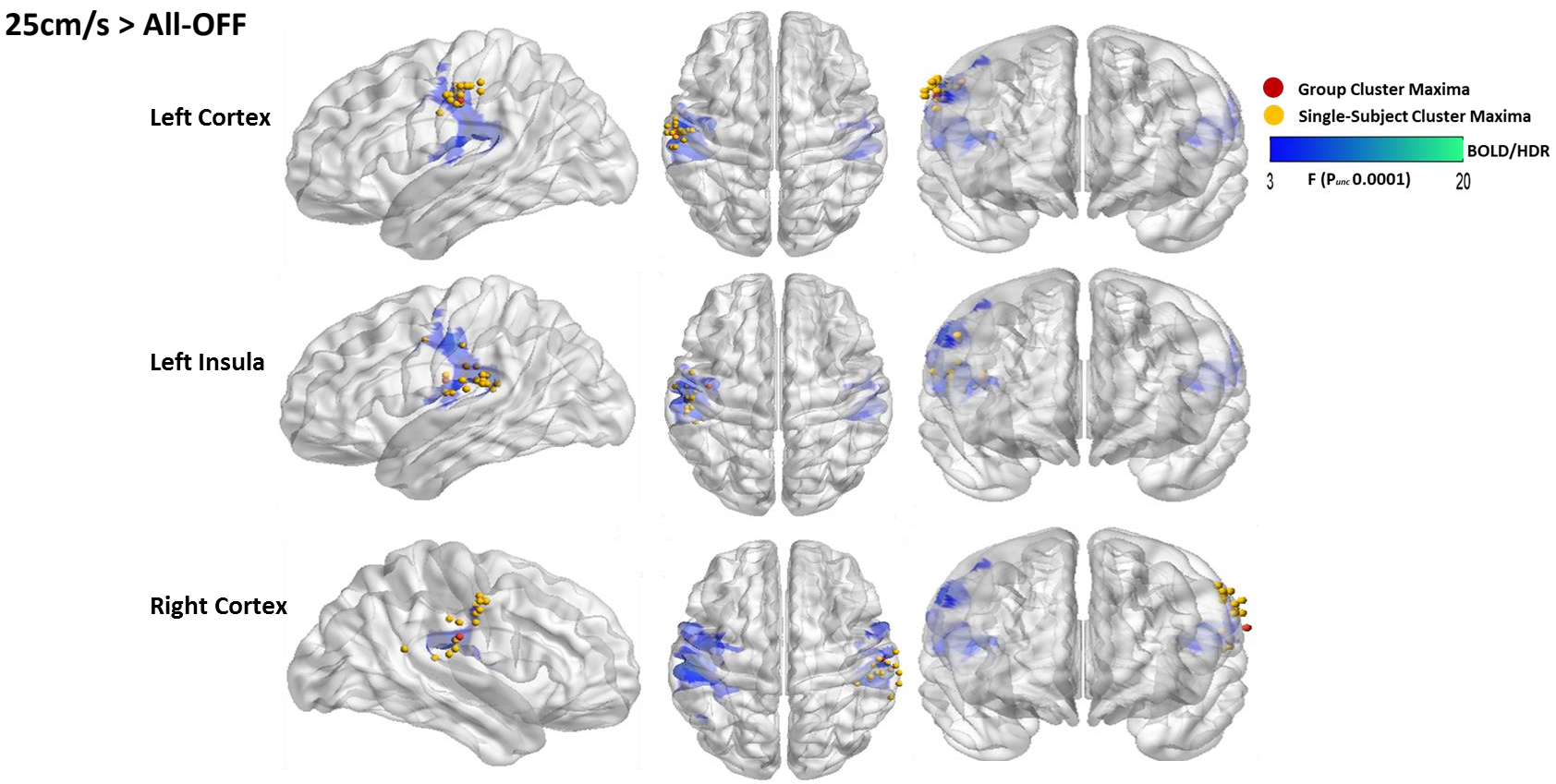

Figure 3.6 Single subject MNI coordinates of cluster maximas (yellow spheres) during 25 cm/s saltatory pneumotactile stimulation plotted with the main effect (group, red sphere) cluster maxima. Blue coloration indicates group BOLD/HRF.

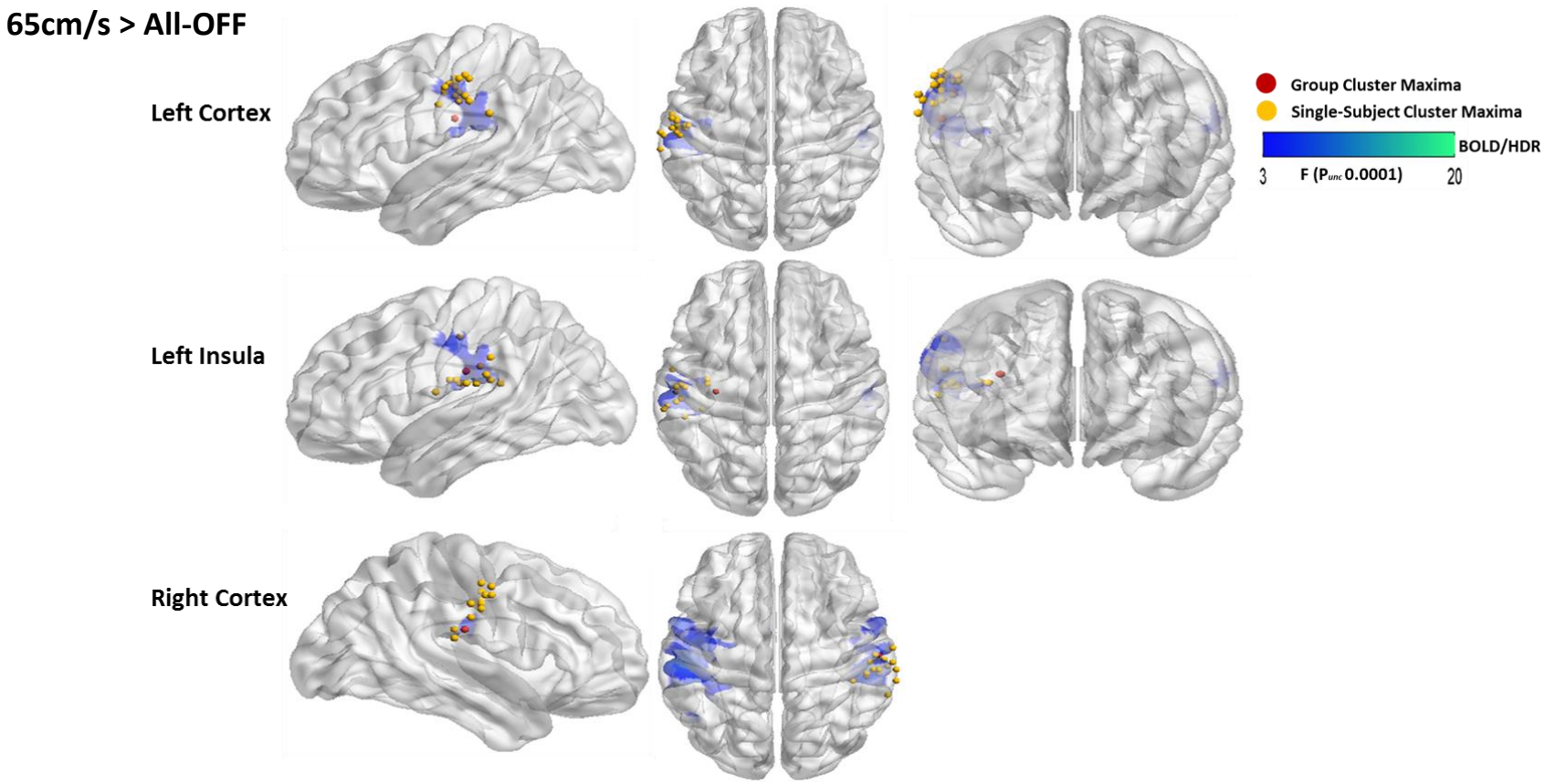

Figure 3.7 Single subject MNI coordinates of cluster maximas (yellow spheres) during 65 cm/s saltatory pneumotactile stimulation plotted with the main effect (group, red sphere) cluster maxima. Blue coloration indicates group BOLD/HRF.

Results indicated that single subject data was distributed closely to the main effect maxima, with MNI coordinates relatively well-aligned to the main effect ROI. Single-subject maximas became more tightly clustered (closer to each other and the main effect maxima) as velocity of the saltatory stimulus increased, likely due to the reduction in spatial extent of BOLD/HRF signal as stimulus velocity increased.

Velocities Compared to Control Conditions

Results of one-sample t-tests ($P_{unc} < 0.001$) used to monitor the change in BOLD signal associated with individual velocities (5, 25, 65 cm/s) compared to the two control conditions (ALL-OFF, ALL-ON), showed that HRF was modulated by corresponding changes in saltatory stimulus velocity. As seen in Figures 3.8 - 3.10, when compared to the ALL-OFF (no stimulation) control condition, sensorimotor cortical HRF was seen at all three velocity presentations, with the largest spatial extent of activation seen in the '5 cm/s > ALL-OFF' condition. The transformation of size, shape and region of HRF activation associated with changing stimulus conditions may reflect underlying changes active neural networks. At the '5cm/s > ALL-OFF' condition, activation in bilateral sensorimotor and insular cortices was recorded, in addition to right (ipsilateral to the stimulus) cerebellum. The largest and most statistically significant cluster of activation was recorded in primary somatosensory cortex (BA 1, BA 3, insula) contralateral to the stimulus (Figure 3.8). Clusters of activation consistent with *a priori* ROIs are listed in Table 3.2. In the '25 cm/s > ALL-OFF' condition (Figure 3.9), bilateral sensorimotor activation was again present, but reduced in spatial extent, with no cerebellar response

recorded (Table 3.3). In the '65cm/s > ALL-OFF' condition (Figure 3.10), the spatial extent of bilateral activation was further reduced, with only a single cluster recorded in ipsilateral cortex (Table 3.4).

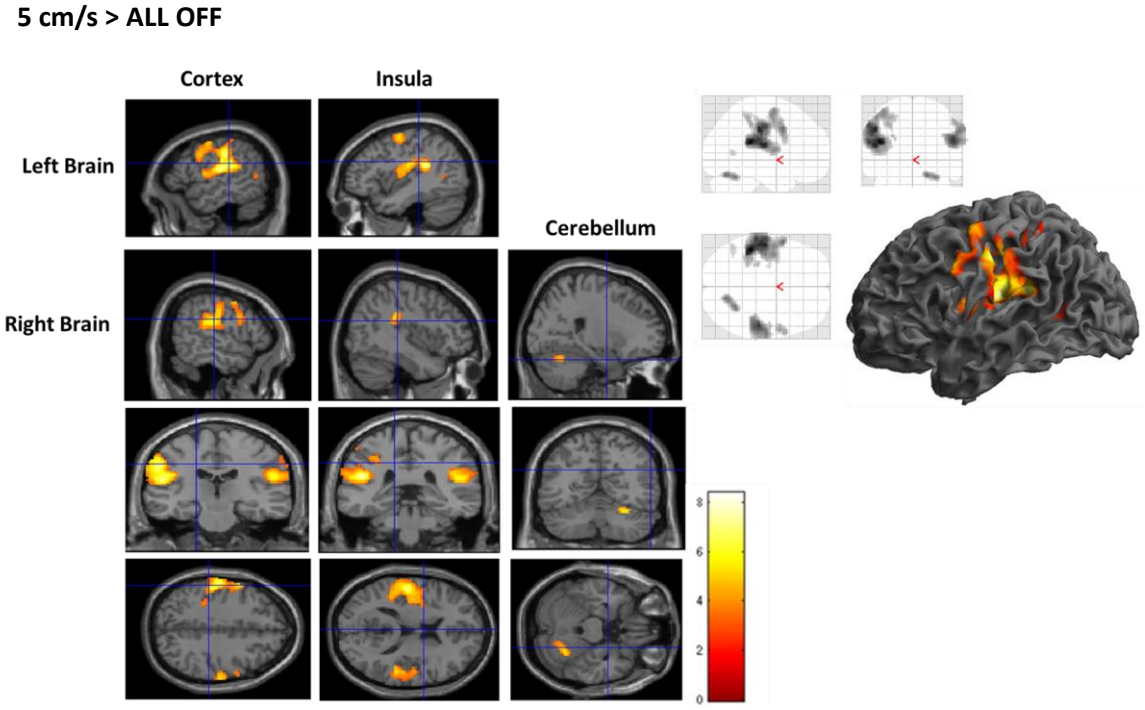

Figure 3.8 BOLD response for 5 cm/s > ALL-OFF (second-level t-test, $P_{unc} < 0.001$)

Table 3.2 Velocity vs. control (5 cm/s > ALL-OFF, second-level) per cluster analysis of BOLD activation

5 cm/s > ALL-OFF (P_{unc} <0.001, k>10)

Region	MNI Coordinates			Stat Value (T)	Cluster Size (mm^3)
	X	Y	Z		
L insula	-45	-37	20	9.72	2020
L postcentral gyrus (BA 1)	-52	-17	18	8.70	
L postcentral gyrus (BA 3)	-52	-23	38	8.57	
R inferior parietal lobe (PPC)	53	-25	23	7.96	756
R precentral gyrus (BA 6)	58	-17	33	6.30	
R insula	53	-12	15	4.72	
R precentral gyrus (BA 9)	58	3	45	5.30	140
R posterior cerebellum (declive)	16	-70	-23	6.45	134
R posterior cerebellum (culmen)	28	-57	-25	6.32	
L inferior parietal lobe (PPC)	-35	-37	45	5.12	128

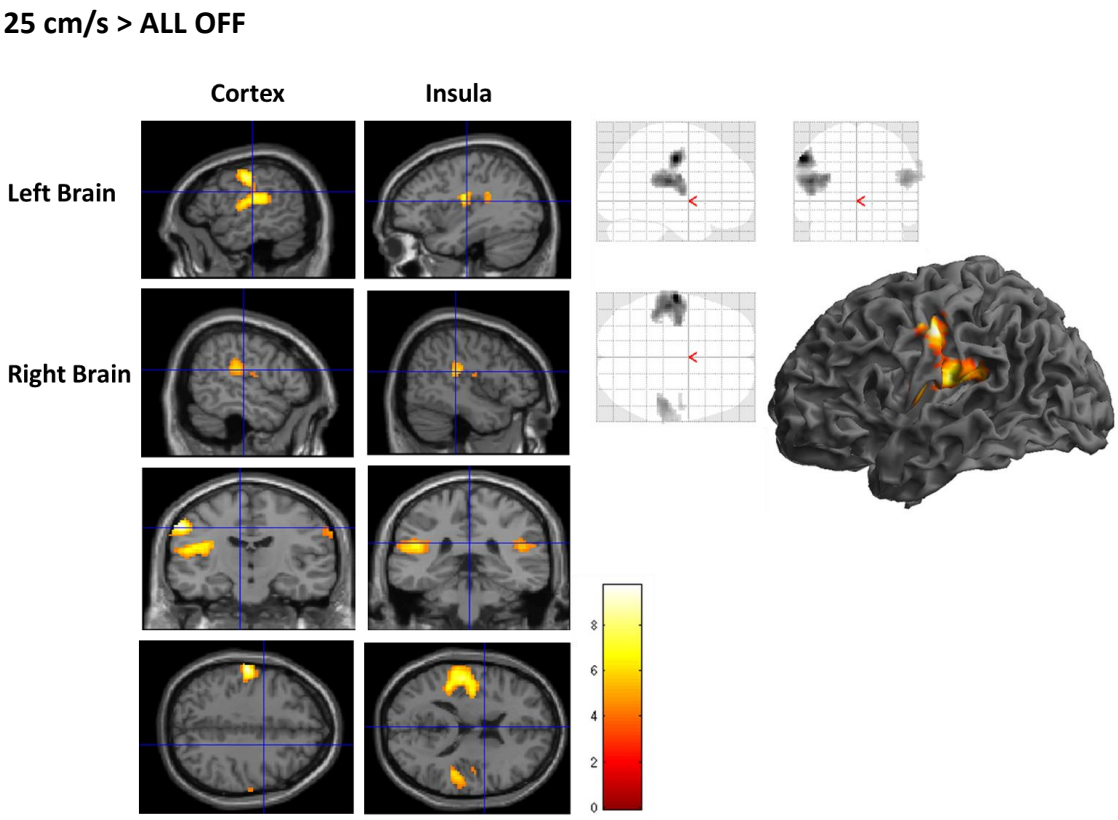

Figure 3.9 BOLD response for 25 cm/s > ALL-OFF (second-level t-test, $P_{unc} < 0.001$)

Table 3.3 Velocity vs. control (25 cm/s > ALL-OFF, second-level) per cluster analysis of BOLD activation

25 cm/s > ALL-OFF (P_{unc} <0.001, k>10)

Region	MNI Coordinates			Stat Value (T)	Cluster Size (mm^3)
	X	Y	Z		
L precentral gyrus (BA 6)	-60	-17	43	8.63	1030
L postcentral gyrus (BA 3)	-52	-22	18	7.15	
L insula	-45	-35	20	6.11	
R inferior lobe (PPC)	51	-27	20	5.55	306
R precentral gyrus (BA 9)	68	-20	25	4.29	
R postcentral gyrus	54	-10	15	4.28	
R precentral gyrus (BA 6)	68	-15	35	4.16	
R insula	41	-10	20	3.77	23

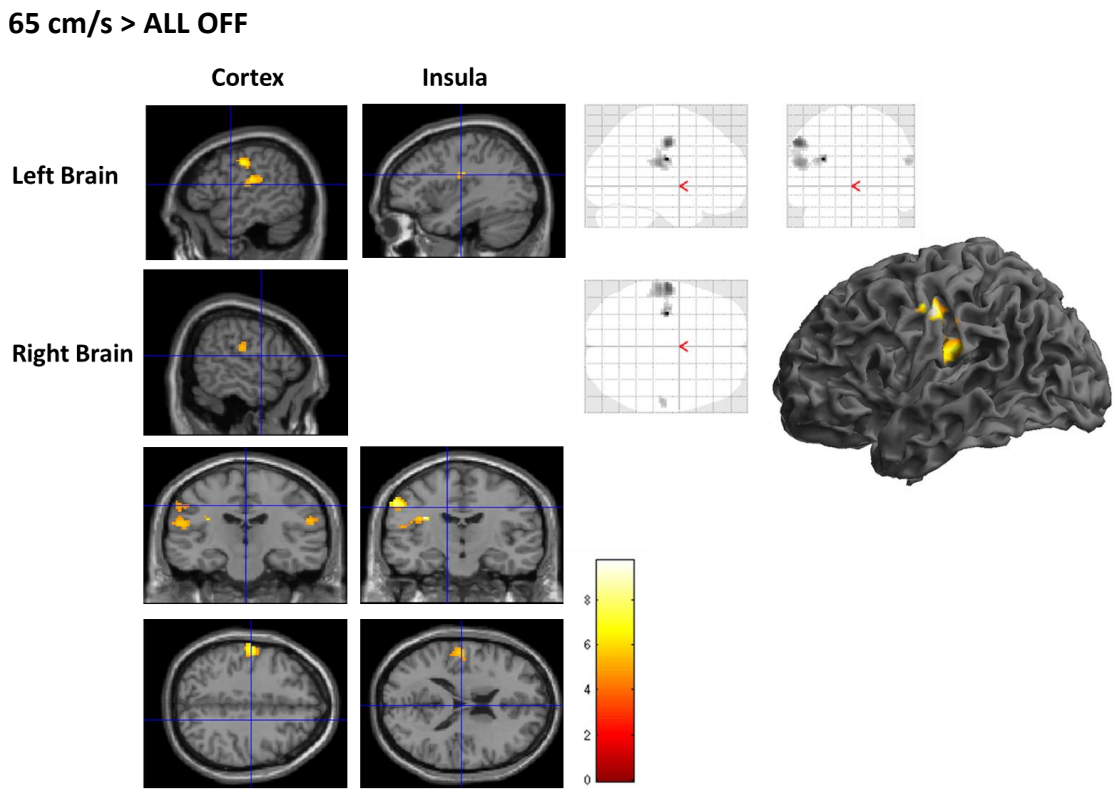

Figure 3.10 BOLD response for 65 cm/s > ALL-OFF (second-level t-test, $P_{unc} < 0.001$)

Table 3.4 Velocity vs. control (65 cm/s > ALL-OFF, second-level) per cluster analysis of BOLD activation

65 cm/s > ALL-OFF (P_{unc} <0.001, k>10)

Region	MNI Coordinates			Stat Value (T)	Cluster Size (mm^3)
	X	Y	Z		
L insula	-32	-15	25	7.62	287
L postcentral gyrus (BA 1)	-57	-15	40	6.04	
L postcentral gyrus (BA 3)	-57	-22	20	5.10	
R postcentral gyrus (BA 3)	58	-20	23	4.35	30

As shown in Figures 3.11- 3.13, when each velocity was compared to the ALL-ON (stimulator cells activated simultaneously at 1 Hz) control condition, sensorimotor cortical HRF at the uncorrected threshold ($p < 0.001$) was again observed at all three velocity presentations (5, 25, 65 cm/s), but with bilateral cortical activation noted only at the '5cm/s > ALL-ON' condition (Table 3.5). In the '25 cm/s > ALL-ON' condition, two significant clusters emerged that were consistant with cortical *a priori* ROI left primary somatosensory (SI) cortex (Table 3.6). In the '65 cm/s > ALL-ON' condition (Table 3.7), only a single, small cluster was recorded in left somatosensory cortex (BA 3).

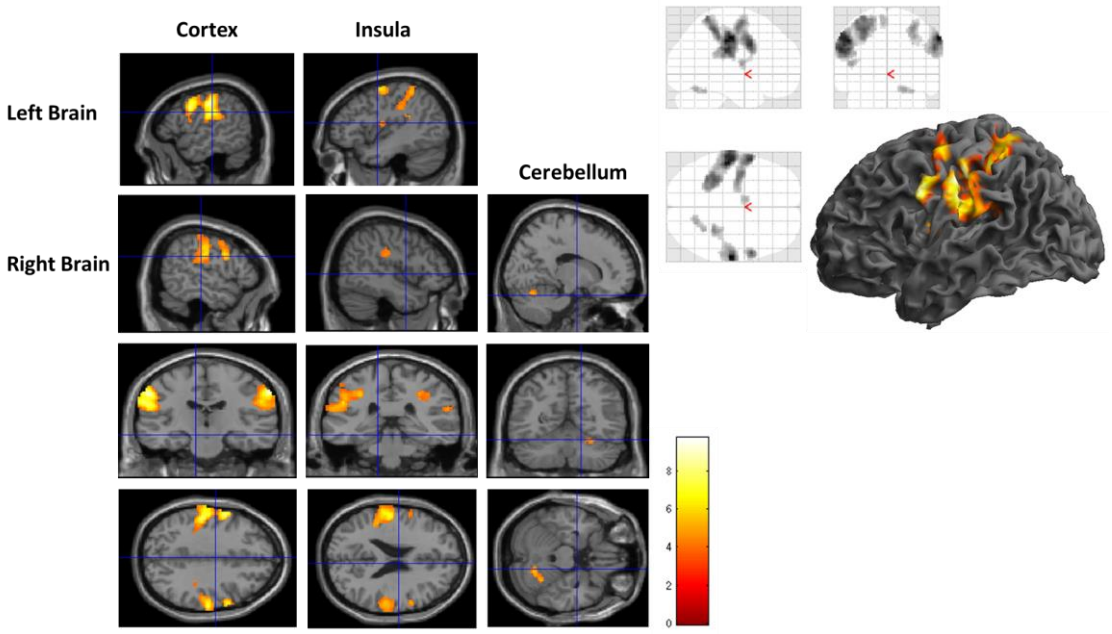

Figure 3.11 BOLD response for 5 cm/s > ALL-ON (second-level t-test, $P_{unc} < 0.001$)

Table 3.5 Velocity vs. control (5 cm/s > ALL-ON, second-level) per cluster analysis of BOLD activation

5 cm/s > ALL-ON (P_{unc} <0.001, k>10)

Region	MNI Coordinates			Stat Value (T)	Cluster Size (mm^3)
	X	Y	Z		
L postcentral gyrus (BA 3)	-52	-25	38	8.69	2002
L precentral gyrus (BA 6)	-60	-22	28	8.08	
L precentral gyrus (BA 9)	-57	6	35	7.74	
R precentral gyrus (BA 6)	63	-20	43	9.31	533
R inferior parietal lobe (PPC)	56	-20	30	5.91	
R precentral gyrus (BA 3)	61	-25	23	5.15	
R postcentral gyrus (BA 40)	31	-40	55	5.85	188
R insula	33	-37	45	5.33	
R precentral gyrus (BA 9)	58	6	30	6.90	163
R posterior cerebellum (declive)	21	-65	-23	5.24	71
R posterior cerebellum (culmen)	31	-55	-23	5.01	

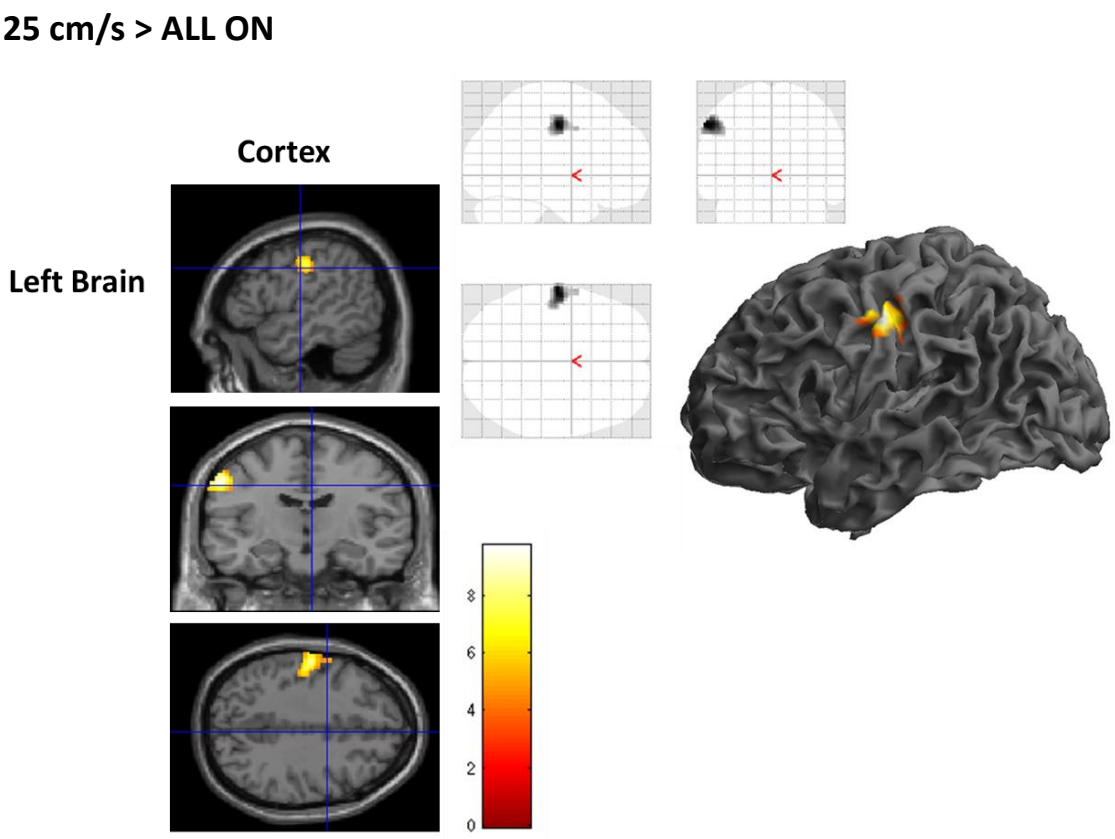

Figure 3.12 BOLD response for 25cm/s > ALL-ON (second-level t-test, $P_{unc} < 0.001$)

Table 3.6 Velocity vs. control (25 cm/s > ALL-OFF, second-level) per cluster analysis of BOLD activation

25 cm/s > ALL-ON (P_{unc} <0.001, k>10)

Region	MNI Coordinates			Stat Value (T)	Cluster Size (mm^3)
	X	Y	Z		
L postcentral gyrus (BA 3)	-62	-15	43	8.18	225
L precentral gyrus (BA 9)	-60	1	38	4.48	

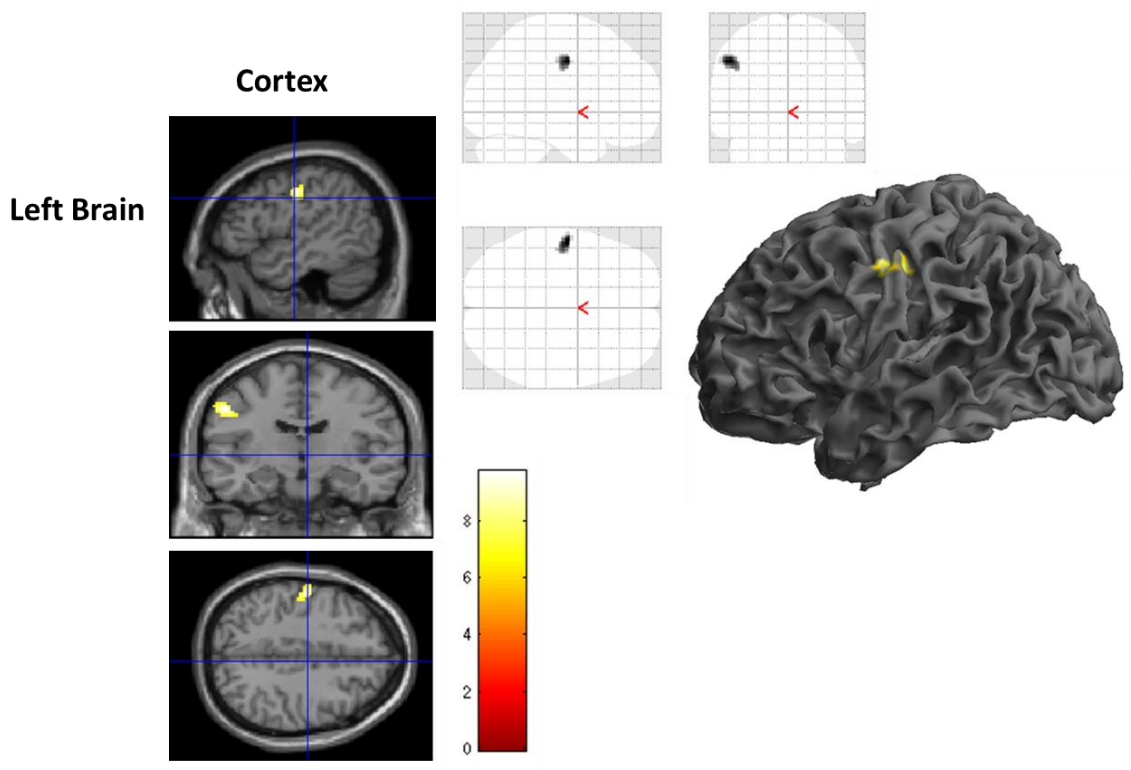

Figure 3.13 BOLD response for 65cm/s > ALL-ON (second-level t-test, $P_{unc} < 0.001$)

Table 3. 7 Velocity vs. control (65 cm/s > ALL-ON, second-level) per cluster analysis of BOLD activation

65 cm/s > ALL-ON (P_{unc} <0.001, k>10)

Region	MNI Coordinates			Stat Value (T)	Cluster Size (mm^3)
	X	Y	Z		
L postcentral gyrus (BA 3)	-52	-12	40	5.47	76

CHAPTER 4: DISCUSSION

Overview of Current Findings

In this study, BOLD responses from 20 healthy, adult subjects revealed a unique transformation of the HRF signal as a function of punctate, saltatory stimulation varied by velocity. In addition to activation in *a priori* contralateral facial somatosensory regions (SI, SII, MI, SMA, PPC, insula), 95% (19/20) of our participants showed regions of activation in the hemisphere ipsilateral to the stimulus, particularly in deeper insular regions of cortex, and in the cerebellum. The extent and region of BOLD/HRF signal was appreciably modulated by changes in the velocity of pneumotactile stimuli, and may represent key dynamic neural networks underlying moving tactile stimulus processing, motion perception and neural organization.

Outcomes of Specific Aims and Hypotheses

Distributed Neural Networks for Velocity Encoding

The overarching specific aim of this study was to map the spatiotemporal organization of the cortical and subcortical networks that encode velocity during discontinuous pneumotactile stimulation of the lower, right face. Using the described paradigm, evaluation of both single subject and group fMRI data showed tight coupling of BOLD activations with changes in stimulus velocity, which matched well with our predominant hypothetical question regarding underlying neural networks involved in the processing of moving sensory stimuli.

We found not only a significant main effect of velocity, but also a markedly different pattern of BOLD response as a function of individual velocities (5 cm/s, 25 cm/s, 65 cm/s) when compared to control (ALL-OFF, ALL-ON) conditions. In nearly all participants (with the exception of participant 06 who showed overall reduced BOLD signal), the spatial extent of the BOLD response was inversely related to stimulus velocity.

These findings strongly support an underlying, adapting neural network, capable of encoding tactile stimulus velocity (Hypotheses 1, 2, 3). Additionally, activations of neural regions associated with motion perception, processing and planning were observed (Hypothesis 4), which included bilateral cortical, insular and cerebellar circuits.

Lateralization vs. Bilateral Cortical Activation

In 'main effect of velocity' data, we found that the largest area of activation (cluster size 1540 mm^3) occurred in the contralateral hemisphere in left precentral, postcentral and insular regions. The second largest area of activation, however, occurred in the ipsilateral hemisphere in right inferior temporal, precentral, postcentral and insular regions. Similarly, in 'velocity vs. control' data, at the lowest velocity (5 cm/s > ALL-OFF, ALL-ON), there was bilateral BOLD response with the largest and most statistically significant cluster of activity seen on the contralateral side. As stimulus velocity increased, the smaller, ipsilateral (right-sided) activation was reduced until at the highest stimulus velocity (65 cm/s > ALL-OFF), there was only a single small cluster of

right-sided activation, and in the higher ’25 cm/s > ALL-ON’ and ‘65 cm/s > ALL-ON’ conditions, ipsilateral activation was absent.

This type of bilateral activation during repeating stimulus trains to the face are likely due to transcallosal intra-cortical fibers extending between SII and SI regions during touch processing. As discussed in previous sections, neural activity can propagate via these long-range axons to cortex ipsilateral to the stimulus, often appearing in regions of frontal cortex, MI, SII, insula and PPC (Trulsson et al., 2000; Aronoff et al., 2010).

In perioral regions however, studies have shown that there is also some anatomical bilateral projection through thalamus to right and left cortical face representation in primates (Rausell & Jones, 1991; Lin et al., 1994). In some cases, strong bilateral activation of the trigeminothalamic tract may occur during noxious or nociceptive stimulus processing (Jantsch et al., 2005; Nash et al., 2010). It may be that repeated stimulation of the sensitive perioral area in our paradigm not only produced signal propagation along some uncrossed trigeminolemniscal (discriminative touch) pathways, but also activated the anterior trigeminothalamic (nociception) tract as well, contributing to the pronounced bilateral effect.

Insular Activation

Results of this study indicated unpredicted, significant activation in deeper, mostly posterior insular regions during facial stimulation, particularly at the lower velocities (5 cm/s, 25 cm/s). This is an interesting finding as research has implicated deeper layers of cortex and insula in higher processing circuit connectivity, beyond

cortical columnar-unit topography. It is these deeper layers of cortex that likely allow stimulus feature selectivity through hierarchical 'gain' and inhibition via ancillary regions of cortex and thalamus (Carandini & Heeger, 2012; Miller, 2016). Insular cortex has also been identified as a key structure in the modulation of trigeminal nocioception (Wang et al., 2015; Schulte & Sprenger, 2016), and its activation has been correlated with the perceived intensity of noxious sensory input (Derbyshire et al., 1997). This may indicate another layer of neural coding occurring during stimulation of the sensitive perioral area that contribute to complex sensory activation in our paradigm (Coghill et al., 1999; Starr et al., 2009; Lotsch et al., 2012).

Relevant to future directions for study, deep cortical regions appear to make strong excitatory and inhibitory links between primary sensory, frontal integrating, and motor processing areas (Elston, 2003; Murphy & Miller, 2009; Chaudhuri et al., 2015). In both animal study of ingestive behavior (Schneider et al., 1993; Jezzini et al., 2012) and human study of speech production (Eckers et al., 2013; Poeppel, 2014; Simonyan & Fuertinger, 2015), insular regions are functionally connected to sensorimotor and orofacial motor networks, and comprise a majority of neural 'communities' which include prefrontal cortex, basal ganglia and thalamus (Eickhoff et al., 2009; Fuertinger et al., 2015). Stimulation of these complex communities may prove highly beneficial for encouraging sensorimotor connectivity and plastic reorganization after neurological disruption.

Cerebellar Activation

The finding of cerebellar activation proximal to the dentate and interpositus nuclear regions provide further evidence for refined signal integration during sensory movement discrimination. The dentato-rubro-olivary loop (Guillain-Mollaret triangle), has long been associated with precision fine motor control, but also holds a key component in sensory processing, proprioceptive tuning, and sensory discrimination (Habas et al., 2009, 2010; Cullen & Brooks, 2015). Damage to cortico-ponto-cerebellar or dento-thalamic-cortical feedback pathways results in characteristic ataxic hemiparesis, or dysmetria, where patients exhibit a lack of limb coordination and undershoot or overshoot intended limb position (Schmahmann et al., 2004; Manto 2009; Caplan, 2012). Similarly, the interpositus cerebellar region (globose and emboliform nuclei) is heavily innervated by climbing fibers originating in the inferior olivary complex, and appears to modulate excitability changes in motor cortex. Activity in these regions is associated with healthy motor learning (Small et al., 2005; Luft et al., 2005; Farias da Guarda & Conforto, 2014), and may play a substantial role in early recovery after infarct (Bannister et al., 2015; Ishida et al., 2016).

In this study, we observed that 70% (14/20) of the participants manifest ipsilateral cerebellar activation. Close examination of single subject vs. group BOLD cluster maxima distribution showed that single subject data was well-aligned to the main effect (group) cerebellar ROI which matches dentate and interpositus regions (Figure 4.1).

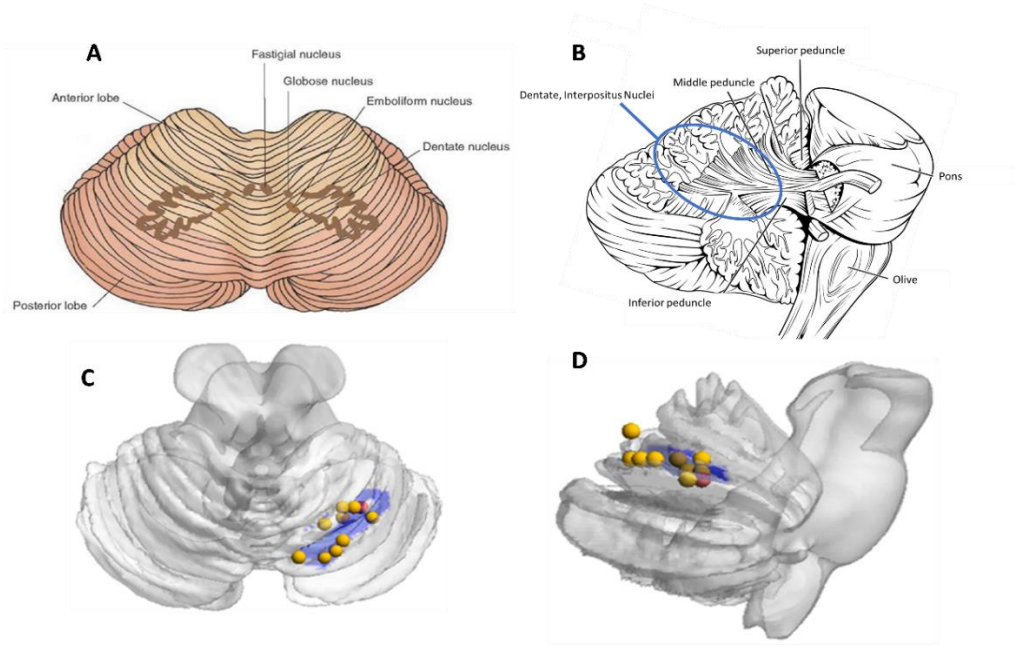

Figure 4.1 Distribution of cerebellar activation. Cartoons (A, B) illustrate human cerebellar arrangement and positions of cerebellar nuclei (retrieved from http://what-when-how.com/neuroscience/brainstem-ii-pons-and-cerebellum-part-2/). Images (C) and (D) show single subject (yellow) and group (red) BOLD cluster maximas aligned with cerebellar ROI.

New research on the role of cerebellum in healthy sensory processing suggests that cerebellar circuits act as the 'predictive' brain, continuously generating internal models of temporally and spatially structured events that can be used to make sensorimotor predictions (Leggio & Molinari, 2015; Fujita, 2016). In neurological disease states, direct damage to the cerebellum can lead to deficits in somatosensory mismatch negativity (Restuccia at al., 2007; Spencer & Ivry, 2013), while cerebellar activation has been has been closely linked to improvement in stroke limb paresis, likely

due hemodynamic shifts associated with post-lesion diaschisis (Pantano et al., 1986; Small et al, 2015). It follows that the significant cerebellar activity seen in our paradigm is prospectively a key component of stimulus velocity coding during these repeating pneumotactile trains, particularly during the slower presentations when individual stimuli (single pulses) are discernable.

Study Limitations and Future Directions

Neurotypical Population

In our study, the participant pool comprised only healthy, neurotypical adults without any known aberrancies of somatosensory processing. The ultimate goal of any human research, however, is to explore the realms of disorder and develop potential therapeutics that can improve the quality of life for individuals with disability. This study presents a first step in mapping somatosensory networks that discriminate changes in tactile velocity, and holds the potential to serve as a neurotypical map for future research that may be applied to cerebrovascular stroke, traumatic brain injury, Parkinson's disease and even developmental disorders such as cerebral palsy, Down syndrome and Autism Spectrum Disorder.

Temporal Assessment

The use of high resolution fMRI to elucidate neural networks that encode velocity during discontinuous stimulation worked well for this preliminary study, and there are

several ways this project could be expanded. A primary assumption of this general *linear* model was that the BOLD response was relatively linear, and noise associated with the hemodynamic changes followed a Gaussian distribution and was stable over time. In fact, because of the known nonlinearity of BOLD signal in short inter-stimulus intervals (less than 6-10 seconds), acquisition sequences must allow for adequate HRF decay. In our experiment, we provided a 20 second 'off' interval between velocity blocks to allow for HRF decay, but that interval may be reduced in future paradigms to shorten the amount of time participants are in the scanner. Additionally, more temporally sensitive fMRI protocols could be employed in next-step research, such as multiband EPI, which permits full-brain coverage through the acquisition of multiple slices simultaneously in the amount of time it takes to acquire a single slice image in standard EPI (Smith et la., 2012; Xu et al., 2013; Todd et al., 2016). This would allow access to important timing characteristics of the BOLD signal and its evolution across processing networks, maintain high spatial resolution, and decrease the amount of scan time for less tolerant, neuro-diverse populations.

For truly effective response network mapping, a further examination of the cortical and subcortical signal should be performed. Following peripheral stimulation, neural activity occurs not only on the order of seconds (hemodynamic, BOLD response), but also on the order of milliseconds (neuronal activity, network fluctuation). By assessing BOLD voxel maximas over an entire scan sequence as we did in this initial study, much of the intricacies of temporal resolution are overlooked. To address this issue, imaging techniques offering millisecond temporal resolution, such as electroencephalography (EEG) or magnetoencephalography (MEG) could be combined

with the excellent spatial resolution of fMRI. Both combinations have been used successfully to monitor neural changes in health (Chun et al., 2016; McWhinney et al., 2016) and disease (Irimia & Van Horn, 2015; Kieler et al., 2016), and can improve detection of subtle differences in perfusion associated with neuronal activity.

Lastly, from an algorithmic standpoint, the data from this fMRI scan analysis could be subdivided into shorter time windows that are either overlapping (Hutchison et al., 2013) or non-overlapping (Bassett et al., 2011; Siebenhuhner et al., 2013), depending on the desired temporal resolution of the HRF data. In some cases, algorithms with 'sliding' time windows can be used in independent component analysis (ICA) of response signals, and can identify transient characteristics of BOLD signals over much shorter timescales (Telesford et al., 2016). These techniques could greatly improve assessment of moving tactile stimulation processing networks across different disordered populations, or across a broad expanse of age ranges in healthy populations.

Connectivity and Advanced Network Mapping

Another approach that could be incorporated in to future study would be structural connectivity assessment with diffusion tensor imaging (DTI), particularly for the evaluation of higher processing and integrative brain regions that showed significant activation in the main effect and low velocity data. Tractography studies of both insular (Cloutman et al., 2012) and posterior parietal (PPC) cortices (Caspers et al., 2011) during somatosensory processing have described intricate parcellation of sensory signals, and that these regions can show dynamic, plastic changes in structural connectivity during

neurological disruption and repair (Yamada et al., 2004; Jang, 2011; Kou & Iraji, 2014). Similarly, alterations in white matter integrity associated with deficits in resting state and active functional connectivity have been reported in cerebral ischemia (Meyer et al., 2015; Cha et al., 2016) and TBI (Chong & Schwedt, 2015; Harris et al, 2016). A future hypothesis would be that there are definable differences in higher level sensory signal management in many disease states, and these differences play a key role sensorimotor and functional recovery.

Sensory Links to Motor Function in Brain Injured Populations

The mapping of trigeminal somatosensory processing networks such as those described in this project can provide a template that can be used in a comparative manner when evaluating network dysfunction in disordered populations. In disease states, motor deficits associated with sensory damage can profoundly impact subsequent recovery, risk for re-injury and overall quality of life. Sensorimotor damage to orofacial regions can inhibit speech, safe and comfortable oral intake, and human interaction.

In all instances of motor rehabilitation after injury, sensory integration plays a critical role in recovery as injured networks remap sensorimotor interactions through recruitment of primary sensory, secondary motor and higher-order association areas involved in touch and movement processing (Nudo, 2013; Bolognini et al., 2016). In our study, we found rapid dynamic changes occurring in not only distinct regional, but also distant bilateral, insular and cerebellar neural networks during the processing of moving tactile stimulation varied by velocity.

In stroke research, lesion studies have shown that these intra- and interhemispheric changes in sensorimotor coupling can greatly effect motor outcomes. Infarct to sensorimotor integration 'hubs' that link anatomically distant processing regions, produces more severe motor deficit than infarcts to local motor regions alone (Grefkes & Fink, 2011; Cheng et al., 2015). Conversely, it may be that activation of integration hubs such as those putatively reported in our study, could be ideal mechanisms to adjunct functional improvement. An immediate future direction for this study will be to establish a 'dose' specific regimen in disordered populations that promotes optimal network activity and plasticity during a stimulation schedule. As an example, velocity varied pneumotactile stimulation might be applied once or twice daily for 5-20 days in individuals who have hemiparesis related to stroke. Standardized behavioral testing combined with functional neuroimaging could be conducted before and after therapeutic application to monitor physiological and performance change.

In addition to passive sensory stimulation, participants could be asked to perform purposeful, task-oriented motor movements (such as reaching, grasping, or orofacial movement) while undergoing pneumotactile stimulation. Asking participants to match their motor tasks with the perceived stimulus velocity or direction may produce the most robust rehabilitative changes. Many studies have shown that purposeful movement combined with sensory training have the most beneficial and lasting effect (Dinse et al., 2011; Kattenstroth et al., 2012; Kato & Izumiyama, 2013).

Conclusion

The research presented here illustrates a method for assessing the neural networks associated with velocity encoding during tactile stimulation to the human orofacial somatosensory system. We found statistically significant neural adaptive responses and network scalability associated with tactile inputs varied by velocity. These findings also indicate that the networks involved in proprioception and motor planning become active during tactile velocity processing, which should lead to further experimental paradigms in sensorimotor disordered populations such as stroke and traumatic brain injury. The described project has the potential to create not only a neurotypical HRF model of cortical velocity processing networks following a novel stimulation paradigm, but should also lead to a long line of new neurodiagnostic and neurotherapeutic applications.

REFERENCES

Ackerley R, Carlsson I, Wester H, Olausson H, Backlund Wasling H. Touch perceptions across skin sites: differences between sensitivity, direction discrimination and pleasantness. Frontiers in Behavioral Neuroscience 2014, (8)54:1-10.

Ahissar E, Sosnik R, Haidarliu S. Transformation from temporal to rate coding in a somatosensory thalamocortical pathway. Nature 2000; 406:302–306.

Ahmed B, Anderson J, Douglas R, Martin K, Nelson J. Polyneuronal innervation of spiny stellate neurons in cat visual cortex. Journal of Comparative Neurology 1994, 341: 39–49.

Alloway K, Zhang M, Chakrabarti S. Septal columns in rodent barrel cortex: functional circuits for modulating whisking behavior. Journal of Comparative Neurology 2004, 480: 299–309.

Andreatta R, Barlow S, Biswas A, Finan D. Mechanosensory modulation of perioral neuronal groups during active force dynamics. Journal of Speech and Hearing Research 1996, October 39(5): 1006-17.

Antal A, Bikson M, Datta A, Lafon B, Dechent P, Parra LC, Paulus W. Imaging artifacts induced by electrical stimulation during conventional fMRI of the brain. NeuroImage 2014, 15(85); 1040-7.

Arleo A, De´jean C, Allegraud P, Khamassi M, Zugaro M, Wiener S. Optic flow stimuli update anterodorsal thalamus head direction neuronal activity in rats. The Journal of Neuroscience 2013, 33(42): 16790-16795.

Aronoff R, Matyas F, Mateo C, Ciron, C, Schneider B, Peterson C. Long-range connectivity of mouse primary somatosensory barrel cortex. European Journal of Neuroscience 2010, 31: 2221-2233.

Aronoff R, Peterson C. Layer- and column-specific knockout of NMDA receptors in pyramidal neurons of the mouse barrel cortex. Frontiers of Integrated Neuroscience 2007,1.doi:10.3389/neuro.07.001.2007.

Bannister L, Crewther S, Gavrilescu M, Carey L. Improvement in Touch Sensation after Stroke is Associated with Resting Functional Connectivity Changes. Frontiers in Neurology 2015, 6:165.

Barlow S. Real time modulation of speech--orofacial motor performance by means of motion sense. Journal of Communication Disorders 1998, Nov-Dec; 31(6):511-33.

Barlow S, Bradford P. Comparsion of perioral reflex modulation in the upper and lower lip. Journal of Speech and Hearing Research 1996, 39: 55-75.

Barlow S, Finan D, Lee J, Chu S. Synthetic orocutaneous stimulation entrains preterm infants with feeding difficulties to suck. Journal of Perinatology 2008, Aug; 28(8): 541-8.

Barlow S, Jegatheesan P, Weiss S, Govindaswami B, Wang J, Lee J, Oder A, Song D. Amplitude-integrated EEG and range-EEG modulation associated with pneumatic orocutaneous stimulation in preterm infants. Journal of Perinatology 2014a, Mar; 34(3): 213-9.

Barlow S, Lee J, Wang J, Oder A, Hall S, Knox K, Weatherstone K, Thompson, D. Frequency-modulated orocutaneous stimulation promotes non-nutritive suck

development in preterm infants with respiratory distress syndrome or chronic lung disease. Journal of Perinatology 2014b, Feb; 34(2): 136-42.

Barlow, S, Lee J, Wang J, Oder A, Oh H, Hall S, Knox K, Weatherstone K, Thompson D. Effects of oral stimulus frequency spectra on the development of non-nutritive suck in preterm infants with respiratory distress syndrome or chronic lung disease, and preterm infants of diabetic mothers. Journal of Neonatal Nursing 2014c, Aug 1; 20(4): 178-188.

Bassett D, Wymbs N, Porter M, Mucha P, Carlson J, Grafton S. Dynamic reconfiguration of human brain networks during learning. Proceedings of the National Academy of Sciences 2011, 108: 7641-7646.

Beckmann C, Jenkinson M, Smith S. General multilevel linear modeling for group analysis in fMRI. Neuroimage 2003, 20:1052–106310.

Bensmaia S. Tactile intensity and population codes. Behavioral Brain Research 2008, 190(2): 165-173.

Berger T, Borgdorff A, Crochet S, Neubauer F, Lefort S, Fauvet B, Ferezou I, Carleton A, Luscher H, Petersen C. Combined voltage and calcium epifluorescence imaging in vitro and in vivo reveals subthreshold and suprathreshold dynamics of mouse barrel cortex. Journal of Neurophysiology 2007, 97:3751–3762.

Bing Y, Zhang G, Sun L, Chu C, Qiu D. Dynamic properties of sensory stimulation evoked responses in mouse cerebellar granule cell layer and molecular layer. Neuroscience Letters 2015, Jan 12; 585:114-8.

Blankenburg F, Ruben J, Meyer R, Schwiemann J, Villringer A. Evidence for a rostral-to-caudal somatotopic organization in human primary somatosensory cortex with mirror-reversal in areas 3b and 1. Cerebral Cortex 2003, 13; 987–993.

Blatow M, Nennig E, Durst A, Sartor K, Stippich C. fMRI reflects functional connectivity of human somatosensory cortex. Neuroimage 2007, 37: 927–936.

Bogousslavsky J, van Melle G, Regli F. The Lausanne stroke registry: analysis of 1,000 consecutive patients with first stroke. Stroke 1988; 19:1083–1092.

Bolognini N, Russo C, Edwards D. The sensory side of post-stroke motor rehabilitation. Restorative Neurology and Neuroscience 2016, PMID: 27080070 (Epub ahead of print].

Briggs R, Dy-Liacco I, Malcolm M, Lee H, Peck K, Gopinath K, et al. A pneumatic vibrotactile stimulation device for fMRI. Magnetic Resonance in Medicine 2004, 51; 640–643.

Brown A. The termination of cutaneous nerve fibers in the spinal cord. Trends in Neuroscience 1981, 4: 64-67.

Brown C, Aminoltejari K, Erb H, Winship I, Murphy T. In vivo voltage-sensitive dye imaging in adult mice reveals that somatosensory maps lost to stroke are replaced over weeks by new structural and functional circuits with prolonged modes of activation within both the peri-infarct zone and distant sites. Journal of Neuroscience 2009, 29: 1719-1734.

Brown I, Bower J. The influence of somatosensory cortex on climbing fiber responses in the lateral hemispheres of the rat cerebellum after peripheral tactile stimulation. The Journal of Neuroscience 2002, 22(15): 6819-29.

Caplan L. Ataxia in patients with brain infarcts and hemorrhages. Handbook of Clinical Neurology 2012, 103: 147-60.

Capra NF, Dessem D. Central connections of trigeminal primary afferent neurons: topographical and functional considerations. Critical Reviews in Oral Biology and Medicine; 1992; 4: 1-52.

Carandini M, Heeger D. Normalization as a canonical neural computation, Nature Reviews Neuroscience 2012, 13: 51–62.

Carmicheal S, Archibeque I, Luke L. Growth-associated gene expression after stroke: evidence for a growth-promoting region in pre-infarct cortex. Experimental Neurology 2005, 193: 291-311.

Carsea, I., Froemke, R., 2013. Cortical plasticity, excitatory-inhibitory balance, and sensory perception. Progress in Brain Research, 207: 65-90.

Caspers S, Eickhoff S, Rick T, von Kapri A, Kuhlen T, Huang R, Shah N, Zilles K. Probabilistic fibre tract analysis of cytoarchitectonically defined human inferior parietal lobule areas reveals similarities to macaques. Neuroimage 2011, 58(2):362-80.

Castro-Alamancos M. Role of thalamocortical sensory suppression during arousal: focusing sensory inputs in neocortex. Journal of Neuroscience 2002, 22:9651–9655.

Celnik P, Hummel F, Harris-Love M, Wolk R, Cohen L. Somatosensory stimulation enhances the effects of training functional hand tasks in patients with chronic stroke. Archives of Physical Medicine and Rehabilitation 2007, 88(11): 1369-1376.

Cerkevich C, Qi H, Kaas J. Thalamic input to representations of the teeth, tongue, and face in somatosensory area 3b of macaque monkeys. Journal of Comparative Neurology 2013, 521(17): 3954-3971.

Cha J, Kim S, Jung W, Han Y, Im G, Lee J. Altered white matter integrity and functional connectivity of hyperacute-stage cerebral ischemia in a rat model. Magnetic Resonance Imaging 2016, Apr 20, pii: S0730-725X (16)30016-9 [Epub ahead of print].

Chaudhuri R, Knoblauch K, Gariel M, Kennedy H, Wang X. A large-scale circuit mechanism for hierarchical dynamical processing in the primate cortex, Neuron 2015, 88: 419–431.

Chakrabarti S, Zhang M, Alloway K. MI neuronal responses to peripheral whisker stimulation: relationship to neuronal activity in S1 barrels and septa. Journal of Neurophysiology 2008, 100:50–63.

Chen L, Friedman R, Roe A. Optical imaging of a tactile illusion in area 3b of the primary somatosensory cortex. Science 2003, Oct 31;302(5646):881-5.

Cheng L, Wu Z, Sun J, Fu Y, Wang X, Yang GY, Miao F, Tong S. Reorganization of Motor Execution Networks During Sub-Acute Phase After Stroke. IEEE Transactions on Neural systems and Rehabilitation 2015, 23(4):713-23.

Chong C, Schwedt T. White matter damage and brain network alterations in concussed patients: a review of recent diffusion tensor imaging and resting-state functional connectivity data. Current Pain and Headache Reports 2015, 19(5): 485.

Chouchkov C. The fine structure of small encapsulated receptors in human digital glabrous skin. Journal of Anatomy-London 1973, 114: 25-33.

Christensen A, Corey D. TRP channels in mechanosensation: direct or indirect activation? Nature Reviews Neuroscience 2007, 8:510-521.

Chu S, Barlow S, Kieweg D, Lee J. OroSTIFF: Face-referenced measurement of perioral stiffness in health and disease. Journal Biomechanics 2010, 43: 1476-1482.

Chung S, Li X, Nelson S. Short-term depression at thalamocortical synapses contributes to rapid adaptation of cortical sensory responses in vivo. Neuron 2002, 34:437–446.

Chun J, Peltier S, Yoon D, Manschreck T, Deldin P. Prolongation of ERP latency and reaction time (RT) in simultaneous EEG/fMRI data acquisition. Journal of Neuroscience Methods 2016, 268:78-86.

Cloutman L, Binney R, Drakesmith M, Parker G, Lambon Ralph M. The variation of function across the human insula mirrors its patterns of structural connectivity: evidence from in vivo probabilistic tractography. Neuroimage 2012, 59(4): 3514-21.

Coghill R, Sang C, Maisog J, Iadarola M. Pain intensity processing within the human brain: a bilateral, distributed mechanism. Journal of Neurophysiology 1999, 82:1934–1943.

Cohen J, Hirata A, Castro-Alamancos M. Vibrissa sensation in superior colliculus: wide-field sensitivity and state-dependent cortical feedback. Journal of. Neuroscience 2008, 28:11205–11220.

Conforto A, Ferreiro K, Tomasi C, Laurenti dos Santos R, Moreira V, Marie S, Baltieri S, Scaff M, Cohen L. Effects of somatosensory stimulation on motor function after subacute stroke. Neurorehabilitation and Neural Repair 2010, 24: 263-272.

Conner N, Abbs J. Orofacial proprioception: analyses of cutaneous mechanoreceptor population properties using artificial neural networks. Journal of Communication Disorders 1998, Nov-Dec; 31(6): 535-42.

Costanzo R, Gardner E. A quantitative analysis of responses of direction-sensitive neurons in somatosensory cortex of awake monkeys. Journal of Neurophysiology 1980, 43: 1319–1341.

Cruikshank S, Urabe H, Nurmikko A, Connors B. Pathway-specific feedforward circuits between thalamus and neocortex revealed by selective optical stimulation of axons. Neuron 2010, 65:230–245.

Cullen K, Brooks J. Neural correlates of sensory prediction errors in monkeys: evidence for internal models of voluntary self-motion in the cerebellum. Cerebellum 2015, 14(1): 31-4.

Custead R, Oh H, Rosner A, Barlow S. Adaptation of the cortical somatosensory evoked potential following pulsed pneumatic stimulation of the lower face in adults. Brain Research 2015, 1622: 81-90.

Darian-Smith I, Goodwin A, Sugitani M, Heywood J (1984) The tangible features of textured surfaces: Their representation in the monkey's somatosensory cortex. In *Dynamic Aspects of Neocortical Function*, Edelman G, Cowan W, Gall W, eds: 475-500, Wiley, New York.

DeFelipe J, Farinas I. The pyramidal neuron of the cerebral cortex: morphological and chemical characteristics of the synaptic inputs. Progressive Neurobiology 1992, 39: 563–607.

Delmas P, Hao J, Rodat-Despix L. Molecular mechanisms of mechanotransduction in mammalian sensory neurons. Nature Reviews: Neuroscience 2011, 12: 139-153.

Dépeault A, Meftah E, Chapman C. Neuronal correlates of tactile speed in primary somatosensory cortex. Journal of Neurophysiology 2013, 110: 1554-1566.

Derbyshire S, Jones A, Gyulai F, Clark S, Townsend D, Firestone L. Pain processing during three levels of noxious stimulation produces differential patterns of central activity. Pain 1997, 73:431–445.

Diamond M, Armstrong-James M, Ebner F. Somatic sensory responses in the rostral sector of the posterior group (POm) and in the ventral posterior medial nucleus (VPM) of the rat thalamus. Journal of Computational Neuroscience 1992, 318: 462–476.

Diaz-Quesada M, Martini F, Ferrati G, Bureau I, Maravall M. Diverse thalamocortical short-term plasticity elicited by ongoing stimulation. The Journal of Neuroscience 2014, 34(2): 515-526.

Dileep G, Hawkins J. Towards a mathematical theory of cortical micro-circuits. PLOS Computational Biology 2009, doi: 10.1371/journal.pcbi.1000532.

Dimitrova A, Weber J, Redies C, Kindsvater K, Maschke M, Kolb F, Forsting S, Diener H, Timmann D. MRI atlas of the human cerebellar nuclei. NeuroImage 2002, 17: 240-255.

Dinse, H., Kattenstroth, J., Gattica Tossi, M., Tegenthoff, M., Kalisch, T., 2011. Sensory stimulation for augmenting perception, sensorimotor behavior and cognition. Augmenting Cognition, 11-39.

Dreyer D, Hollins A, Whitsel B. Factors influencing cutaneous directional sensitivity. Sensory Processes 1978, 2: 71-79.

Dubbioso R, Pellegrino G, Antenora A, De Michele G, Filla A, Santoro L, Manganelli F. The effect of cerebellar degeneration on human sensori-motor plasticity. Brain Stimulation 2015, doi: 10.1016/j.brs.2015.05.012. [Epub ahead of print].

Eastwood J, Lev M, Azhari T, Lee T, Barboriak D, Delong D, Fitzek C. et al. CT Perfusion Scanning with deconvolution analysis: pilot study in patients with acute middle cerebral artery stroke 1. Radiology 222, no. 1 (2002): 227-236.

Eckers C, Kroger B, Sass K, Heim S. Neural representation of the sensorimotor speech-action repository. Frontiers in Human Neuroscience 2013, 7:121.

Edin B, Essick G, Trulsson M, Olsson K. Receptor encoding of moving tactile stimuli in humans. I. Temporal pattern of discharge of individual low-threshold mechanoreceptors. The Journal of Neuroscience 1995, 15(1): 830-847.

Edin B, Essick G, Trulsson M, Olsson K. Receptor encoding of moving tactile stimuli in humans. I. Temporal pattern of discharge of individual low-threshold mechanoreceptors. The Journal of Neuroscience 1995, 15(1): 830-847.

Eickhoff S, Heim S, Zilles K, Amunts K. A systems perspective on the effective connectivity of overt speech production. Philosophical transactions Series A, Mathematical, Physical, and Engineering Sciences 2009; 367:2399–421.

Eimer M, Forster B, Vibell J. Cutaneous saltation within and across arms: A new measure of the saltation illusion in somatosensation. Perception & Psychophysics 2005, 67(3): 458-468.

Elston G. Cortex, cognition and the cell: new insights into the pyramidal neuron and prefrontal function, Cerebral Cortex 2003, 13: 1124–1138.

Erdfelder, E., Faul, F., & Buchner, A. (1996). GPOWER: A general power analysis program. Behavior Research Methods, Instruments, & Computers, 28, 1-11.
Essick G, Afferica T, Aldershof B, Nestor J, Kelly D, Whitsel B. Human Perioral direction sensitivity. Experimental Neurology 1988b, 100: 506-523.
Essick G, Bredehoeft K, McLaughlin D, Szaniszlo. Directional sensitivity along the upper limb. Somatosensory and Motor Research 1991, 8(1): 13-22.
Essick G, Edin B. Receptor encoding of moving tactile stimuli in humans. II. The mean response of individual low-threshold mechanoreceptors to motion across the receptive field. The Journal of Neuroscience 1995, 15(1): 848-864.
Essick G, Franzen O, Whitsel B. Discrimination and scaling of velocity stimulus motion across the skin. Sensory and Motor Research 1988a, 6(1): 21-40.
Essick G. Factors affecting direction discrimination of moving tactile stimulation. Advances in Psychology-Amsterdam 1998, 127:1-54.
Essick G, McGuire M, Joseph A, Franzen O. Characterization of the percepts evoked by discontinuous motion over the perioral skin. Somatosensory and Motor Research 1992, (9) 2: 175-184.
Farkas T, Kis Z, Toldi J, Wolff J. Activation of the primary motor cortex by somatosensory stimulation in adult rats is mediated mainly by associational connections from the somatosensory cortex. Neuroscience 1999, 90: 353–361.
Fasano A, Herzog J, Raethjen J, Rose F, Muthuraman M, Volkmann J, Falk D, Elble R, Deuschl G. Gait ataxia in essential tremor is differentially modulated by thalamic stimulation. Brain 2010, 133: 2635-3648.
Favorov O, Diamond M. Demonstration of discrete place-defined columns segregates in the cat SI. Journal of Comparative Neurology 1990. 298: 97–112.
Ferezou I, Bolea S, Petersen C. Visualizing the cortical representation of whisker touch: voltage-sensitive dye imaging in freely moving mice. Neuron 2006, 50: 617–629.
Ferezou I, Haiss F, Gentet L, Aronoff R, Weber B, Petersen C. Spatiotemporal dynamics of cortical sensorimotor integration in behaving mice. Neuron 2007, 56: 907–923.
Fox M. Raichle M. Spontaneous fluctuations in brain activity observed with functional magnetic resonance imaging. Nature Review Neuroscience 2007, 8: 700-711.
Friston K, Jezzard P, Turner R. Analysis of functional MRI time-series. Human Brain Mapping 1994, 1:153–17110.
Frostig R, Chen-Bee C. Visualizing adult cortical plasticity using intrinsic signal optical imaging. In: Frostig, RD., editor. In vivo optical imaging of brain function. Second Edition. CRC Press; Boca Raton, FL, 2009: 255-87.
Frostig R, Lay C, Davis M. A rat's whiskers point the way toward a novel stimulus-dependent, protective stroke therapy. The Neuroscientist 2012, 19(3): 313-328.
Fucile, S., Gisel, E., 2010. Sensorimotor interventions improve growth and motor function in preterm infants. Neonatal Network, Nov-Dec; 29(6): 359-66.
Fucile. S., McFarland D., Gisel, E., Lau, C., 2012. Oral and nonoral sensorimotor interventions facilitate suck-swallow-respiration functions and their coordination in preterm infants. Early Human Development, Jun; 88(6): 345-50.
Fuertinger S, Horwitz B, Simonyan K. The Functional Connectome of Speech Control. PLos Biology 2015, 13: 2399-421.

Fujita M. A theory of cerebellar cortex and adaptive motor control based on two types of universal function approximation capability. Neural Networks 2016, 75: 173-96.

Gao J, Parsons L, Bower J, Xiong J, Li J, Fox P. Cerebellum implicated in sensory acquisition and discrimination rather than motor control. Science 1996, 272(5261): 545-7.

Gardner E, Costanzo R. Neuronal mechanisms underlying direction sensitivity of somatosensory cortical neurons in awake monkeys. Journal of Neurophysiology 1980, 43: 1342-1354.

Geldard F, Sherrick C. The cutaneous "rabbit": A perceptual illusion. Science 1972, 178, 178-179.

Geldard F, Sherrick C. The cutaneous saltatory area and its presumed neural basis. Perception & Psychophysics, 33, 299-304.

Goldreich D. A Bayesian perceptual model replicates the cutaneous rabbit and other tactile spatiotemporal illusions. PLoS One 2007, Mar 28;2(3):e333.

Goldreich D, Tong J. Prediction, postdiction, and perceptual length contraction: a bayesian low-speed prior captures the cutaneous rabbit and related illusions. Frontiers of Psychology 2013, May 10; 4:221.

Goodwin A, Morley J. Sinusoidal movement of a grating across the monkey's finger pad: representation of grating and movement features in afferent fiber responses. Journal of Neuroscience 1987, 7: 2168-2180.

Grabski K, Lamalle L, Vilain C, Schwartz J, Vallée N, Tropres I, Baciu M, Le Bas J, Sato M. Functional MRI assessment of orofacial articulators: neural correlates of lip, jaw, larynx, and tongue movements. Human Brain Mapping 2012, 33(10): 2306-21.

Greenlee M, Heitger F. The functional role of contrast adaptation. Vision Research 1988, 28:791-8.

Grefkes C, Fink G. Reorganization of cerebral networks after stroke: new insights from neuroimaging with connectivity approaches. Brain 2011, 134(5):1264-76.

Groh A, de Kock C, Wimmer V, Sakmann B, Kuner T. Driver or coincidence detector: modal switch of a corticothalamic giant synapse controlled by spontaneous activity and short-term depression. Journal of Neuroscience 2008, 28: 9652–9663.

Gruber P, Gould D. The red nucleus: Past, present and future. Neuroanatomy 2010, 9: 1-3.

Guillery R, Sherman S. Thalamic relay functions and their role in corticocortical communication: generalizations from the visual system. Neuron 2002, 33: 163-175.

Habas C. Functional imaging of the deep cerebellar nuclei: A review. Cerebellum 2010, 9(1):22-8.

Habas C, Guillevin R, Abanou A. In vivo structural and functional imaging of the human rubral and inferior olivary nuclei: A mini-review. Cerebellum 2010, 9(2):167-73.

Habas C, Kamdar N, Nguyen D, Prater K, Beckmann C, Menon V, Greicius M. Distinct cerebellar contributions to intrinsic connectivity networks. Journal of Neuroscience 2009, 29: 8586–8594.

Hamada M, Strigaro G, Murase N, Sadnicka A, Galea J, Edwards M, Rothwell J. Cerebellar modulation of human associative plasticity. The Journal of Physiology 2012, 590(10): 2365-74.

Hamada Y, Otsuka S, Okamoto T, Suzuki R. The profile of the recovery cycle in human primary and secondary somatosensory cortex: a magnetoencephalography study. Clinical Neurophysiology 2002, 113: 1787–1793.

Hamdy S, Rothwell J, Aziz Q, Singh K, Thompson D. Long-term reorganization of human motor cortex driven by short-term sensory stimulation. Nature Neuroscience 1998, 1(1): 64-68.

Harrington G, Wright C, Hunter Downs J. A new vibrotactile stimulator for functional MRI. Human Brain Mapping 2000, 10: 140–145.

Harris N, Verley D, Gutman B, Sutton R. Bi-directional changes in fractional anisotropy after experiment TBI: Disorganization and reorganization? Neuroimage 2016, 133: 129-43.

Heiss, J., Katz, Y., Ganmor, E., Lampl, I., 2008. Shift in the balance between excitation and inhibition during sensory adaptation of S1 neurons. The Journal of Neuroscience, 28(49): 13320-13330.

Hendelman W. Dorsal column-medial lemniscus discriminative touch, joint position and vibration. In: Functional Neuroanatomy: Second Edition. Boca Raton: CRC Press; 2006.

Hogri R, Segalis E, Mintz M. Cerebellar inhibitory output shapes the temporal dynamics of its somatosensory inferior olivary input. Cerebellum 2014, 13(4): 452-61.

Huang R, Sereno M. Dodecapus: An MR-compatible system for somatosensory stimulation. Neuroimage 2007, 34(3):1060-73.

Hubener, M., Bonhoeffer, T., 2014. Neuronal plasticity: beyond the critical period. Cell, Nov 6; 159(4): 727-37.

Hu L, Zhang Z, Hu Y. A time-varying source connectivity approach to reveal human somatosensory information processing. NeuroImage 2012, 62: 217-228.

Hu X, Le T, Ugurbil K. Evaluation of the early response in fMRI in individual subjects using short stimulus duration. Magnetic Resonance in Medicine 1997, 37(6): 877-84.

Hursh J. Conduction velocity and diameter of nerve fibers. American Journal of Physiology 1939, 127: 131-139.

Hutchison R, Womelsdorf T, Allen E, Bandettini P, Calhoun V, Corbetta M, Della Penna S, Duyn J, Glover G, Gonzalez-Castillo J, Handwerker D, Keilholz S, Kiviniemi V, Leopold D, DePasquale F, Sporns O, Walter M, Chang C. Dynamic functional connectivity: Promise, issues, and interpretations. NeuroImage 2013, 80: 360-378.

Irimia A, Van Horn J. Functional neuroimaging of traumatic brain injury: advances and clinical utility. Neuropsychiatric Disease and Treatment 2015, 11: 2355-65.

Ito T, Gomi H. Cutaneous mechanoreceptors contribute to the generation of a cortical reflex in speech. Sensory and Motor Systems 2007, 18(9): 907-910.

Iwamura Y, Tanaka M, Iriki A, Taoka M, Toda T. Processing of tactile and kinesthetic signals from bilateral sides of the body in the postcentral gyrus of awake monkeys. Behavioral Brain Research 2002, 135: 185–190.

Jacobs K, Donoghue J. Reshaping the cortical motor map by unmasking latent intracortical connections. Science 1990, 251: 944–47.

Jacquin M, Wiegand R, Renehan, W. Structure-function relationships in rat brain stem subnucleus interpolaris, VIII Cortical inputs. Journal of Neurophysiology 1990, 64:3–27.

Jang S. A review of diffusion tensor imaging studies on motor recovery mechanisms in stroke patients. NeuroRehabilitation 2011, 28(4): 245-52.

Jantsch H, Kemppainen P, Ringler R, Handwerker H, Forster C. Cortical representation of experimental tooth pain in humans. Pain 2005, 118(3): 390-9.

Jenkins, W., Merzenich, M., 1990. Functional reorganization of primary somatosensory cortex in adult owl monkeys after behaviorally controlled tactile stimulation. Journal of Neurophysiology, 63: 82-103.

Jenny A, Saper C. Organization of the facial nucleus and corticofacial projection in the monkey: a reconsideration of the upper motor neuron facial palsy. Neurology 1987, 37(6):930-9.

Jezzini A, Caruana F, Stoianov I, Gallese V, Rizzolatti G. Functional organization of the insula and inner perisylvian regions. Proceedings of the National Academy of Sciences of the United States of America 2009, 109(25): 10077-82.

Jiang Y, Zaaimi B, Martin J. Competition with primary sensory afferents drives remodeling of corticospinal axons in mature spinal motor circuits. Journal of Neuroscience 2016, 6; 36: 193-203.

Johansson R, Trulsson M, Olsson K, Westberg K. Mechanoreceptor activity from the human face and oral mucosa. Experimental Brain Research 1988, 72: 204-208.

Johnson B, Frostig R. Long, intrinsic horizontal axons radiating through and beyond rat barrel cortex have spatial distributions similar to horizontal spreads of activity evoked by whisker stimulation. Brain Structure and Function 2015, Epub ahead of print, PMID: 26438334.

Johnson K. The roles and functions of cutaneous mechanoreceptors. Current Opinion in Neurobiology 2001, 11:455-461.

Johnson K, Lamb G. Neural mechanisms of spatial tactile discrimination: Neural patterns evoked by Braille-like dot patterns in the monkey. Journal of Physiology 1981. 310*:* 117-144.

Jones E. Anatomy of cerebral cortex: columnar input–output organization. In: Schmitt, F.O. (Ed.), The Organization of the Cerebral Cortex. MIT Press; 1992, Cambridge, MA, pp. 199–235.

Kaas J. Somatosensory system. In: Paxinos G, Mai JK, editors. The human nervous system, 2nd edition. New York: Elsevier Academic Press 2004, 1059–1092.

Kaas J, Qi H, Iyengar S. Cortical network for representing the teeth and tongue in primates. The Anatomical record Part A 2006, 288A: 182-190.

Kaelin-Lang A, Luft A, Sawaki L, Burstein A, Sohn Y, Cohen L. Modulation of human corticomotor excitability by somatosensory input. Journal of Physiology 2002, 540:623- 633.

Kamishina H, Yurcisin G, Corwin J, Reep R. Striatal projections from the rat lateral posterior thalamic nucleus. Brain Research 2008, 1204: 24–39.

Kato, H., Izumiyama. M., 2013. Activation of Brain Sensorimotor Network by Somatosensory Input in Patients with Hemiparetic Stroke: A Functional MRI Study. Available from: http://dx.doi.org/10.5772/51693.

Kattenstroth, J., Kalisch, T., Peters, S., Tegenthoff, M., Dinse, H., 2012. Long-term sensory stimulation therapy improves hand function and restores cortical

responsiveness in patients with chronic cerebral lesions. Three single case studies. Frontiers in Human Neuroscience, 6: 244.
Kedarnath N, Shruthi R. MRI as an essential diagnostic approach for trigeminal neuralgia. Journal of Maxillofacial and Oral Surgery 2015, 14(1): 462-4.
Kelly E, Folger S. EEG evidence of stimulus-directed response dynamics in human somatosensory cortex. Brain Research 1999, 815:326-36.
Kennedy T, Grimm R, Towe A. The role of cerebral cortex in evoked somatosensory activity in cat cerebellum. Experimental Neurology 1966, 14(1): 13-23.
Kielar A, Deschamps T, Chu R, Jokel R, Khatamian Y, Chen J, Meltzer J. Identifying Dysfunctional Cortex: Dissociable Effects of Stroke and Aging on Resting State Dynamics in MEG and fMRI. Frontiers in Aging Neuroscience 2016; 8: 40.
Kim, H., Beierlein, M., Connors, B., 1995. Inhibitory control of excitable dendrites in neocortex. Journal of Neurophysiology, 74(4): 1810-1814.
Kitazawa S. The science of the mental present: implications of temporal illusions. Brain Nerve 2013 Aug; 65(8):911-21.
Kohn A, Whitsel B. Sensory cortical dynamics. Behavioral Brain Research 2002, 135: 119-126.
Kou Z, Iraji A. Imaging brain plasticity after trauma. Neural Regeneration Research 2014, 9(7): 693–700.
Krubitzer L, Kaas J. The organization and connections of somatosensory cortex in marmosets. Journal of Neuroscience 1990, 10:952–974.
Küper M, Dimitrova A, Thürling M, Maderwald S, Roths J, Elles HG, Gizewski ER, Ladd ME, Diedrichsen J, Timmann D. Evidence for a motor and a non-motor domain in the human dentate nucleus--an fMRI study. NeuroImage 2011, 54(4): 2612-22.
Kwong K, Belliveau J, Chesler D, Goldberg I, Weisskoff R, Poncelet B, Kennedy D, Halpemet Halpemet E, Rosen B. (1992) Dynamic magnetic resonance imaging of human brain activity during primary sensory stimulation. Proceedings of the National Academy of Sciences, 1992. 89: 5675-9.
LaCara G, Ursino M. Direction selectivity of simple cells in the primary visual cortex: comparison of two alternative mathematical models. II: Velocity tuning and response to moving bars. Computers in Biology and Medicine 2007, 37(5): 589-610.
Lamb G. Tactile discrimination of textured surfaces: Psychophysical performance measurements in humans. Journal of Physiology 1983, May, 338: 551-65.
Lapash-Daniels C, Ayers K, Finley A, Culver J, Goldberg P. 2009. Axon sprouting in adult mouse spinal cord after motor cortex stroke. Neuroscience Letters 2009, 450:191–5.
Lay, C, Davis M, Chen-Bee C, Frostig R. Mild sensory stimulation reestablishes cortical function during the acute phase of ischemia. The Journal of Neuroscience 2011, 31(32): 11495-11504.
Lay C, Davis M, Chen-Bee C, Frostig R. Mild sensory stimulation completely protects the adult rodent cortex from ischemic stroke. PLoS ONE 2012, 5(6): e11270. doi:10.1371/journal.pone.0011270.
Lay C, Frostig R, Complete protection from impending stroke following permanent middle cerebral artery occlusion in awake, behaving rats. The European Journal of Neuroscience 2014, Nov; 40(9): 3413-21.

Leggio M, Molinari M. Cerebellar Sequencing: a Trick for Predicting the Future. Cerebellum 2015, 14:35–38.

Lee C, Imaizumi K. Functional convergence of thalamic and intrinsic projections to layers 4 and 6. Neurophysiology 2013, 45(5-6): 396-406.

Lee C, Whitsel B. Mechanisms underlying somatosensory cortical dynamics: I. In vivo studies. Cerebral Cortex 1992, 2:81-106.

Lee M, Kim S, Choi B, Chang C, Ann S, Jang S. Functional MRI finding by proprioceptive input in patients with thalamic hemorrhage. Neuro Rehabilitation 2012, 30(2): 131-6.

Liebeskind D. Trials of endovascular therapies or collaterals? International Journal of Stroke 2012, 8: 258–259.

Lin L, Murray G, Sessle B. Functional properties of single neurons in the primate face primary somatosensory cortex. I. Relations with trained orofacial motor behaviors. Journal of Neurophysiology 1994, 71: 2377-90.

Lipworth G, Ensworth J, Seetharam K, Lee J, Schmalenberg P, Nomura T, Reynolds M, Smith D, Urzhumov Y. Quasi-static magnetic field shielding using longitudinal mu-near-zero metamaterials. Scientific Reports 2015, 3(5):12764. doi: 10.1038/srep12764.

Lin C, Sun Y, Huang C, Yu C, Ju M. Cortical activation by tactile stimulation to face and anterior neck areas: an fMRI study with three analytic methods. Human Brian Mapping 2010, 31(12): 1876-85.

Liu Y, Pu Y, Gao J, Parsons L, Xiong J, Liotti M, Bower J, Fo P. The human red nucleus and lateral cerebellum in supporting roles for sensory information processing. Human Brain Mapping 2000, 10(4): 147-59.

Logothetis N, Pauls J, Augath M, Trinath T, Oeltermann A. Neurophysiological investigation of the basis of the fMRI signal. Nature 2001, 412 150-7.

Lötsch J, Walter C, Felden L, Nöth U, Deichmann R, Oertel B. The human operculo-insular cortex is pain-preferentially but not pain-exclusively activated by trigeminal and olfactory stimuli. PLoS One 2012, 7(4): e34798.

Luhmann H, Mudrick-Donnon L, Mittmann T, Heinemann U. Ischemia-induced long-term hyperexcitability in rat neocortex. European Journal of Neuroscience 1995, 7:180-191.

Luken L, Evert M, Wessberg J. Pleasantness of touch in human glabrous and hairy skin: order effects on affective ratings. Brain Research 2011. 1417: 9-15.

Lundblad L, Olausson H, Hermansson A, Wasling H. Cortical processing of tactile direction discrimination based on spatiotemporal cues in man. Neuroscience Letters 2011. 21: 50(1): 45-9.

Magee J. In: Stuart G, Spruston N, Hausser M, editors. Voltage-gated ion channels in dendrites. Dendrites, New York: Oxford University Press, 1999:139-160.

Malina, K., Jubran, M., Katz, Y., Lampl, I., 2013. Imbalance between excitation and inhibition in the somatosensory cortex produces postadaptation facilitation. The Journal of Neuroscience, 33(19): 8463-8471.

Mano T, Iwase S, Toma S. Microneurography as a tool to investigate peripheral neural traffic in humans. Clinical Neurophysiology 2006, 117(11): 2357-84.

Manto M. Mechanisms of human cerebellar dysmetria: experimental evidence and current conceptual bases. Journal of Neuroengineering and Rehabilitation 2009, 6:10.

Mayer J, Schuster H, Claussen J. Role of inhibitory feedback for information processing in thalamocortical circuits. Physical Review, E, Statistical, Nonlinear and Soft Matter Physics 2006, 73(1): 031908.

McCormick D, Bal T. Sensory gating mechanisms of the thalamus. Current Opinion in Neurobiology 1994, 4(4): 550-6.

McGlone F, Kelly E, Trulsson M, Francis S, Westling G, Bowtel R. Functional neuroimaging studies of human somatosensory cortex. Behavioral Brain Research 2002, 135: 147–158.

McGlone F, Reilly D. The cutaneous sensory system. Neuroscience and Biobehavioral Reviews 2010, 34(2): 148-59.

McWhinney S, Bardouille T, D'Arcy R, Newman A. Asymmetric Weighting to Optimize Regional Sensitivity in Combined fMRI-MEG Maps. Brain Topography 2016, 1:1-12.

Merzenich M, Kaas J, Sur M, Lin C. Double representation of the body surface within cytoarchitectonic areas 3b and 1 in "SI" in the owl monkey (Aotus trivirgatus). Journal of Computational Neurology 1978, 181:41–73.

Merzenich, M., Kaas, J., Wall, J., Nelson, R., Sur, M., Felleman, D., 1983a. Topographic reorganization of somatosensory cortical areas 3b and 1 in adult monkeys following restricted deafferentation. Neuroscience, 8: 33–55.

Merzenich, M., Kaas, J., Wall, J., Sur,M., Nelson, R., Felleman, D., 1983b. Progression of changes following median nerve section in the cortical representation of the hand in areas 3b and 1 in adult owl and squirrel monkeys. Neuroscience, 10(3): 639-65.

Merzenich, M., Nelson, R., Stryker, M., Cynader, M., Schoppmann, A., Zook, J., 1984. Somatosensory map changes following digit amputation in adult monkeys. Journal of Comparative Neurology, 224(4): 591–605.

Meyer S, Kessner S, Cheng B, Bönstrup M, Schulz R, Hummel F, De Bruyn N, Peeters A, Van Pesch V, Duprez T, Sunaert S, Schrooten M, Feys H, Gerloff C, Thomalla G, Thijs V, Verheyden G. Voxel-based lesion-symptom mapping of stroke lesions underlying somatosensory deficits. Neuroimage Clinical 2015, 10: 257-66.

Miller K. Canonical computations of cerebral cortex. Neurobiology of Cognitive Behavior, 2016, 37: 75-84.

Miyazaki M, Hirashima M, Nozaki D. The "cutaneous rabbit" hopping out of the body. Journal of Neuroscience 2010, Feb 3; 30(5):1856-60.

Monti M. Statistical analysis of fMRI time series: A critical review of the GLM approach. Frontiers in Human Neuroscience 2011, 5: 28.

Morecraft R, Stilwell-Morecraft S, Rossing W. The motor cortex and facial expression: new insights from neuroscience. Neurologist 2004, 10(5):235-49.

Moskowitz M, Lo E, Iadecola C. The science of stroke: mechanisms in search of treatments. Neuron 2010, 67(2): 181-198.

Mountcastle V. In: Edelman, G.M., Mountcastle, V.B. (Eds.) The Mindful Brain. MIT Press, 1978; Cambridge, MA, pp. 51–100.Murphy T, Corbett D. Plasticity during stroke recovery: from synapse to behavior. Nature Reviews; Neuroscience 2009, 10: 861–72.

Murphy B, Miller K. Balanced amplification: a new mechanism of selective amplification of neural activity patterns, Neuron 2009, 61: 635–648.

Nash P, Macefield V, Klineberg S, Gustin S, Murray G, Henderson L. Bilateral activation of the trigeminothalamic tract by acute orofacial cutaneous and muscle pain in humans. Pain 2010, 151: 384-393.

Nordin M, Hagbarth K. Mechanoreceptive units in the human infraorbital nerve. Acta Physiologica Scandinavica. 1989; 135:149-161.

Nordin M, Thomander L. Intrafascicular multi-unit recordings from the human infra-orbital nerve. Acta Physiologica Scandinavica 1989, 135(2): 139-48.

Nudo, R., McNeal, D., 2013. Plasticity of cerebral functions. Handbook of Clinical Neurology, 110: 13-21.

Ogawa S, Lee T, Kay A, Tank D. Brain Magnetic Resonance Imaging with Contrast Dependent on Blood Oxygenation Proceedings of the National Academy of Science 1990, 87: 9868-9872.

Ogawa S, Tank D, Menon R, Ellermann J, Kim S, Merkle H, Ugurbil K. (1992), Intrinsic Signal Changes Accompanying Sensory Stimulation: Functional Brain Mapping With Magnetic Resonance Imaging. Proceedings of the National Academy of Science 1992, 89: 5951-5955.

Ohmae S, Uematsu A, Tanaka M. Temporally specific sensory signals for the detection of stimulus omission in the primate deep cerebellar nuclei.

Pantano P, Baron J, Samson Y, Bousser M, Derouesne C, Comar D. Crossed cerebellar diaschisis: Further studies. Brain 1986, 109: 677-94.

Parent M, Parent A. Single-axon tracing and three-dimensional reconstruction of center median-parafascicular thalamic neurons in primates. The Journal of Comparative Neurology 2005, 481 (1): 127–44.

Parsons L, Bower J, Gao J, Xiong J, Li J, Fox P. Lateral cerebellar hemispheres actively support sensory acquisition and discrimination rather than motor control. Learning & Memory 1997, 4(1): 49-62

Pauling L, Coryell C. The magnetic properties and structure of hemoglobin, oxyhemoglobin and carbonmonoxy hemoglobin. Proceedings of the National Academy of Science 1936, 22: 210-216.

Pei Y, Bensmaia S. The neural basis of tactile motion perception. Journal of Neurophysiology 2014, 112(12): 3023-32.

Pereira A, Ribeiro S, Wiest M, Moore L, Pantoja J, Lin S, Nicolelis M. Processing of tactile information by the hippocampus. Proceedings of the National Academy of Science USA 2007, 104:18286–18291.

Peron S, Freeman J, Iyer V, Guo C, Svoboda K. A cellular resolution map of barrel cortex activity during tactile behavior. Neuron 2015, 6; 86(3): 783-99.

Petreanu L, Huber D, Sobczyk A, Svoboda K. Channelrhodopsin-2-assisted circuit mapping of long-range callosal projections. Nature Neuroscience 2007, 10:663–668.

Peurala S, Pitkänen K, Sivenius J, Tarkka I. Cutaneous electrical stimulation may enhance sensorimotor recovery in chronic stroke. Clinical Rehabilitation 2002, 16(7): 709-716.

Phillips J, Johnson K. neural mechanisms of scanned and stationary touch. The Journal of the Acoustic Society of America 1985, 77(1): 220-4.

Pinto D, Brumberg J, Simons D. Circuit dynamics and coding strategies in rodent somatosensory cortex. J. Neurophysiology 2000, 83:1158–1166.

Pita-Almenar J, Ranganathan G, Koester H. Impact of cortical plasticity on information signaled by populations of neurons in the cerebral cortex. Journal of Neurophysiology 2011, 106(3):1118-24.

Poeppel D. The neuroanatomic and neurophysiological infrastructure for speech and language. Current Opinion Neurobiology 2014, 28:142–9.

Popescu E, Barlow S, Venkatesan L, Wang J. Popescu M. Adaptive changes in the neuromagnetic response of the primary and association somatosensory areas following repetitive tactile hand stimulation in humans. Human Brain Mapping 2013, 34(6): 1415-1426.

Popescu M, Barlow S, Popescu M, Estep M, Popescu E-A, Venkatesan L, Auer E, Brooks W. Cutaneous stimulation of the digits and lips evokes responses with different adaptation patterns in primary somatosensory cortex. NeuroImage 2010, 52: 1477–1486.

Porter J, Johnson C, Agmon A. Diverse types of interneurons generate thalamus-evoked feedforward inhibition in the mouse barrel cortex. The Journal of Neuroscience 2001, 21(8): 2699-2710.

Rao V, Finkbeiner, S. NMDA and AMPA receptors: old channels, new tricks. Trends in Neurosciences 2007, 30(6): 284-291.

Rausell E, Jones E. Histochemical and immunocytochemical compartments of the thalamic VPM nucleus in monkeys and their relationship to the representational map. Journal of Neuroscience 1991, 11: 210-25.

Restuccia D, Della Marca G, Valeriani M, Leggio M, Molinari M. Cerebellar damage impairs detection of somatosensory input changes. A somatosensory mismatch-negativity study. Brain 2007, 130: 276–87.

Rocchi L, Casula E, Tocco P, Berardelli A, Rothwell J. Somatosensory temporal discrimination threshold involves inhibitory mechanisms in the primary somatosensory area. Journal of Neuroscience 2016, 13; 36(2): 325-35.

Rosner A, Barlow S. Sensorimotor cortical hemodynamics following hand and orofacial motor tasks and pulsed cutaneous stimulation. Nanosymposium on Oral Motor and Speech at the annual meeting for the Society for Neuroscience 2015, Chicago, IL.

Rowe M, Ferrington D, Fisher G, Freeman B. Parallel processing and distributed coding for tactile vibratory information within sensory cortex. In: Rowe, M.J., Willis, W.D. (Eds.), Development, Organization, and Processing In Somatosensory Pathways. Alan R. Liss, Inc., New York, 1985: 247–258.

Rowland N, Jaeger D. Responses to tactile stimulation in deep cerebellar nucleus neurons result from recurrent activation in multiple pathways. Journal of Neurophysiology 2008, 99(2): 704-17.

Schmahmann J, Ko R, MacMore J. The human basis pontis: motor syndromes and topographic organization. Brain 2004, 127: 1269-91.

Schneider R, Friedman D, Mishkin M. A modality specific somatosensory area within the insula of the rhesus monkey. Brain Research 1993, 621:116–120.

Schnepel, P., Kumar, A., Zohar, M., Aertsen, A., Boucsein, C., 2014. Physiology and impact of horizontal connections in rat neocortex. Cerebral Cortex, Nov 19. pii bhu265 (Epup ahead of print).

Schulte L, Sprenger C, May A. Physiological brainstem mechanisms of trigeminal nociception: An fMRI study at 3T. Neuroimage 2016, 124: 518-25.

Servos P, Engel S, Gati J, Menon R. fMRI evidence for an inverted face representation in human somatosensory cortex NeuroReport 1999, 10:1393–1395.

Sherman S. Guillery R, On the actions that one nerve cell can have on another: distinguishing ‘‘drivers’’ from ‘‘modulators’’. Proceedings of the National Academy of Science 1998, USA, 95:7121–7126.

Siebenhuhner F, Weiss S, Coppola R, Weinberger D, Bassett D. Intra- and Inter-Frequency Brain Network Structure in Health and Schizophrenia. PLoS ONE 2013, 8, e72351.

Simonyan K, Fuertinger S. Speech networks at rest and in action: Interactions between functional brain networks controlling speech production. Journal of Neurophysiology 2015, 113(7): 2967-78.

Shuaib A, Butcher K, Mohammad A, Saqqur M, Liebeskind D. Collateral blood vessels in acute ischemic stroke: a potential therapeutic target. Lancet Neurology 2011, 10: 909–921.

Small S, Hlustik P, Noll D, Genovese C, Solodkin A. Cerebellar hemispheric activation ipsilateral to the paretic hand correlates with functional recovery after stroke. Brain 2002, 125: 1544-1557.

Smith S, Millera K, Moellerb S, Xub J, Auerbachb E, Woolricha M, Beckmanna C, Jenkinsona M, Anderssona J, Glasserf M, Van Essenf D, Feinbergg D, Yacoubb E, Ugurbilb K. Temporally-independent functional modes of spontaneous brain activity. Proceedings of the National Academy of Sciences of the United States of America 2012, 109(8): 3131-3126.

Spackman L, Boyd S, Towell T. Identification and characterization of somatosensory off responses. Brain Research 2006, 1114(1): 53-62.

Spencer R, Ivry R. Cerebellum and timing. In: Manto M, Gruol D, Schmahmann J, Koibuchi N, Rossi F, editors. Handbook of the cerebellum and cerebellar disorders. New York: Springer 2013, 1201–19.

Stal P, Eriksson P, Eriksson A, Thornell. Enzyme-histochemical and morphological characteristics of muscle fibre types in the human buccinator and orbicularis oris. Archives of Oral Biology 1990, 35(6): 449-58.

Staines R, Black S, Graham S, McIlroy W. Somatosensory gating and recovery from stroke involving the thalamus. Stroke 2002, 33: 2642-2651.

Staines R, Brooke J, McIlroy W. Task-relevant selective modulation of somatosensory afferent paths from the lower limb. Neuroreport 2000, 11:1713–1719.

Starr C, Sawaki L, Wittenberg G, Burdette J, Oshiro Y, Quevedo A, Coghill R. Roles of the insular cortex in the modulation of pain: Insights from brain lesions. Journal of Neuroscience 2009, 29(9): 2684-2694.

Stephani C, Fernandez-Baca Vaca G, Maciunas R, Koubeissi M, Lüders H. Functional neuroanatomy of the insular lobe. Brain Structure & Function 2011, 216(2):137-49.

Steriade M, McCormick D, Sejnowski T. Thalamocortical oscillations in the sleeping and aroused brain. Science 1993, 262:679–685.

Strick P, Dum R, Fiez J. Cerebellum and nonmotor function. Annual Review of Neuroscience 2009, 32:413–434.

Swadlow A, Gusev A. The impact of 'bursting' thalamic impulses at a neocortical synapse. Nature Neuroscience 2001, 4:402–408.

Szaniszlo J, Essick G, Kelly D, Joseph A, Bredehoeft. Evocation and characterization of percepts of apparent motion on the face. Perceptions & Psychophysics 1998, 60(5): 785-804.

Telesford Q, Lynall M, Vettel J, Miller M, Grafton S, Bassett D. Detection of functional brain network reconfiguration during task-driven cognitive states. Neuroimage 2016, May 31. pii: S1053-8119 (16)30198-7 [Epub ahead of print].

Tesche C, Karhu J. Anticipatory cerebellar responses during somatosensory omission in man. Human Brain Mapping 2000, 9(3): 119-42.

Thulborn K, Warterton J, Matthews P, Radda G. Oxygenation dependence of the transverse relaxation time of water protons in whole blood at high field. Biochim Biophys Acta 1982, 714:265-70.

Todd G. Anisotropy and spatial acuity on human lips. Clinical Neurophysiology 2012, 123(8): 1593-98.

Todd N, Moeller S, Auerbach E, Yacoub E, Flandin G, Weiskopf N. Evaluation of 2D multiband EPI imaging for high-resolution, whole-brain, task-based fMRI studies at 3T: Sensitivity and slice leakage artifacts. Neuroimage 2016, 124: 32-42.

Tomita A, Kato T, Sato F, Hague T, Oka A, Yamamoto M, Ono T, Maeda Y, Sessle B, Yoshida A. Somatotopic direct projections from orofacial areas of primary somatosensory cortex to pons and medulla, especially to trigeminal sensory nuclear complex, in rats. Neuroscience 2012, 200(3): 166-185.

Tommerdahl M, Favorov O, Whitsel B. Dynamic representations of the somatosensory cortex. Neuroscience and Biobehavioral Reviews 2010, 34: 160-170.

Tommerdahl M, Simons S, Chiu J, Favorov O, Whitsel B. Ipsilateral input modifies the primary somatosensory cortex response to contralateral skin flutter. Journal of Neuroscience 2006, 26: 5970–5977.

Tommerdahl M, Simons S, Chiu J, Favorov O, Whitsel B. Response of SI cortex to ipsilateral, contralateral and bilateral flutter stimulation in the cat. BMC Neuroscience 2005, 6: 29.

Trulsson M, Francis S, Kelly E, Westling G, Bowtell R, McGlone F. Cortical responses to single mechanoreceptive afferent microstimulation revealed with fMRI. NeuroImage 2000, 13: 613–622.

Trulsson M, Johansson R. Orofacial mechanorecptors in humans: encoding characteristics and responses during natural orofacial behaviors. Behavioral Brain Research 2002, 135.

Tsunozaki M, Bautista D. Mammalian somatosensory mechanotransduction. Current Opinion in Neurobiology 2009, 19:362–369.

Valbo A, Johansson R. Properties of cutaneous mechanoreceptors in the human hand related to touch sensation. Human Neurobiology 1984, 3:3-14.

Valle M, Bosco G, Casabona A, Garifoli A, Perciavalle V, Coco M, Perciavalle V. Representation of movement velocity in the rat's interpositus nucleus during passive forelimb movements. Cerebellum 2010, 9(2): 249-58.

Van Ede F, Maris E. Somatosensory demands modulate muscular Beta oscillations, independent of motor demands. Journal of Neuroscience 2013, 33(26): 10849-57.

Venkatesan L, Barlow S, Popescu M, Popescu A. Integrating approach for studying adaptation mechanisms in the human somatosensory cortical network. Experimental Brain Research 2014, 232, 3545-3554.

Venkatesan, L., Barlow, S., Popescu, M., Popescu, A., Auer, E., 2010. TAC-Cell inputs to human hand and lip induce short-term adaptation of the primary somatosensory cortex. Brain Research, 1348: 63-70.

Venkatesan L, Barlow S, Popescu M, Popescu A, Auer E. TAC-Cell inputs to human hand and lip induce short-term adaptation of the primary somatosensory cortex. Brain Research 2010, 1348: 63-70.

Wacker E, Spitzer B, Lützkendorf R, Bernarding J, Blankenburg F. Tactile motion and pattern processing assessed with high-field fMRI. PlosOne 2011, 6(9): e24860

Wang Q, Webber R, Stanley G. Thalamic synchrony and the adaptive gating of information flow to cortex. Nature Neuroscience 2010, 13(12): 1534-1543.

Wang J, Li Z, Feng B, Zhang T, Zhang H, Li H, Chen T, Cui J, Zang WD, Li Y. Corticotrigeminal projections from the insular cortex to the trigeminal caudal subnucleus regulate orofacial pain after nerve injury via extracellular signal-regulated kinase activation in insular cortex neurons. Frontiers in Cellular Neuroscience 2015, 9: 493.

Wardman D, Gandevia S, Colebatch J. Cerebral, subcortical, and cerebellar activation evoked by selective stimulation of muscle and cutaneous afferents: an fMRI study. Physiological Reports 2014, 2(4):e00270.

Warren J, Santello M, Helms Tillery S. Effects of fusion between tactile and proprioceptive inputs on tactile perception. PLoS One. 2011 Mar 25; 6(3):e18073.

Warren S, Hamalainen H, Gardner E. Objective classification of motion- and direction-sensitive neurons in primary somatosensory cortex of awake monkeys. Journal of Neurophysiology 1986, 56(3): 598-622.

Whitsel B, Favorov O, Delemos K, Tommerdahl M, Essick G, Nakhle B. SI neuron response variability is stimulus tuned and NMDA receptor dependent. Journal of Neurophysiology 1999, 81: 2988-3006.

Whitsel B, Franzen O, Dreyer A, Hollins M, Young M, Essick G, Wong C. Dependence of subjective transverse length on velocity of moving tactile stimuli. Somatosensory Research 1986, 3: 185-196.

Whitsel B, Kelly E, Delemos K, Xu M, Quibrera P. Stability of rapidly adapting afferent entrainment vs. responsivity. Somatosensory and Motor Research 2000, 17:13-31.

Whitsel B, Roppolo J, Werner G. Cortical information processing of stimulus motion on primate skin. Journal of Neurophysiology 1972, 35: 691–717.

Wu C, Seo H, Cohen L. Influence of electric somatosensory stimulation on paretic-hand function in chronic stroke. Archives of Physical Medicine and Rehabilitation 2006, 87(3): 351–357.

Xerri C, Merzenich M, Peterson B, Jenkins W. Plasticity of primary somatosensory cortex paralleling sensorimotor skill recovery from stroke in adult monkeys. J Neurophysiology 1998, 79: 2119-2148.

Xu J, Moeller S, Auerbach EJ, Strupp J, Smith SM, Feinberg DA, Yacoub E, Uğurbil K. Evaluation of slice accelerations using multiband echo planar imaging at 3 T. Neuroimage 2013, 83: 991-1001.

Yildiz S, Bademkiran F, Yildiz N, Aydogdu I, Uludag B, Ertekin C. Facial motor cortex plasticity in patients with unilateral peripheral facial paralysis. NeuroRehabilitation 2007, 22(2):133-40.

Yamada K, Ito H, Nakamura H, Kizu O, Akada W, Kubota T, Goto M, Konishi J, Yoshikawa K, Shiga K, Nakagawa M, Mori S, Nishimura T. Stroke patients' evolving symptoms assessed by tractography. Journal of Magnetic Resonance Imaging 2004. 20(6): 923-9.

Yamashiro K, Inui K, Otsuru N, Urakawa T, Kakigi R. Temporal window of integration in the somatosensory modality: an MEG study. Clinical Neurophysiology 2011, 122(11): 2276-81.

Yu C, Horev G, Rubin N, Derdikman D, Haidarliu S, Ahissar E. Coding of object location in the vibrissal thalamocortical system. Cerebral Cortex 2013, ahead of print; doi: 10.1093.

Zembrzycki A, Chou S, Ashery-Padan R, Stoykova A, O'Leary D. Sensory cortex limits cortical maps and drives top-down plasticity in thalamocortical circuits. Nature Neuroscience 2013, Aug; 16(8): 1060-7.

Website Images:

Banos, J. NBL 120: Basic Neuroscience Virtual Gross Lab (Retrieved from http://www.opt.uab.edu/class2011/1st%20year/NeuroAnatomy/NBL120VirtualLab.htm, date accessed; August 28, 2015).

Imgarcade.com, The human cortical homunculus (retrieved from http://imgarcade.com/1/cortical-homunculus/ , date accessed September 10, 2015).

National Institute of Neurological Disorders and Stroke, Trigeminal Neuralgia; Fact Sheet (retrieved from http://www.ninds.nih.gov/disorders/trigeminalneuralgia/detail-trigeminal-neuralgia.htm, date accessed September 20, 2015).

The Clever Machine, Characterizing the BOLD Signal-The Hemodynamic Response Function (retrieved from https://theclevermachine.wordpress.com, date accessed September 16, 2015).

Study Blue, Cerebellum (retrieved from https://www.studyblue.com/notes/note/n/ch-9cerebellum/deck/4085835, date accessed January 5, 2016).

Study Blue, Somatosensory Cortex (retrieved from https://www.studyblue.com/notes/note/n/somatic-sensory-system/deck/6227652, date accessed October 30, 2015).

What-When-How In-Depth Tutorials and Information, The Upper Motor Neurons (Motor and Sensory Systems) Part 1 (Retrieved from http://what-when-how.com/neuroscience/the-upper-motor-neurons-motor-systems-part-1/, date accessed; August 24, 2015).

What-When-How In-Depth Tutorials and Information, Brainstem, Pons and Cerebellum Part 2 (Retreived from http://what-when-how.com/neuroscience/brainstem-ii-pons-and-cerebellum-part-2/, date accessed May 20, 2016).

APPENDICES

Appendix A: Sample Velocity Program (.xml)

```
<Series>
  <Date>7/28/2015 10:00 AM</Date>
  <File>D:\USERS\Rebecca\fMRI_sequence\FACE_09
velocity.xml</File>
  <Description>Velocity Set</Description>
  <Continuous>False</Continuous>
  <Sequence Num="1">
    <On>True</On>
    <Runs>10</Runs>
    <CycleTime>2000</CycleTime>
    <Description>All 60ms pulses 5 cm/sec</Description>
    <Channel Num="1">
      <OnTime>0</OnTime>
      <OffTime>60</OffTime>
    </Channel>
    <Channel Num="2">
      <OnTime>500</OnTime>
      <OffTime>560</OffTime>
    </Channel>
    <Channel Num="3">
      <OnTime>1000</OnTime>
      <OffTime>1060</OffTime>
    </Channel>
    <Channel Num="4">
      <OnTime>1400</OnTime>
      <OffTime>1460</OffTime>
    </Channel>
    <Channel Num="5">
      <OnTime>1800</OnTime>
      <OffTime>1860</OffTime>
    </Channel>
    <Channel Num="6">
      <OnTime>0</OnTime>
      <OffTime>0</OffTime>
    </Channel>
    <Channel Num="7">
      <OnTime>0</OnTime>
      <OffTime>0</OffTime>
    </Channel>
    <Channel Num="8">
      <OnTime>0</OnTime>
```

```
    <OffTime>0</OffTime>
  </Channel>
</Sequence>
<Sequence Num="2">
  <On>True</On>
  <Runs>40</Runs>
  <CycleTime>500</CycleTime>
  <Description>All 60ms pulses, 25 cm/sec</Description>
  <Channel Num="1">
    <OnTime>0</OnTime>
    <OffTime>60</OffTime>
  </Channel>
  <Channel Num="2">
    <OnTime>100</OnTime>
    <OffTime>160</OffTime>
  </Channel>
  <Channel Num="3">
    <OnTime>200</OnTime>
    <OffTime>260</OffTime>
  </Channel>
  <Channel Num="4">
    <OnTime>280</OnTime>
    <OffTime>340</OffTime>
  </Channel>
  <Channel Num="5">
    <OnTime>360</OnTime>
    <OffTime>420</OffTime>
  </Channel>
  <Channel Num="6">
    <OnTime>0</OnTime>
    <OffTime>0</OffTime>
  </Channel>
  <Channel Num="7">
    <OnTime>0</OnTime>
    <OffTime>0</OffTime>
  </Channel>
  <Channel Num="8">
    <OnTime>0</OnTime>
    <OffTime>0</OffTime>
  </Channel>
</Sequence>
<Sequence Num="3">
  <On>True</On>
  <Runs>80</Runs>
  <CycleTime>250</CycleTime>
  <Description>All 60ms pulses, 65 cm/sec</Description>
```

```
    <Channel Num="1">
      <OnTime>0</OnTime>
      <OffTime>60</OffTime>
    </Channel>
    <Channel Num="2">
      <OnTime>38</OnTime>
      <OffTime>98</OffTime>
    </Channel>
    <Channel Num="3">
      <OnTime>76</OnTime>
      <OffTime>136</OffTime>
    </Channel>
    <Channel Num="4">
      <OnTime>107</OnTime>
      <OffTime>167</OffTime>
    </Channel>
    <Channel Num="5">
      <OnTime>138</OnTime>
      <OffTime>198</OffTime>
    </Channel>
    <Channel Num="6">
      <OnTime>0</OnTime>
      <OffTime>0</OffTime>
    </Channel>
    <Channel Num="7">
      <OnTime>0</OnTime>
      <OffTime>0</OffTime>
    </Channel>
    <Channel Num="8">
      <OnTime>0</OnTime>
      <OffTime>0</OffTime>
    </Channel>
  </Sequence>
  <Sequence Num="4">
    <On>True</On>
    <Runs>20</Runs>
    <CycleTime>1000</CycleTime>
    <Description>All 60ms pulses, non-stim</Description>
    <Channel Num="1">
      <OnTime>0</OnTime>
      <OffTime>0</OffTime>
    </Channel>
    <Channel Num="2">
      <OnTime>0</OnTime>
      <OffTime>0</OffTime>
    </Channel>
```

```
    <Channel Num="3">
      <OnTime>0</OnTime>
      <OffTime>0</OffTime>
    </Channel>
    <Channel Num="4">
      <OnTime>0</OnTime>
      <OffTime>0</OffTime>
    </Channel>
    <Channel Num="5">
      <OnTime>0</OnTime>
      <OffTime>0</OffTime>
    </Channel>
    <Channel Num="6">
      <OnTime>0</OnTime>
      <OffTime>0</OffTime>
    </Channel>
    <Channel Num="7">
      <OnTime>0</OnTime>
      <OffTime>0</OffTime>
    </Channel>
    <Channel Num="8">
      <OnTime>0</OnTime>
      <OffTime>0</OffTime>
    </Channel>
  </Sequence>
<Sequence Num="5">
    <On>True</On>
    <Runs>20</Runs>
    <CycleTime>1000</CycleTime>
    <Description>All 60ms pulses, same OnTime</Description>
    <Channel Num="1">
      <OnTime>0</OnTime>
      <OffTime>60</OffTime>
    </Channel>
    <Channel Num="2">
      <OnTime>0</OnTime>
      <OffTime>60</OffTime>
    </Channel>
    <Channel Num="3">
      <OnTime>0</OnTime>
      <OffTime>60</OffTime>
    </Channel>
    <Channel Num="4">
      <OnTime>0</OnTime>
      <OffTime>60</OffTime>
    </Channel>
```

```
    <Channel Num="5">
      <OnTime>0</OnTime>
      <OffTime>60</OffTime>
    </Channel>
    <Channel Num="6">
      <OnTime>0</OnTime>
      <OffTime>0</OffTime>
    </Channel>
    <Channel Num="7">
      <OnTime>0</OnTime>
      <OffTime>0</OffTime>
    </Channel>
    <Channel Num="8">
      <OnTime>0</OnTime>
      <OffTime>0</OffTime>
    </Channel>
  </Sequence>
</Series>
```

Appendix B: Velocity Protocol Calculation

```
<Series>
  <Date>7/28/2015 10:00 AM</Date>
  <File>D:\USERS\Rebecca\fMRI_sequence\FACE_09
velocity.xml</File>
  <Description>Velocity Set</Description>
  <Continuous>False</Continuous>
  <Sequence Num="1">
    <On>True</On>
    <Runs>10</Runs>
    <CycleTime>2000</CycleTime>
    <Description>All 60ms pulses 5 cm/sec</Description>
    <Channel Num="1">
      <OnTime>0</OnTime>
      <OffTime>60</OffTime>
    </Channel>
    <Channel Num="2">
      <OnTime>500</OnTime>
      <OffTime>560</OffTime>
    </Channel>
    <Channel Num="3">
      <OnTime>960</OnTime>
      <OffTime>1020</OffTime>
    </Channel>
    <Channel Num="4">
      <OnTime>1360</OnTime>
      <OffTime>1420</OffTime>
    </Channel>
    <Channel Num="5">
      <OnTime>1740</OnTime>
      <OffTime>1800</OffTime>
    </Channel>
```

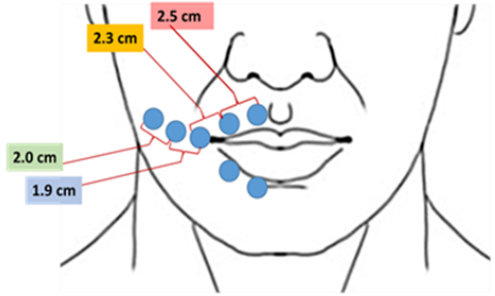


```
  <Sequence Num="2">
    <On>True</On>
    <Runs>40</Runs>
    <CycleTime>500</CycleTime>
    <Description>All 60ms pulses, 25 cm/sec</Description>
    <Channel Num="1">
      <OnTime>0</OnTime>
      <OffTime>60</OffTime>
    </Channel>
    <Channel Num="2">
      <OnTime>100</OnTime>
      <OffTime>160</OffTime>
    </Channel>
    <Channel Num="3">
      <OnTime>200</OnTime>
      <OffTime>260</OffTime>
    </Channel>
    <Channel Num="4">
      <OnTime>280</OnTime>
      <OffTime>340</OffTime>
    </Channel>
    <Channel Num="5">
      <OnTime>360</OnTime>
      <OffTime>420</OffTime>
    </Channel>
```

500 + 460 = 960

Galileo Velocity Table (cm/s)

SPAN(cm)	TIME1(s)	VELOCITY1(cm/s)	TIME2(s)	VELOCITY2(cm/s)	TIME3(s)	VELOCITY3 (cm/s)
1.5	0.3000	5	0.0600	25	0.0231	65
1.6	0.3200	5	0.0640	25	0.0246	65
1.7	0.3400	5	0.0680	25	0.0262	65
1.8	0.3600	5	0.0720	25	0.0277	65
1.9	0.3800	5	0.0760	25	0.0292	65
2	0.4000	5	0.0800	25	0.0308	65
2.1	0.4200	5	0.0840	25	0.0323	65
2.2	0.4400	5	0.0880	25	0.0338	65
2.3	0.4600	5	0.0920	25	0.0354	65
2.4	0.4800	5	0.0960	25	0.0369	65
2.5	0.5000	5	0.1000	25	0.0385	65
2.6	0.5200	5	0.1040	25	0.0400	65
2.7	0.5400	5	0.1080	25	0.0415	65
2.8	0.5600	5	0.1120	25	0.0431	65
2.9	0.5800	5	0.1160	25	0.0446	65

Appendix C: Sample Galileo Output

Series - START
Date: 7/28/2015 4:31:31 PM
File:D:\USERS\Rebecca\fMRI_Velocity\LastDownloadedSeries.xml
Description: Velocity Set
Continuous: False
Hardware Trigger: 2
Runs: 1
CB Runs: 4
Random Runs: 1

SEQ: 1 True
Runs: 10
Cycle Time: 2000
Description: All 60ms pulses 5 cm/sec
VALID: True
1: 0-60
2: 500-560
3: 1000-1060
4: 1400-1460
5: 1800-1860

SEQ: 2 True
Runs: 40
Cycle Time: 500
Description: All 60ms pulses, 25 cm/sec
VALID: True
1: 0-60
2: 100-160
3: 200-260
4: 280-340
5: 360-420

SEQ: 3 True
Runs: 80
Cycle Time: 250
Description: All 60ms pulses, 65 cm/sec
VALID: True
1: 0-60
2: 38-98
3: 76-136
4: 107-167
5: 138-198

SEQ: 4 True

Runs: 20
Cycle Time: 1000
Description: All 60ms pulses, non-stim
VALID: True

SEQ: 5 True
Runs: 20
Cycle Time: 1000
Description: All 60ms pulses, same On Time
VALID: True
1: 0-60
2: 0-60
3: 0-60
4: 0-60
5: 0-60

SEQ: 6 OFF
SEQ: 7 OFF
SEQ: 8 OFF
SEQ: 9 OFF
SEQ: 10 OFF
SEQ: 11 OFF
SEQ: 12 OFF
SEQ: 13 OFF
SEQ: 14 OFF
SEQ: 15 OFF
SEQ: 16 OFF
SEQ: 17 OFF
SEQ: 18 OFF
SEQ: 19 OFF
SEQ: 20 OFF
SEQ: 21 OFF
SEQ: 22 OFF
SEQ: 23 OFF
SEQ: 24 OFF
SEQ: 25 OFF
Series - END

OPENED: 7/28/2015 4:32:12 PM
DESCRIPTION: RANDOM BALANCED

Seq, Repeat
1, 1
1, 1
1, 2
1, 3

1, 4
1, 5
1, 6
1, 7
1, 8
1, 9
1, 10
3, 1
3, 2
3, 3
3, 4
3, 5
3, 6
3, 7
3, 8
3, 9
3, 10
3, 11
3, 12
3, 13
3, 14
3, 15
3, 16
3, 17
3, 18
3, 19
3, 20
3, 21
3, 22
3, 23
3, 24
3, 25
3, 26
3, 27
3, 28
3, 29
3, 30
3, 31
3, 32
3, 33
3, 34
3, 35
3, 36
3, 37
3, 38
3, 39

3, 40
3, 41
3, 42
3, 43
3, 44
3, 45
3, 46
3, 47
3, 48
3, 49
3, 50
3, 51
3, 52
3, 53
3, 54
3, 55
3, 56
3, 57
3, 58
3, 59
3, 60
3, 61
3, 62
3, 63
3, 64
3, 65
3, 66
3, 67
3, 68
3, 69
3, 70
3, 71
3, 72
3, 73
3, 74
3, 75
3, 76
3, 77
3, 78
3, 79
3, 80
1, 1
1, 2
1, 3
1, 4
1, 5

1, 6
1, 7
1, 8
1, 9
1, 10
5, 1
5, 2
5, 3
5, 4
5, 5
5, 6
5, 7
5, 8
5, 9
5, 10
5, 11
5, 12
5, 13
5, 14
5, 15
5, 16
5, 17
5, 18
5, 19
5, 20
4, 1
4, 2
4, 3
4, 4
4, 5
4, 6
4, 7
4, 8
4, 9
4, 10
4, 11
4, 12
4, 13
4, 14
4, 15
4, 16
4, 17
4, 18
4, 19
4, 20
2, 1

2, 2
2, 3
2, 4
2, 5
2, 6
2, 7
2, 8
2, 9
2, 10
2, 11
2, 12
2, 13
2, 14
2, 15
2, 16
2, 17
2, 18
2, 19
2, 20
2, 21
2, 22
2, 23
2, 24
2, 25
2, 26
2, 27
2, 28
2, 29
2, 30
2, 31
2, 32
2, 33
2, 34
2, 35
2, 36
2, 37
2, 38
2, 39
2, 40
5, 1
5, 2
5, 3
5, 4
5, 5
5, 6
5, 7

5, 8
5, 9
5, 10
5, 11
5, 12
5, 13
5, 14
5, 15
5, 16
5, 17
5, 18
5, 19
5, 20
4, 1
4, 2
4, 3
4, 4
4, 5
4, 6
4, 7
4, 8
4, 9
4, 10
4, 11
4, 12
4, 13
4, 14
4, 15
4, 16
4, 17
4, 18
4, 19
4, 20
2, 1
2, 2
2, 3
2, 4
2, 5
2, 6
2, 7
2, 8
2, 9
2, 10
2, 11
2, 12
2, 13

2, 14
2, 15
2, 16
2, 17
2, 18
2, 19
2, 20
2, 21
2, 22
2, 23
2, 24
2, 25
2, 26
2, 27
2, 28
2, 29
2, 30
2, 31
2, 32
2, 33
2, 34
2, 35
2, 36
2, 37
2, 38
2, 39
2, 40
2, 1
2, 2
2, 3
2, 4
2, 5
2, 6
2, 7
2, 8
2, 9
2, 10
2, 11
2, 12
2, 13
2, 14
2, 15
2, 16
2, 17
2, 18
2, 19

2, 20
2, 21
2, 22
2, 23
2, 24
2, 25
2, 26
2, 27
2, 28
2, 29
2, 30
2, 31
2, 32
2, 33
2, 34
2, 35
2, 36
2, 37
2, 38
2, 39
2, 40
4, 1
4, 2
4, 3
4, 4
4, 5
4, 6
4, 7
4, 8
4, 9
4, 10
4, 11
4, 12
4, 13
4, 14
4, 15
4, 16
4, 17
4, 18
4, 19
4, 20
2, 1
2, 2
2, 3
2, 4
2, 5

2, 6
2, 7
2, 8
2, 9
2, 10
2, 11
2, 12
2, 13
2, 14
2, 15
2, 16
2, 17
2, 18
2, 19
2, 20
2, 21
2, 22
2, 23
2, 24
2, 25
2, 26
2, 27
2, 28
2, 29
2, 30
2, 31
2, 32
2, 33
2, 34
2, 35
2, 36
2, 37
2, 38
2, 39
2, 40
5, 1
5, 2
5, 3
5, 4
5, 5
5, 6
5, 7
5, 8
5, 9
5, 10
5, 11

5, 12
5, 13
5, 14
5, 15
5, 16
5, 17
5, 18
5, 19
5, 20
5, 1
5, 2
5, 3
5, 4
5, 5
5, 6
5, 7
5, 8
5, 9
5, 10
5, 11
5, 12
5, 13
5, 14
5, 15
5, 16
5, 17
5, 18
5, 19
5, 20
4, 1
4, 2
4, 3
4, 4
4, 5
4, 6
4, 7
4, 8
4, 9
4, 10
4, 11
4, 12
4, 13
4, 14
4, 15
4, 16
4, 17

4, 18
4, 19
4, 20
3, 1
3, 2
3, 3
3, 4
3, 5
3, 6
3, 7
3, 8
3, 9
3, 10
3, 11
3, 12
3, 13
3, 14
3, 15
3, 16
3, 17
3, 18
3, 19
3, 20
3, 21
3, 22
3, 23
3, 24
3, 25
3, 26
3, 27
3, 28
3, 29
3, 30
3, 31
3, 32
3, 33
3, 34
3, 35
3, 36
3, 37
3, 38
3, 39
3, 40
3, 41
3, 42
3, 43

3, 44
3, 45
3, 46
3, 47
3, 48
3, 49
3, 50
3, 51
3, 52
3, 53
3, 54
3, 55
3, 56
3, 57
3, 58
3, 59
3, 60
3, 61
3, 62
3, 63
3, 64
3, 65
3, 66
3, 67
3, 68
3, 69
3, 70
3, 71
3, 72
3, 73
3, 74
3, 75
3, 76
3, 77
3, 78
3, 79
3, 80
1, 1
1, 2
1, 3
1, 4
1, 5
1, 6
1, 7
1, 8
1, 9

1, 10
3, 1
3, 2
3, 3
3, 4
3, 5
3, 6
3, 7
3, 8
3, 9
3, 10
3, 11
3, 12
3, 13
3, 14
3, 15
3, 16
3, 17
3, 18
3, 19
3, 20
3, 21
3, 22
3, 23
3, 24
3, 25
3, 26
3, 27
3, 28
3, 29
3, 30
3, 31
3, 32
3, 33
3, 34
3, 35
3, 36
3, 37
3, 38
3, 39
3, 40
3, 41
3, 42
3, 43
3, 44
3, 45

3, 46
3, 47
3, 48
3, 49
3, 50
3, 51
3, 52
3, 53
3, 54
3, 55
3, 56
3, 57
3, 58
3, 59
3, 60
3, 61
3, 62
3, 63
3, 64
3, 65
3, 66
3, 67
3, 68
3, 69
3, 70
3, 71
3, 72
3, 73
3, 74
3, 75
3, 76
3, 77
3, 78
3, 79
3, 80
3, 1
3, 2
3, 3
3, 4
3, 5
3, 6
3, 7
3, 8
3, 9
3, 10
3, 11

3, 12
3, 13
3, 14
3, 15
3, 16
3, 17
3, 18
3, 19
3, 20
3, 21
3, 22
3, 23
3, 24
3, 25
3, 26
3, 27
3, 28
3, 29
3, 30
3, 31
3, 32
3, 33
3, 34
3, 35
3, 36
3, 37
3, 38
3, 39
3, 40
3, 41
3, 42
3, 43
3, 44
3, 45
3, 46
3, 47
3, 48
3, 49
3, 50
3, 51
3, 52
3, 53
3, 54
3, 55
3, 56
3, 57

3, 58
3, 59
3, 60
3, 61
3, 62
3, 63
3, 64
3, 65
3, 66
3, 67
3, 68
3, 69
3, 70
3, 71
3, 72
3, 73
3, 74
3, 75
3, 76
3, 77
3, 78
3, 79
3, 80
1, 1
1, 2
1, 3
1, 4
1, 5
1, 6
1, 7
1, 8
1, 9
1, 10

CLOSED: 7/28/2015 4:46:14 PM